NTNU – Trondheim
Norwegian University of
Science and Technology

ROV Control System for Positioning of Subsea Modules

Eirik Hexeberg Henriksen

Marine Technology
Submission date: June 2014
Supervisor: Asgeir Johan Sørensen, IMT
Co-supervisor: Brede Thorkildsen, FMC Technologies

Norwegian University of Science and Technology
Department of Marine Technology

NTNU Trondheim
Norwegian University of Science and Technology
Department of Marine Technology

MASTER THESIS IN MARINE CYBERNETICS

SPRING 2014

FOR

STUD. TECH. Eirik Hexeberg Henriksen

ROV control system for positioning of subsea modules

Work description

Remotely Operated Vehicles (ROVs) are common in deepwater industries. As the oil industry, and also other relevant industries, moves into deeper water, the use of subsea technology has increased. Due to safety and practical reasons it is not convenient to use manned diving for maintenance and surveys. The solution is to use ROVs that are unoccupied, highly maneuverable and operated by a person onboard a vessel.

When subsea equipment is installed on the seabed there is a need for precise placement. The modules are often supposed to interface with existing equipment or structures, and proper alignment is required. In the "tree on wire" installation method for Xmas trees an ROV is used for this alignment. The control of the ROV is manual today. The objective of this thesis is to investigate mathematical models and automated control methods and functions of the ROV during seabed installation of subsea equipment. These should be implemented and tested

Scope of work

- Review relevant literature on ROV control systems and subsea installations.
- Formulate a mathematical simulation model (process plant model) for the installation phase both for model scale and full scale. The process plant model should include current loading model, ROV and subsea tree models as well as interaction forces and moments. Installations in the wave zone should also be investigated.
- Define control objectives and propose control strategies and algorithms for the ROV to control the motions of the X-mas tree. Different controllers should be investigated. The controller should be robust, and capable of controlling the motions of the Xmas tree even the physical properties are not perfectly known.
- Conduct simulation for controller tuning and testing.

- Prepare plan for testing the control system in NTNU AUR-lab. The testing should be done on R/V Gunnerus using ROV Minerva and a scaled model of a subsea module (e.g. a Xmas tree model).
- Conduct planned experiments for testing of the control system during May 2014.
- Document each step in the process

The report shall be written in English and edited as a research report including literature survey, description of mathematical models, description of control algorithms, simulation results, model test results, discussion and a conclusion including a proposal for further work. Source code should be provided on a CD with code listing enclosed in appendix. It is supposed that Department of Marine Technology, NTNU, can use the results freely in its research work, unless otherwise agreed upon, by referring to the student's work. The thesis should be submitted in three copies within June xx.

Advisers: Brede Thorkildsen (FMC Technologies)

Professor Asgeir J. Sørensen
Supervisor

Preface

This thesis is written during spring 2014 as the final part of my studies for the Master of Science degree in Marine Technology at the Norwegian University of Science and Technology (NTNU) in Trondheim. The problem of the thesis was given by FMC Technologies, a company that is a global provider of equipment and services for the energy industry. The Norwegian part of the company is mainly focused on subsea technology. The work done in this thesis is a continuation of the work done in Henriksen [2013].

Abstract

Installation of deep water Xmas trees for subsea oil production is sometimes done by lowering the tree using one wire. Xmas trees are interfacing with other equipment on the seafloor and will therefore need to be positioned, and oriented correct. Today aligning the Xmas tree to existing interfacing structures on the seabed during installation is done by manual control of an ROV. In this thesis it is proposed to automate this process. The benefits of doing this is to gain a faster and more precise control of the position of the tree, as well as being less prone to human errors. This will make the operation faster, safer and less expensive.

This thesis is a feasibility study of this new solution for aligning the Xmas tree in the installation process. In order to investigate the feasibility of the solution a mathematical model of an ROV and a Xmas tree that is hanging in a wire has been developed. Interaction forces between these objects are then defined. A model of the environment and sensor output from the ROV is also developed.

A controller algorithm has been defined that uses the position of the Xmas tree to calculate the control forces the ROV need to control the motions of the Xmas tree. This controller algorithm is a nonlinear PID-controller where the output is translated from the body-centre of the Xmas tree to the body centre of the ROV in order to use some of the existing control system in the ROV. In addition to the controller an extended kalman filter has been implemented in order to handle the sensor feedback, and a reference model has been made to generate smooth and feasible trajectories as input to the control system.

The mathematical model is used to simulate the behavior of the system, when the control system is connected. The simulations shows very promising results.

An experimental setup has been made in order to test the control system in real life. The experimental setup consists of a downscaled Xmas tree model, a docking frame, and a small scale ROV. This setup was used to test the control system in the Trondheim fjord using R/V Gunnerus. Due to an error in the programming the testing was not able to fully verify the simulation results. The results obtained during the test did however seem promising when this error is taken into account, and thus proof of concept was established.

Sammendrag

Installasjon av juletrær (Xmas tree) for oljeproduksjon blir av og til gjort ved at treet blir senket ned til havbunnen ved hjelp av kun en wire. Juletreet skal kobles til utsyr som allerede er på havbunnen og det er derfor nødvending med med presis posisjonering of orientering av treet før det settes på plass. I dag gjøres dette ved hjelp av en ROV som styres manuelt. I denne avhandlingen blir det forelått å automatisere denne prosessen. Fordelene ved dette er at man får raskere og mer presis kontroll over posisjonen til juletreet, og det er mindre sjangse for at menneskelige feil blir gjort. Dette vil gjøre installasjonen raskere, mer sikker og billigere.

Denne avhandlingen er en mulighetsstudie av et slikt kontrollsystem. For å studere problemet er det blitt utviklet en matematisk modell av et juletre som henger i en wire, som er sammenkoblet med en ROV. I denne modellen er også modeller av miljøpåvirkninger fra havstrømmer og bølger blitt implementert, samt en modell av sensorsignalene fra ROVen.

En kontrollalgoritme som bruker posisjonen til juletreet til å regne ut hvilke krefter ROVen må yte for å posisjonere juletreet er blitt designet. Dette er gjort ved hjelp av ulineær PID-kontroll, der utgangskraften blir transformert fra juletresenteret til senteret av ROVen. Dette er gjort for å kunne bruke det eksisterende kontrollsystemet som allerede finnes for denne. I tilleg til er det implementert et utvidet kalman filter (extended kalman filter) for å håndtere de støyete sensorsignalene, samt en referansemodell for å gi kontrollsystemet en jevn og gjennomførbar referanse.

Den matematiske modellen er brukt til å simulere systemet med implementasjonen av kontrollsystemet. Simuleringene har vist gode resultater.

For å kunne teste kontrollsystemet i virkeligheten har et eksperimentoppsett blitt laget. Dette består av en nedskalert juletremodell, en bunnramme og en liten ROV. Oppsettet ble brukt for å teste kontrollsystemet i Trondheimsfjorden ombord på R/V Gunnerus. På grunn av en programmeringsfeil klarte man ikke under testingen å fullstendig verifisere de gode resultatene fra simuleringene. Resultatene viste seg imidlertid å være meget lovende når man tar denne feilen i betraktning, og konseptet kan derfor betraktes som verifisert.

Acknowledgements

During the work with this thesis I have received help and assistance from a number of people.

First I would like to thank my enthusiastic supervisor, Asgeir Sørensen. During the course of writing this thesis, he provided me with help and feedback on my progress, providing me with ideas for improvement and additions. At the same time, he did not restrict me in any way, and allowed me to approach the problems that I faced at my own pace.

FMC Technologies, and especially Brede Thorkildsen also deserves thanks. Brede has alway been available to answer questions and has provided me with confidence. I would also thank him for the possibility of working with solutions of the future, both in this thesis and in the summers I have spent at FMC Technologies in Kongsberg. I also thank FMC Tecnologies for providing the founds to make an experimental setup for real life testing.

I also want to thank Martin Ludvigsen for all his help in planning the testing in the Trondheim fjord, Oddvar Paulsen for helping me design the modules needed in the experimental setup, and for making sure time and manpower was allocated in the workshop for production of these. Fellow student Robert Kajanus also deserves a thanks for all the hours he spent setting up the HIL-simulator for the control system, and for his help with the thrust allocation.

The whole crew at R/V Gunnerus has my sincere gratitude for all the help they provided during the experimental testing. They were always positive even when we encountered problems, and without them the testing would not have been possible.

A special thanks is also given to Siri for always being there, and believing in me.

Table of Contents

List of Figures

List of Abbreviations

AUV Autonomus Underwater Vehicle

CW Clockwise

CCW Counter Clockwise

EKF Extended Kalman Filter

HIL Hardware In the Loop

OOP Object Oriented Programming

RMS Root Meas Squared

ROV Remotely Operated Vehicle

SSC Supervisory Switched Control

TMS Thether Management System

URV Underwater Robotic Vehicle

UUV Unmanned Underwater Vehicle

XT Xmas Tree

Chapter 1

Introduction

The objective of this thesis is to investigate mathematical models and control methods of an ROV interacting with subsea equipment during seabed installation. The goal of this work is to make a control algorithm for the ROV so it is able to govern the movement of a subsea tree during a wireline installation in order to align the tree to the wellhead connector. The algorithm should be able of doing this even if there is a varying current present. This thesis is a continuation of the work done in Henriksen [2013]. For completeness the relevant results from this work is included in this text.

This chapter is presenting the starting point for the thesis. It will present some background material as well as the motivation for the thesis. A brief presentation of underwater vehicles and subsea technology will be given. The installation of subsea Xmas trees is presented with focus on the placement on the seabed. This is the design application of the control system presented and designed in this thesis.

1.1 Underwater Vehicles

Underwater vehicles are common in deepwater industries. As the oil industry, and also other relevant industries, moves into deeper water, the use of subsea technology has increased. Due to safety and practical reasons it is not convenient to use manned diving for maintenance and surveys. The solution is to use underwater vehicles that are unoccupied, highly maneuverable and operated autonomously or from a vessel.

An Underwater vehicle is according to Fossen [2011] defined as follows in *Encyclopedia Britannica*:

"Underwater vehicle: "small vehicle that is capable of propelling itself beneath the water surface as well as on the water's surface. This includes unmanned underwater vehicle (UUV), remotely operated vehicle (ROV), autonomous underwater vehicles (AUV) and underwater robotic vehicles (URV). Underwater vehicles are used both commercially and by the navy".

This definition include both manned and unmanned vehicles. This thesis are however focusing on ROVs that are unmanned vehicles that are remotely controlled and powered using a tether. AUVs are also unmanned vehicles, but these have no connection with the surface during missions. They are controlled by preprogrammed autonomous algorithms and brings with them the energy needed to perform the mission.

Typical tasks for ROVs include missions such as sea bottom and pipeline surveys, cable maintenance as well as installation, maintenance and monitoring of subsea structures and equipment. ROVs are also used for ocean science, marine archeology and military applications such as neutralization of sea mines.

NTNU AUR-lab is a multi discipline laboratory that is used for research in technology, natural science and archeology. The laboratory operates the research vessel Gunnerus, two ROVs, and one AUV among other equipment. A picture of R/V Gunnerus can bee seen in figure 1.1.

Figure 1.1: R/V Gunnerus, courtesy of Fredrik Skoglund (NTNU)

The ROVs operated by NTNU AUR lab is one 400 kg observation class ROV with an installed manipulator, and one larger ROV that weighs 1850 kg. The smaller ROV is called Minerva, and the bigger one is called SF30k or Neptune. Both ROVs are made by Sperre AS, a Norwegian ROV company.

1.2 Subsea Petroleum Production

Subsea technology and subsea oil production is referring to the trend were more and more equipment used for producing oil or gas is placed on the seabed instead of on structures above or on the ocean surface. The reason we want to put the equipment on the seabed is basically to avoid the cost of building expensive platforms, or to be able to drill wells that is outside the effective drilling zone of an existing platform. The benefits of putting equipment on the seabed increases as the oil or gas fields are getting deeper. As the subsea technology matures, it also facilitates the development of deeper fields. The development of subsea processing, boosting and compression are increasing the oil recovery from existing reservoirs as well as making undeveloped reservoirs economically feasible to develop.

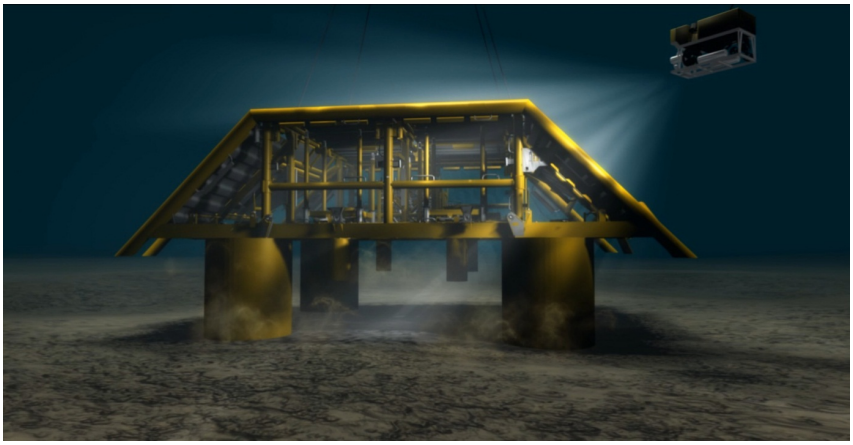

Figure 1.2: Template structure during installation, courtesy of FMC Technologies

A subsea production system often consists of several subsea trees tied together via flow-lines to a manifold. These components can be spread around the seabed in a so called satellite field, or they can be colocalized in a template structure. There are typically 4 or 6 wells that are drilled through one template, each with one subsea Xmas tree (XT) on top. The wells are drilled into different parts of the reservoir, in order to maximize the oil/gas recovery. This is possible due to directional drilling techniques that makes it possible to control the path of the drill-string, so one can drill into different parts of a reservoir starting from the

same place. A template structure can be seen in figure 1.3 and 1.2.

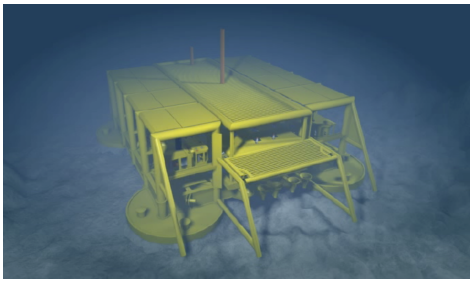

Complete template structure

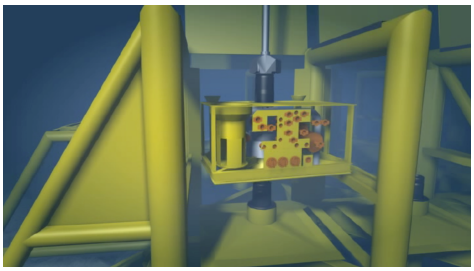

Xmas tree installed in template

Figure 1.3: A subsea template, courtesy of FMC Technologies

1.3 Xmas Tree Installation

A Xmas tree is basically a collection of valves that functions as the final barrier between the well and the environment. They are placed on top of the wellhead which is the top end of the well. There are both dry trees placed on a platform deck, and subsea trees placed on the seabed. The subsea trees on the seabed have valves that are remotely operated through an umbilical. These valves are most commonly actuated by hydraulic pressure. The valves are so called fail-safe. That means that if the communication is lost they will automatically close, leaving the system in a safe state.

When Xmas trees are installed they are placed on top of an oil or gas well. The well is essentially a pipe that goes into the ground. The wellhead is connected to the top of this pipe, and the Xmas tree are connected to the wellhead. In order to make a tight connection to the wellhead there are a set of seals that need to fit perfectly. In order to not damage these seals during the installation it is important that the Xmas tree is properly aligned when it is lowered down on to the wellhead. There are several ways to ensure that the Xmas tree is aligned when its weight is let down on the wellhead. The most usual is the use of guidelines. When using this method the long guidewires need to be fastened to the subsea structure at the seabed before the immersion of the Xmas tree can start. These wires will guide the Xmas tree into position. This can be seen in figure 1.4 and 1.5. If something happens and the Xmas tree is dropped during the lowering it is important that the Xmas tree do not hit the equipment already at the bottom. To avoid this the guidewires are not being tensioned before the Xmas tree is close to the depth it is going to be installed. This makes it possible that the guidewires get tangled up while the tree is lowered, especially is this a risk in deepwater fields.

Traditionally the Xmas tree is lowered down using the drill string of a drilling

rig or ship. The drill string is built up from a lot of smaller pipes that need to be connected while it is lowered down. This is a slow process. The drill string is connected to a unit called a running tool attached to the top of the XT. This is used to balance the Xmas tree so it is hanging straight. The running tool is connected to the surface through an umbilical supplying hydraulic and electrical power. This power is directed to the XT and is used to make a secure and sealed connection to the wellhead. It is also used to perform valve function testing, seal testing and control module testing after the XT is landed.

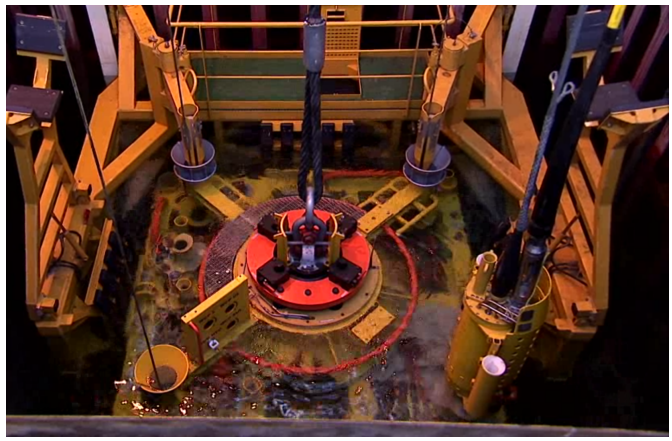

Figure 1.4: Xmas tree lowered down through moon-pool with guidelines, courtesy of FMC Technologies

Figure 1.5: Xmas tree with guidelines lowered down on template, courtesy of FMC Technologies

The traditional way of performing the XT installation requires a lot of time consuming procedures. In addition these procedures are performed by drilling rigs with high day rates. In order to save both time and money a new method for installing Xmas trees is emerging. This is called the *Three On Wire* (TOW) method.

When using the tree on wire method, the installation is done using an installation vessel, and the tree is lowered down to the seabed using one single wire and no guidewires, as seen in Figure 2.2. The wire is lowered using a winch, and is a lot faster than lowering a drill string. The wire however gives very little or no possibility for exact alignment, therefore an ROV is used. The ROV grabs the Xmas tree and rotates and pushes it into position, and the vessel may also be repositioned in order to move the tree.

Hull [2004] describes the use of the TOW method in the Gulf of Mexico in 2004. It was used to install a Xmas trees at approximately 350 m depth, using a construction vessel without a heave compensated crane. This was however no problem as the wave height was about 60 cm (2 ft). During this installation a Xmas tree running tool was used to lock the connection and perform tests. It was stated that the installation was done between twice and four times as fast as a regular installation.

In 2008 Shell wanted to investigate the use of this method in the North Sea in order to install Xmas trees in the Ormen Lange field, located at about 850 m depth outside the city of Kristiansund (Yarrow [2009]). It is stated that the installation at this depth it takes about five to seven days using the traditional method, where most of the time is used lowering and rising the drill string. Due to harsh conditions the installation season in the North Sea is quite short, and it was necessary to save time in order to make all the planned installations in one season.

In the installations in the North Sea the installation window was specified with a maximum wave height of 5.8 m. This made the operation a lot more challenging than the operations performed in the Gulf of Mexico. Skandi Seven, a ship owned by Subsea 7 was given the task. The vessel is equipped with a heave compensated crane, and has two working class ROVs (Subsea 7 [2014]). As seen in Figure 2.2 the trees were lowered without a running tool, but a special tool-skid was mounted to one of the ROVs that supplied the Xmas tree with the power needed to perform the connection lock in, and barrier tests. In Yarrow [2009] it is estimated that this installation method caused savings of $ 4 million a tree.

1.4 Problem Formulation

During installation proper alignment of the XT is required. As mentioned earlier this is done by using an ROV, combined with moving the vessel in order to get the XT into the correct position. The control of the ROV is manual today and there is ample possibility for the ROV operator to misjudge the location of the X-mas

tree and in additon ocean currents may further influence position. Hence it is a rather unpredictable operation and several attempts may have to be made.

An automated control system installed in the ROV, that is designed to position the Xmas tree would most likely make this operation more predictable, effective and with lower risk for misplacing the tree.

To ensure that the Xmas tree does not hit the existing subsea structures if something should happen to the winch or wireline, the Xmas tree is lowered down some distance away from the structures. It is then moved into position by moving the ship. This is a very slow process because one need to avoid transient motions of the Xmas tree. This process could be made much faster using an ROV with an automated control system could control the motions of the Xmas tree.

An automated controller will use position measurements, whereas a human ROV pilot in many cases will use a video stream to get information about the position of the Xmas tree. This will probably make a difference in accuracy, favoring the measurements. However video verification is needed to make sure the Xmas tree is aligned before it is placed. An automated controller will also be capable of faster response to changes e.g. in the environment than a human pilot.

This thesis is going to investigate the methods for using an automated ROV to position a Xmas tree during installation using a wireline, and the feasibility for such a system. The ROV should be able of keeping the Xmas tree in position, rotating it as well as moving it some distance. The problem is illustrated in figure 1.6 and 1.7.

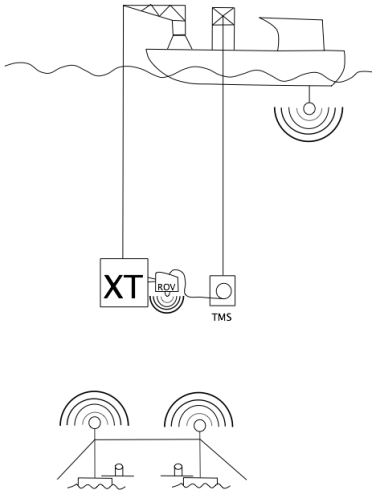

Figure 1.6: Installation set-up

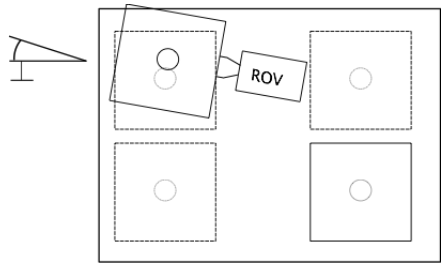

Figure 1.7: Positioning and alignment of the Xmas tree

In order to investigate methods and feasibility of the described system a model of an ROV and a Xmas tree hanging in a wire shall be developed, and the interaction

forces between these two shall be specified. Further a controller algorithm for the ROV should be proposed, and simulations shall be conducted in order to study the system. This will also show that the proposed solution is feasible.

To further study this installation experiments shall be done using an experimental setup including a downscaled Xmas tree model and ROV Minerva, a ROV owned and operated by NTNU.

1.5 Contributions

The contributions of this thesis are the following:

In **Chapter 2** a Xmas tree hanging in a wire is modelled. The model is then extended to include an ROV that is connected to the XT in order to position and orient this. The model is based on the model presented in Henriksen [2013], but in this thesis it is developed further and sensor models and a wave model is included. The is made to predict the behavior of a Xmas tree during a *Tree on Wire* installation.

In **Chapter 3** a control strategy for using a ROV for governing of XT movements in order to position it is proposed. This strategy is then implemented as a nonlinear PID-controller. In addition an Extended Kalman filter, and a reference model is implemented. Two different thrust allocation algorithms is discussed, and implemented.

In **Chapter 4** a series of simulations is done using the model developed in Chapter 2, and the controller from Chapter 3.

In **Chapter 5** the design of an experimental setup for testing the XT installation is presented. This experimental setup was used for experimental testing in the Trondheim Fjord May 2014. The results from the testing is presented.

In **Chapter 6** both the simulation results and the experimental results are discussed. The simulation results indicate that the control system is performing quite good, however due to an programming error this was not 100% verified during experimental testing. The experimental results do however seem promising.

1.6 Outline of Thesis

Chapter 2 is presenting the modelling of a Xmas tree, an ROV and a system where these are connected. In addition environmental loads and subsea vehicle measurements are discussed. A proposal for modelling these are also given.

Chapter 3 presents the design procedure for the control system. A hybrid system is proposed, and a controller, observer and reference model for controlling the

motions of the Xmas tree is presented.

Chapter 4 is presenting simulation result for simulations done both with a full scale model of the Xmas tree, and simulations done using an experimental scale model.

Chapter 5 is presenting both the experimental setup and results from the testing done in the Trondheim fjord May 2014.

Chapter 6 is discussing the results obtained through simulations and during experimental testing.

Chapter 7 is presenting the conclusions of this thesis, as well as some recomendations for further work.

Appendix A Is presenting the drawings of the Xmas tree that are the basis for the Xmas tree model.

Appendix B Lists the model parameters used in the simulations and in the experimental testing.

Appendix C Is containing the operation manual that was made before the experimental testing.

Appendix D Is containing additional plots that was not included in the main text.

Appendix E Is the results from a HIL-simulation where the error that was made in the control system during testing is simulated.

Appendix F Is a digital appendix containing the simulation models and the control system that are made in this thesis.

Chapter 2

Modelling

2.1 Preliminaries

This section will present a preliminary background for the modeling that is presented in the later sections. The focus in the modeling procedure is to make mathematical models that should be implemented for computer simulation. In this context a vectorial representation of the models has been chosen. The models are made with 6- degrees of freedom (DOFs).

2.1.1 Kinematics

Kinematics can be described as the *geometry of motion*, and is the part of classical mechanics that describes the motions of objects without consideration of the causes of this motion. In the following sections kinematic relations are used to define the relations between motions in different reference frames. This is later used as a tool to express the mathematical models on a simple form called Fossen's Robot-Like Vectorial Model for Marine Craft from Fossen [1991].

Reference frames

In order to express the position, orientation, velocities and accelerations of the ROV we need some reference frames to relate these parameters to for them be meaningful. In the following model the Earth-fixed reference frame (**NED**) is used to express the vessel's position and orientation, while the linear and angular velocities and accelerations are expressed in the body fixed reference frame (**BODY**).

NED: The *North-East-Down* reference frame is a coordinate system, $\{\mathrm{n}\} = (x_n, y_n, x_n)$ with its origin, o_n defined relative to the Earth reference ellipsoid. It is usually defined as the tangent plane on the surface of the Earth moving with the craft, but with x-axis pointing towards true *North*, y-axis pointing towards *East* and the z-axis pointing *downwards* normal to the earth surface. If we are operating in a local area where the latitude and longitude are approximately constant we can assume that the reference frame {n} is inertial. Under this assumption Newtons laws is still applicable.

BODY: The body fixed reference frame $\{\mathrm{b}\} = (x_b, y_b, z_b)$ with origin o_b is a moving frame that is fixed to the craft. The origin, o_b is for surface ships usually chosen to coincide with a point midships on the the waterline, but for our case we choose the origin to coincide with the centre of gravity (CG). The axis in the BODY-frame are chosen to coincide with the *principal axes of inertia*, and they are usually defined as:

x_b - longitudinal axis (directed from aft to fore)

y_b - transversal axis (directed towards starboard)

z_b - normal axis (directed from top to bottom)

Fossen [2011]

The vessels position, velocities and forces are expressed using the SNAME (the Society of Naval Architects and Marine Engineers) notation from 1950. This notation can be found in Table 2.1.

The velocity vector $\boldsymbol{\nu} = [\boldsymbol{p}^n_{b/n}, \boldsymbol{\Theta}_{nb}]^T = [u, v, w, p, q, r]^T$ is given in the BODY-frame, and the position vector $\boldsymbol{\eta} = [\boldsymbol{v}^b_{b/n}, \hat{\mathrm{A}}\dot{\mathrm{t}}\boldsymbol{w}^b_{b/n}]^T = [x, y, z, \phi, \theta, \psi]$ is given in the NED-frame. The kinematic relationship between the vectors is expressed by:

$$\dot{\boldsymbol{\eta}} = \boldsymbol{J}_{\boldsymbol{\Theta}}(\boldsymbol{\eta})\boldsymbol{\nu} \tag{2.1}$$

where

$$\boldsymbol{J}_{\boldsymbol{\Theta}}(\boldsymbol{\eta}) = \begin{bmatrix} \boldsymbol{R}^{\boldsymbol{n}}_{\boldsymbol{b}}(\boldsymbol{\Theta}_{\boldsymbol{nb}}) & \mathbf{0}_{3x3} \\ \mathbf{0}_{3x3} & \boldsymbol{T}_{\boldsymbol{\Theta}}(\boldsymbol{\Theta}_{\boldsymbol{nb}}) \end{bmatrix} \tag{2.2}$$

The rotation matrix for the linear velocity $\boldsymbol{R}^{\boldsymbol{n}}_{\boldsymbol{b}}(\boldsymbol{\Theta}_{\boldsymbol{nb}})$, and the rotation matrix for the angular velocities $\boldsymbol{T}_{\boldsymbol{\Theta}}(\boldsymbol{\Theta}_{\boldsymbol{nb}})$ are given by:

$$\boldsymbol{R}^{\boldsymbol{n}}_{\boldsymbol{b}}(\boldsymbol{\Theta}_{\boldsymbol{nb}}) = \begin{bmatrix} c\psi c\theta & -s\psi c\phi + c\psi s\theta s\phi & s\psi s\phi + c\psi c\theta \\ s\psi c\theta & c\psi c\theta + s\phi s\theta s\psi & -c\psi s\theta + s\theta s\psi c\phi \\ -s\theta & c\theta s\phi & c\theta c\phi \end{bmatrix} \tag{2.3}$$

$$\boldsymbol{T}_{\boldsymbol{\Theta}}(\boldsymbol{\Theta}_{\boldsymbol{nb}}) = \begin{bmatrix} 1 & s\phi t\theta & c\phi t\theta \\ 0 & c\phi & -s\phi \\ 0 & \frac{s\phi}{c\theta} & \frac{c\phi}{c\theta} \end{bmatrix} \tag{2.4}$$

where $c(\cdot) = cos(\cdot), s(\cdot) = sin(\cdot)$ and $t(\cdot) = tan(\cdot)$.

Table 2.1: The notation of SNAME (1950) for marine vessels

DOF	Description	Forces and moments	Velocities	Positions and euler angles
1	motions in the x-direction (surge)	X	u	x
2	motions in the y-direction (sway)	Y	v	y
3	motions in the z direction (heave)	Z	w	z
4	rotations about the x-axis (roll)	K	p	ϕ
5	rotations about the y-axis (pitch)	M	q	θ
6	rotations about the z-axis (yaw)	N	r	ψ

2.1.2 Kinetics

The marine craft will experience a set of forces and moments that will cause movement of the craft. These forces can be divided into rigid-body forces, hydrodynamic forces and hydrostatic forces. The ROV is assumed deeply submerged and it will therefore not be subject to wave or wind forces. It will however experience umbilical forces as well as interaction forces with the subsea tree.

Rigid-Body Kinetics

The rigid-body kinetics can be expressed in a vectorial setting, according to Fossen [1991] as:

$$\boldsymbol{M}_{RB}\dot{\boldsymbol{\nu}} + \boldsymbol{C}_{RB}(\boldsymbol{\nu})\boldsymbol{\nu} = \boldsymbol{\tau}_{RB} \tag{2.5}$$

Where $\boldsymbol{M}_{RB}$ is the rigid-body mass matrix, $\boldsymbol{C}_{RB}$ is the rigid-body Coriolis and centripetal matrix due to the rotation of the BODY-coordinates about the inertial frame NED, $\boldsymbol{\nu} = [u, v, w, p, q, r]^T$ is the generalized velocity vector expressed in BODY-coordinates and $\boldsymbol{\tau}_{RB}$ is a generalized vector of the external forces and moments expressed in BODY-coordinates. The matrices $\boldsymbol{M}_{RB}$ and $\boldsymbol{C}_{RB}(\boldsymbol{\nu})$ can be expressed by the following equations:

$$\boldsymbol{M}_{RB} = \begin{bmatrix} m\boldsymbol{I}_{3x3} & -m\boldsymbol{S}(\boldsymbol{r}_g^b) \\ m\boldsymbol{S}(\boldsymbol{r}_g^b) & \boldsymbol{I}_b \end{bmatrix} \tag{2.6}$$

$$\boldsymbol{C}_{RB}(\boldsymbol{\nu}) = \begin{bmatrix} \boldsymbol{0}_{3x3} & -m\boldsymbol{S}(\boldsymbol{\nu}_1) - m\boldsymbol{S}(\boldsymbol{\nu_2})\boldsymbol{S}(\boldsymbol{r}_g^b) \\ -m\boldsymbol{S}(\boldsymbol{\nu}_1) + m\boldsymbol{S}(\boldsymbol{r}_g^b)\boldsymbol{S}(\boldsymbol{\nu_2}) & -\boldsymbol{S}(\boldsymbol{I}_b\boldsymbol{\nu}_2) \end{bmatrix} \tag{2.7}$$

Where $\boldsymbol{I_{3x3}}$ is the identity matrix, $\boldsymbol{I}_b = \boldsymbol{I}_b^T = \boldsymbol{I_g} - m\boldsymbol{S}^2(r_b^g)$ is the inertia matrix about the origin of the BODY-coordinate system, $\boldsymbol{I}_g$ is the inertia matrix about the centre of gravity. $\boldsymbol{S}$ is the skew-symmetric cross-product operator defined in definition 2.2 in Fossen [2011], $\boldsymbol{\nu_1} := \boldsymbol{v_{b/n}^b} = [u, v, w]T, \boldsymbol{\nu_2} := \boldsymbol{\omega_{b/n}^b} = [p, q, r]T$ and

$\boldsymbol{r_g^b}$ is the vector form of o_b to the centre of gravity. If the origin of the BODY-coordinates is chosen to coincide with the centre of gravity $\boldsymbol{r}_g^b = [0, 0, 0]$ and the mass matrix, $\boldsymbol{M}_R B$ are reduced to:

$$\boldsymbol{M}_{RB} = \begin{bmatrix} m\boldsymbol{I}_{3x3} & \boldsymbol{0}_{3x3} \\ \boldsymbol{0}_{3x3} & \boldsymbol{I}_g \end{bmatrix} \tag{2.8}$$

Hydrostatic Forces and Moments

The hydrostatic forces and moments working on the submerged objects based on Archimedes' laws of fluid statics. This include the gravitational and buoyancy forces. These forces are in hydrostatic terminology called restoring forces and moments, and are equivalent to the spring forces in a mass-damper-spring system. These forces and moments can be expressed in 6 DOF by the vector:

$$\boldsymbol{g}(\boldsymbol{\eta}) = \begin{bmatrix} (W-B)s(\theta) \\ -(W-B)c(\theta)s(\phi) \\ -(W-B)c(\theta)c(\phi) \\ -(y_g W - y_b B)c(\theta)c(\phi) + (z_g W - z_b B)c(\theta)s(\phi) \\ (z_g W - z_b B)s(\theta) + (x_g W - x_b B)c(\theta)c(\phi) \\ -(x_g W - x_b B)c(\theta)s(\phi) - (y_g W - y_b B)s(\theta) \end{bmatrix} \tag{2.9}$$

Here $W = mg$ denotes the weight of the body, and $B = \rho g \nabla$ denotes the boyancy of the body. The vector $\boldsymbol{r}_g^b = [x_g, y_g, z_g]^T$ is the center of gravity (CG) with respect to the origin of the BODY-coordinates (CO). The vector $\boldsymbol{r}_b^b = x_b, y_b, z_b$ denotes the centre of buoyancy (CB) with respect to CO.

Hydrodynamic Forces and Moments

Due to the inertia of the surrounding fluid the motion of a submerged body will introduce an added mass. There will also be a corresponding Coriolis and centripetal matrix. There will also be a damping term due to viscous effects like skin friction, vortex shedding lift/drag effects etc. This damping can be modeled as a linear and a nonlinear term. These hydrodynamic forces is dependent on the velocity relative to the surrounding fluid, and not to the absolute velocity of the body. The relative velocity is denoted as:

$$\boldsymbol{\nu}_r = \boldsymbol{\nu} - \boldsymbol{\nu}_c \tag{2.10}$$

where $\boldsymbol{\nu}_c$ is the current velocity. The hydrodynamic forces will then be:

$$\boldsymbol{\tau}_{hyd} = -\boldsymbol{M}_A \dot{\boldsymbol{\nu}}_r - \boldsymbol{C}_A(\boldsymbol{\nu}_r)\boldsymbol{\nu}_r - \boldsymbol{D}_L \boldsymbol{\nu}_r - \boldsymbol{D}_{NL}(\boldsymbol{\nu}_r)\boldsymbol{\nu}_r \tag{2.11}$$

2.1.3 Fossen's Robot-Like Vectorial Model for Marine Craft

If we collect all the derived terms in one equation we get:

$$\dot{\boldsymbol{\eta}} = \boldsymbol{J}_{\Theta}(\boldsymbol{\eta})\boldsymbol{\nu} \tag{2.12a}$$

$$\begin{aligned} \boldsymbol{M}_{RB}\dot{\boldsymbol{\nu}} + \boldsymbol{C}^*_{RB}(\boldsymbol{\nu})\boldsymbol{\nu} + \boldsymbol{M}_A\dot{\boldsymbol{\nu}}_r \\ +\boldsymbol{C}^*_A(\boldsymbol{\nu}_r)\boldsymbol{\nu}_r + \boldsymbol{D}_L\boldsymbol{\nu}_r + \boldsymbol{D}_{NL}(\boldsymbol{\nu}_r)\boldsymbol{\nu}_r + \boldsymbol{G}(\eta) = \boldsymbol{\tau} \end{aligned} \tag{2.12b}$$

This vectorial way of representing the equations of motion for the marine craft dates back to Fossen [1991]. The motions is represented both in the body-frame and the NED-frame. This vectorial model is well suited for computer implementation and control systems design [Fossen [2011]].

2.2 ROV model

In this section we are going to show how the mathematical model found in Equation 2.12 can be used to model an ROV. The ROVs used as a basis for this are NTNUs ROV sf 30k and Minerva. A short description of these ROVs are given in section 1.1. In this masters thesis two parametrizations of this ROV model are used, one modelling a large working class ROV, and one model of NTNUs ROV Minerva. The parameters for the Working Class ROV is based on the parameters derived in Berg [2012] for Sf 30k. The parameters that is used in the simulations in Chapter 4 can be found in Appendix B.

In Equation 2.12 it is pretty straight forward to put in the inertial-, damping- and coriolis-matrices of the ROV. This section is therefore only presenting the peculiarities of the ROV model and choices made during modelling.

In this model it is assumed that the ROV is deployed through a submersible tether management system (TMS). This is a system where the ROV is connected to a cage or similar while being submerged into the working depth. This cage then has a reel with umbilical that connects the ROV to the ship, via the TMS. The most important advantage of deploying the ROV this way is that the weight of the TMS will take up most of the cross-flow drag forces [Christ and Wernli [2007]]. This is especially important when working at large depths, and most working class ROVs are deployed this way. A schematic drawing of a TMS can be seen in figure 2.1. Due to the TMS it is assumed that the umbilical forces are small and can be neglected.

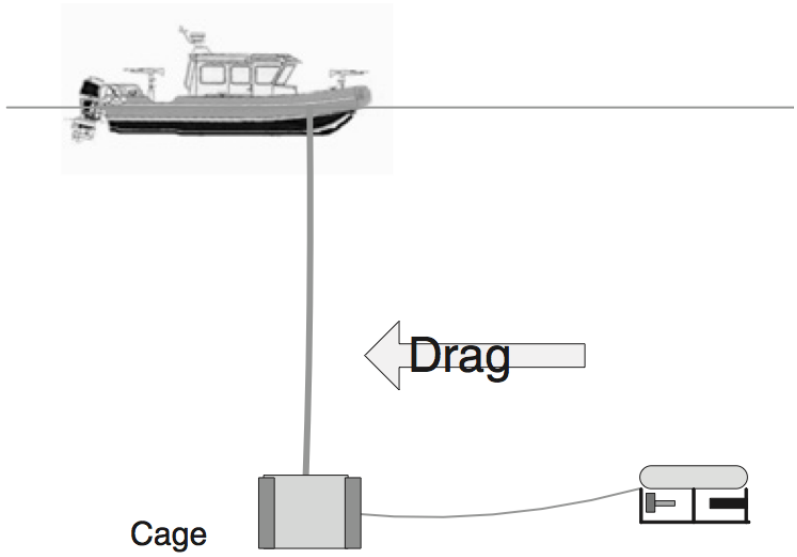

Figure 2.1: Schematic drawing of a TMS, courtesy to Christ and Wernli [2007]

2.2.1 Restoring Forces and Moments

The restoring forces and moments are calculated using equation 2.9. The input to this equation is the mass, and buoyancy of the ROV as well as the positions of the centers of gravity and buoyancy. ROVs are often made to have a slightly larger buoyancy than weight, so the net force is positive.

2.2.2 Control Forces

The control forces and moments are the ones we use to execute control over the vessel. They are generated by the rotation of the propellers in the thrusters. The rotational frequency of each thruster are set by the controller, it is however for the ROV SF30k limited to a maximum rotational frequency of 1500 rpm. We will then need to calculate the force vector made by the sum of all these thrusters.

The thrusters of the ROV is fixed, so direction of the thrust for each thruster is constant and known. By using this information we can set up a thruster configuration matrix, T that maps the force of each thruster into forces and moments acting on the ROV in 6 DOFs. Each column in the thrust allocation matrix corresponds to one thruster and is multiplied by a vector containing the forces each thruster

produce. The following equation gives the control forces in 6 DOFs:

$$\boldsymbol{\tau} = \boldsymbol{T}\boldsymbol{K}_T\boldsymbol{u} \tag{2.13}$$

where $u_i = n_i|n_i|$ is a vector containing the signed square of of the rotational speed of every thruster, and $\boldsymbol{K}_T$ is the thrust coefficients of the thrusters, mapping the rotational speed to a thrust force.

2.2.3 Working Class ROV

The Working class ROV is based on the model of SF30k that is presented in Berg [2012]. The initial plan was to use an unmodified model of this ROV, but during simulations it was found that this ROV did not have enough power to control a Full Scale Xmas tree properly. Other working class ROVs was therefore investigated in order to find out if the concept was feasible at all. In the product charts for Working Class ROVs from Forum [Forum Energy Technologies [2014]] and FMC Technologies [FMC Technologies [2014]] it was found that their ROVs had approximately ten times more thrust power than SF30k, even though the ROV had approximately the same dimensions. A decision was then made to use the model of SF30k, but increase its power output by ten times. This was done by multiplying the thrust coefficients by a factor of ten.

2.2.4 ROV Minerva

As we were going to use the ROV Minerva in the experimental testing it was natural to use an unmodified model of this ROV. The model used for Minerva is the same model that is derived in Kirkeby [2010].

2.2.5 Process and Control Plant Model

The process plant model is a model that is used for simulations of the system, while the control plant model is a simplified model used as a basis for model based controllers and for analytical stability analysis [Sørensen [2013a]].

By summing up the above derivations we get the following process plant model for the ROV:

$$\dot{\boldsymbol{\eta}} = \boldsymbol{J}_\Theta(\boldsymbol{\eta})\boldsymbol{\nu} \tag{2.14a}$$

$$\begin{aligned}\boldsymbol{M}_{RB}\dot{\boldsymbol{\nu}} + \boldsymbol{C}^*_{RB}(\boldsymbol{\nu})\boldsymbol{\nu} + \boldsymbol{M}_A\dot{\boldsymbol{\nu}}_r + \boldsymbol{C}^*_A(\boldsymbol{\nu}_r)\boldsymbol{\nu}_r + \\ \boldsymbol{D}_L\boldsymbol{\nu}_r + \boldsymbol{D}_{NL}(\boldsymbol{\nu}_r)\boldsymbol{\nu}_r + \boldsymbol{g}(\eta) + = \boldsymbol{\tau}_{control} + \boldsymbol{\tau}_{ext}\end{aligned} \tag{2.14b}$$

The control plant model will be defined in section 2.4.2 together with the complete system model.

2.3 Subsea Tree Model

In this section a 6 Degrees Of Freedom (DOF), process plant model of a subsea Xmas tree hanging in a wire between the sea surface and the sea floor will be developed. The subsea Xmas tree that is used as the basis of this modeling is an Enhanced Horizontal Xmas Tree (EHXT) made by FMC Technologies. The structure can be seen in figure 2.2 and appendix A, and its main dimensions and weight is found in table 2.2. As one can see in these figures the Xmas tree has a very complex geometry. This makes it difficult to predict its hydrodynamical properties accurately. In the mathematical model developed, the hydrodynamical properties of the structure has been estimated on the background of two masters thesis on the subject, as well as using analytical coefficients for simplified geometry. The model makes it possible to predict the behavior of a subsea Xmas tree during installation.

Figure 2.2: Photo of Xmas tree during installation, courtesy of FMC Technologies

The formulation of the model is done using Fossen's Robot-Like Vectorial Model for Marine Craft found in 2.12. The forces can be divided into rigid-body forces, hydrodynamical forces, hydrostatic forces, gravitational forces and external forces. The most important of the external forces for the Xmas tree are the wireline forces,

the current forces and forces applied by an ROV.

In these equations $\boldsymbol{\eta}$ represents the position vector in the North-East-Down reference frame (NED), while $\boldsymbol{\nu}$ is the velocity vector specified in the body-frame of the Xmas tree. Equation 2.12a expresses the kinematic relation between these reference frames, while 2.12b expresses the relation between forces and velocity in the body frame. In the equations $J_\Theta(\boldsymbol{\eta})$ is the rotation matrix between the body frame and the NED-frame. The $\boldsymbol{M}$ matrices denotes inertia, $\boldsymbol{C}$ Coriolis and centripetal forces, $\boldsymbol{D}$ denotes damping forces and $\boldsymbol{g}(\boldsymbol{\eta})$ is a vector containing the restoring forces. Subscript RB denotes a rigid body, while A stands for added mass, and denotes hydrodynamic inertia. L stands for linear while NL is nonlinear.

In the following sections the parameters in these equations will be derived. The origin of the body-frame coordinate system has been chosen to coincide with the centre of gravity of the Xmas tree.

Table 2.2: The main physical properties of an FMC Technologies EHXT

Property	**Value**
Length	3.600 m
Width	2.586 m
Height	2.808 m
Weight	36000 kg

2.3.1 Rigid-Body System Inertia Matrix

The mass of the Xmas tree is given in table 2.2. It is assumed that the mass center of the Xmas tree is in the geometric center of the Xmas tree block. From the drawings found in Kjemperud [2011], we see that the pipe on the top of the tree is placed in the center of the block. The Xmas trees are often made to be balanced about this pipe in order to make the installation easier, and to minimize loads in the fixing point at the wellhead.

To find estimates of the moments of inertia it is assumed that the mass is uniformly distributed about the centre of gravity. This assumption makes it possible to calculate the moments of inertia using the following formulas:

$$I_x = \frac{1}{12}m(h^2 + w^2) \tag{2.15a}$$

$$I_y = \frac{1}{12}m(h^2 + l^2) \tag{2.15b}$$

$$I_z = \frac{1}{12}m(l^2 + w^2) \tag{2.15c}$$

Where m is the mass, and l, w, h is the length, width and height respectively. These parameters are found in table 2.2. We assume that the coupled moments of

inertia, $I_{xy}, I_{yx}, I_{xz}, I_{zx}, I_{yz}$ and I_{zy} are small and can be neglected. The resulting rigid body system inertia matrix in the body frame will then be:

$$\boldsymbol{M}_{rb} = \begin{bmatrix} 36000 & 0 & 0 & 0 & 0 & 0 & \\ & 0 & 36000 & 0 & 0 & 0 & 0 \\ & 0 & 0 & 36000 & 0 & 0 & 0 \\ & 0 & 0 & 0 & 43717 & 0 & 0 \\ & 0 & 0 & 0 & 0 & 62535 & 0 \\ & 0 & 0 & 0 & 0 & 0 & 58942 \end{bmatrix} \tag{2.16}$$

2.3.2 Hydrodynamic System Inertia Matrix

The Xmas tree has a complex geometry which makes it difficult to calculate the hydrodynamical inertia for the structure. The problem was approached in Kjemperud [2011]. In his thesis Kjemperud used both experimental and numerical methods to estimate the added mass of the Xmas tree. The results obtained for the reference system (a square prism) in the thesis did however not match the theory. The results gave very high added mass for his models. In the experimental approach Kjemperud tested tree models, one prism, as well as two more complex models where cylinders was put between a top-plate and a bottom-plate. He named his models A,B and C where A is the prism and C is the model with most complexity. If we take a look at table 2.3 we see that the dimensionless added

Table 2.3: Added mass coefficients found by using data from Kjemperud [2011]

Model	**Added mass** m_a	**Displaced mass** $V\rho$	**Added mass coeficient** $Ca = \frac{m_a}{V_r \rho}$
A	79.04 kg	15.18 kg	5.20
B	35.43 kg	3.15 kg	11.11
C	41.42 kg	3.02 kg	13.73

mass coefficient increases as the complexity of the model increases. If we assume that the errors that made Kjemperud experimental results deviate from the theory were systematical errors, i.e they were the same during each run of the experiment. We can then assume that the added mass coefficient is higher for a complex object compared to a simpler object. This assumption seem to be according to theory, as a geometrically complex structure will make a larger disturbance in the water than a well defined smooth structure.

The results found in Kjemperud [2011] can not be used directly, but by using the assumption that the added mass coefficient increases with geometrical complexity of the hydrodynamical object together analytically found added mass coefficients found for simpler structures. The added mass coefficients found in DNV [2010] is used. The added mass in the linear directions are estimated by using the added mass coefficients for a square prism. For the shape of the Xmas tree block this

coefficient is found to be 0.68. In table 2.3 we see that the added mass coefficients of the more complex structures are roughly twice as big as the one for the prism, so we multiply the added mass coefficient by 2 in order to get our estimate of the added mass. Further we assume that 60% of the Xmas tree block volume is steel. This can be summed up by the following equations:

$$C_a = 2C_{a,prism} \tag{2.17}$$

$$V = 0.6C_b = 0.6 \cdot w \cdot l \cdot h \tag{2.18}$$

In order to estimate the added inertia in the rotational degrees of freedom we use a method proposed in Berg [2012] where we use the added mass for the enclosing shape of the structure, and then reduce these values by 20% due to rounded edges and flow through openings. The added inertia is found by using the equation:

$$A = \beta\rho\pi s^4 \tag{2.19}$$

Where β is a factor depending on the ratio between the length of the sides in the rotating plane, and s is the longest side in the same plane. By using these estimates the added mass matrix for the Xmas tree is:

$$\boldsymbol{M}_a = \begin{bmatrix} 21865 & 0 & 0 & 0 & 0 & 0 \\ 0 & 21865 & 0 & 0 & 0 & 0 \\ 0 & 0 & 21865 & 0 & 0 & 0 \\ 0 & 0 & 0 & 37477 & 0 & 0 \\ 0 & 0 & 0 & 0 & 101249 & 0 \\ 0 & 0 & 0 & 0 & 0 & 101249 \end{bmatrix} \tag{2.20}$$

These estimates of the added inertia in pitch and yaw was estimated with very high values. It is believed that this is due to a a wrong β-value in 2.19. The ratio between the sides here is approximately 1.4, and the β-value used is for a ratio of 1.0. The next β-value is for a ratio of 2.0. The β-value decreases with a higher ratio. The β-value for the added inertia in pitch and yaw is therefore reduced from 0.234 to 0.19. This value is in the middle of the 1:1 ratio and the 1:2 ratio. We then get the following matrix, which seems more reasonable:

$$\boldsymbol{M}_a = \begin{bmatrix} 21865 & 0 & 0 & 0 & 0 & 0 \\ 0 & 21865 & 0 & 0 & 0 & 0 \\ 0 & 0 & 21865 & 0 & 0 & 0 \\ 0 & 0 & 0 & 37477 & 0 & 0 \\ 0 & 0 & 0 & 0 & 82211 & 0 \\ 0 & 0 & 0 & 0 & 0 & 82211 \end{bmatrix} \tag{2.21}$$

It shall be noted that if the method described in Berg [2012] is used for the linear added mass the results will be similar to the ones from the method outlined here.

2.3.3 Restoring Forces

The term restoring forces is generally used to describe the hydrostatic forces acting on the marine craft, however for the model of the Xmas tree the main restoring

forces are the ones acting on the tree from the wireline, as well as the weight of the tree.
The restoring forces are calculated according to 2.9

It is assumed that both the center of gravity, and the center of buoyancy is placed in the geometrical centre of the tree. This implies that the restoring moments in the equation is zero. However it is assumed that the tree will act as a 3D pendulum suspended from the attachment point of the wireline. The wireline is attached in the top of the steel pipe of the Xmas tree by using a "running tool". We can then use an equation similar to 2.9 for calculating the set of restoring forces:

$$\boldsymbol{g(\eta)} = \begin{bmatrix} W_0 sin(\theta) \\ -W_0 cos(\theta) sin(\phi) \\ -W_0 cos(\theta) cos(\phi) \\ z_a W_0 cos(\theta) sin(\phi) \\ -z_a W_0 sin(\theta) \\ 0 \end{bmatrix} \tag{2.22}$$

Where W_0 is the submerged weight of the Xmas tree, and z_a is the vertical length between the centre of gravity/buoyancy and the attachment point for the wireline. This distance is found to be $l_p + \frac{h}{2} = 2.584m$ where l_p is the length of the top pipe, and h is the height of the Xmas tree without the pipe.

In addition to these restoring forces the Xmas tree will experience restoring forces in vertical direction and in the horizontal plane due to the wireline.

Vertical stiffness

A load hanging in a wireline will experience a restoring force from the wire that is due to the stiffness in the wire. According to Nielsen [2007] this force can be divided into two parts, namely elastic stiffness and geometric stiffness. The elastic stiffness is due to the material stiffness, or the Young's modulus of the wire. The geometrical stiffness is a result of the horizontal displacement of the cable due to current loading. When the position of the lower end of the line is changed, the geometry of the whole cable has to change. It is this change in geometry that leads to the geometrical part of the stiffness. The stiffness can be expressed by the

following set of equations:

$$\frac{1}{k_E} = \frac{L}{EA} \tag{2.23}$$

$$\begin{aligned}\frac{1}{k_G} =& -\frac{q^2}{w^3}\left[ln\left(\frac{\frac{W_0}{wL}}{\frac{W_0}{wL}+1}\right)+\frac{1}{2}\frac{2\frac{W_0}{wL}+3}{\left(\frac{W_0}{wL}+1\right)^2}\right] \\ &+\frac{q}{w^2}\frac{F_0}{W_0}\frac{1}{\left(\frac{W_0}{wL}+1\right)^2} \\ &+\frac{1}{w}\left(\frac{F_0}{W_0}\right)^2\frac{\frac{W_0}{wL}+\frac{1}{2}}{\left(\frac{W_0}{wL}+1\right)^2}\end{aligned} \tag{2.24}$$

$$k_{tot} = \left(\frac{1}{K_E}+\frac{1}{k_G}\right)^{-1} \tag{2.25}$$

These equations are derived in Nielsen [2007, ch. 5.3]. In this expression q is the drag force on the line per unit length and is calculated according to Morrison's equation found in Faltinsen [1990]:

$$q = \frac{1}{2}\rho d C_D |V_r| V_r \tag{2.26}$$

where d is the diameter of the wire, C_D is the drag coefficient and V_r is the current velocity. w is the weight of the cable per unit length, W_0 is the weight of the load hanging in the cable, i.e the Xmas tree. L is the length of the cable, and F_0 is the external forces acting on the Xmas tree in the horizontal direction. F_0 is calculated according to the following equation:

$$F_0 = D_l V_r + D_{nl}|V_r|V_r + \tau \tag{2.27}$$

Where τ is an external force applied on the Xmas tree e.g by an ROV. The restoring forces in the vertical direction can then be found by multiplying the spring coefficient, k_{tot} by the difference between the initial length of cable and the depth of the Xmas tree.

$$G_z = k_{tot} z_{rel} \tag{2.28}$$

where $z_{rel} = L - z_{Xmas}$. This relation is only valid for $z_{Xmas} > L$, because if $z_{Xmas} < L$ there will be slack in the wire and it will not apply any forces to the Xmas tree.

It is observed that the elastic stiffness dominates for the cases where the current speed is low and/or the cable length is short. However when the current speed increases the geometrical stiffness becomes more important. This can be seen in figure 2.3. This plot shows how the contributions from the elastic and geometrical stiffness changes with the current velocity with a wire length of 1200 m. We see that for current velocities around 0.3 m/s the geometrical stiffness starts affecting the total stiffness, and for velocities higher than 0.8 m/s it is the most important contribution to the total stiffness.

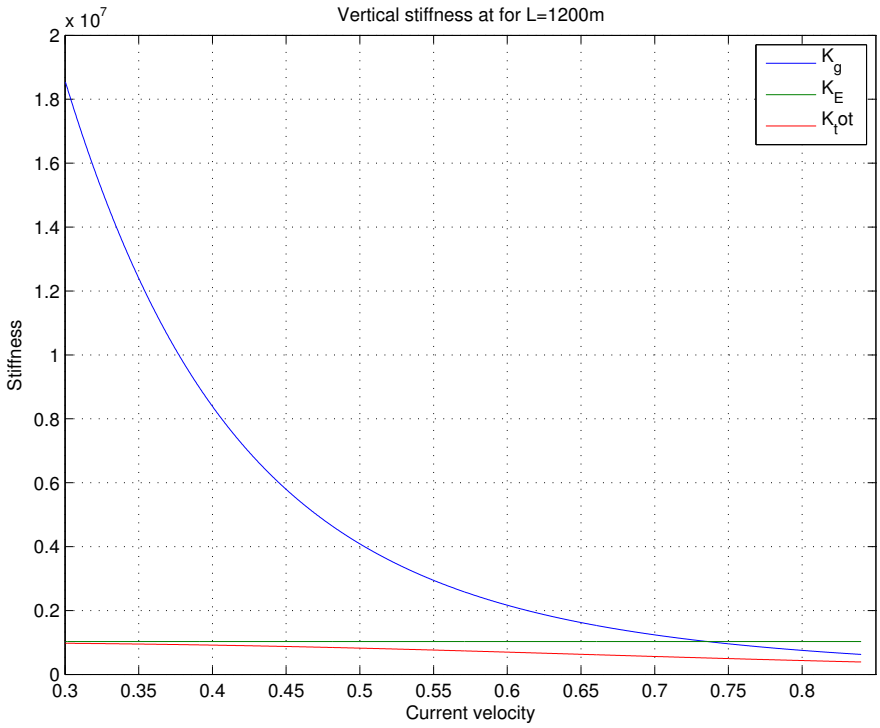

Figure 2.3: Stiffness contributions for different current velocities

Horizontal stiffness

In order to find the horizontal restoring forces on the Xmas tree due to hanging in wire, we differentiate the equation for the horizontal offset of a load hanging in a wire with respect to the external forces. The equation for the horizontal offset is derived in Nielsen [2007, ch. 5.3].

$$\frac{\eta_{wire}(-L)}{L} = \left(\frac{q}{w}\frac{W_0}{wL} - \frac{F_0}{wL}\right) ln\left[\frac{W_0}{W_0 + wL}\right] + \frac{q}{w}L \tag{2.29}$$

$$\frac{1}{k} = \frac{d\eta(-L)}{dF_0}$$

$$\frac{1}{k} = \frac{1}{w} ln\left[\frac{W_0}{W_0 + wL}\right] \tag{2.30}$$

We can see from this equation that the horizontal stiffness is not directly influenced by the cable drag, or the external forces acting on the Xmas tree. However the point where the horizontal restoring forces are zero, i.e the equilibrium point of the

spring forces are influenced by the drag forces acting on the wire. This equilibrium point can be found by using 2.29, setting $F_0 = 0$ and adding this to the position of the crane tip, i.e η_{crane}. The reason we set F_0 to zero is to not include the effect of the forces acting on the Xmas tree twice. The effect of these forces are taken care of by including the horizontal spring stiffness in the equations of motion for the xmas tree. The horizontal restoring forces can be found by the following equation:

$$G_{hor} = k\eta_{rel} \tag{2.31}$$

where $\eta_{rel,hor} = \eta_{Xmas} - (\eta_{wire,hor} + \eta_{crane})$. This is how the wire drag is accounted for in this model.

Total wire restoring forces

In order to fit these restoring forces into Fossen's Robot-Like Vectorial Model for Marine Craft we want to write the forces on the form:

$$\boldsymbol{G}_{wire} = \boldsymbol{K}\boldsymbol{\eta}_{rel} \tag{2.32}$$

This can be done by defining the stiffness matrix:

$$\boldsymbol{K}(U, L) = diag(k_x, k_y, k_z, 0, 0, 0) \tag{2.33}$$

and the vectors

$$\boldsymbol{\eta}_{ship} = \begin{bmatrix} x_{crane-tip} \\ y_{crane-tip} \\ L \\ 0 \\ 0 \\ 0 \end{bmatrix} \tag{2.34}$$

$$\boldsymbol{\eta}_{rel} = \boldsymbol{\eta}_{Xmas} - (\boldsymbol{\eta}_{ship} + \boldsymbol{\eta}_{wire}) \tag{2.35}$$

$$\boldsymbol{\eta}_{rel} = \boldsymbol{\eta}_{Xmas} - \begin{bmatrix} x_{crane-tip} + x_{wire} \\ y_{crane-tip} + y_{wire} \\ L \\ 0 \\ 0 \\ 0 \end{bmatrix} \tag{2.36}$$

The vertical and horizontal stiffness derived above are valid for static loads. In the case of dynamic loads the dynamic drag forces will act on the wire. The dynamic drag forces will restrict the change of geometry of the cable necessary to mobilize the geometric stiffness. As the drag forces increases, less of the geometrical changes will take place, and the effect of the geometrical stiffness will be reduced. However this model is made to model the installation of the Xmas tree, and the dynamics are assumed to be adequately slow in order for these equations to be valid.

2.3.4 Damping and Drag forces

The Xmas tree will experience damping forces due to hydrodynamic drag. It is also assumed that the wire will have a damping effect for the motions in the z-direction, this is supported by Vanderveldt et al. [1973]. According to 2.12 the damping terms is divided into linear damping ($\boldsymbol{D}_l\boldsymbol{\nu}$) and nonlinear damping ($\boldsymbol{D}_{nl}(\boldsymbol{\nu})\boldsymbol{\nu}$). Both in Mukha [2012] and Kjemperud [2011] the drag forces on the Xmas tree are investigated. In Mukha [2012] the results derived in Kjemperud [2011] are investigated more thoroughly by using CFD-analysis on the same model used for the experiments in Kjemperud [2011]. The results in Mukha [2012] are quite similar to the results in Kjemperud [2011] for the drag forces in the flow direction, the results however deviates quite a lot for the forces normal to the flow direction. It is likely that the model used in the theses have more forces acting normal to the flow direction than a real Xmas tree, this is because the model is less symmetrical than a real Xmas tree. Due to the uncertainty about the forces normal to the flow direction they are neglected in this model.

According to Kjemperud [2011] we can use Froude scaling to get the full-scale forces acting on the Xmas tree from this model test. The forces acting in the same direction of the flow from Mukha [2012] are scaled to full scale by using the following formulas found in Steen [2007].

$$U_{FS} = \sqrt{\lambda} U_M \tag{2.37}$$

$$F_{FS} = \frac{\rho_{FS}}{\rho_M} \lambda^3 F_M \tag{2.38}$$

We assume that the total drag forces can be written on the form:

$$F(U) = \frac{1}{2}\rho A D_{d,nl} U^2 + \frac{1}{2}\rho A D_{d,l} \tag{2.39}$$

And then use curve-fitting to find the drag coefficients. This gives us the drag coefficients:

$$D_{d,nl} = 0.6285 \tag{2.40a}$$

$$D_{d,l} = 0.1433 \tag{2.40b}$$

These coefficients represent the drag forces acting in the x-direction of the Xmas tree. This is the only direction that is considered in Mukha [2012]. Kjemperud [2011] also considers the forces acting in the y-direction. The experimental drag coefficients seems to be around 1.8 times larger in the y-direction than in the x-direction. This seems reasonable because the model used has a lot of open space for the water to flow through in the x-direction, while the y-direction has a flat plate blocking the flow. In order to find the drag in the y-direction the coefficients in 2.40 are multiplied by 1.8.

When comparing the real Xmas tree (figure 2.2 and appendix A) to the model

in Kjemperud we can see that the real Xmas tree has less open room for the water to flow through. The drag coefficients in 2.40 are therefore increased by a factor of 1.2 in order to find the drag-coefficients in x-direction.

The damping forces in the heave (z-direction) includes both hydrodynamical as well as damping from the wire. It is assumed that the damping in the wire is linear. The nonlinear damping in heave is then due to drag forces, and is assumed to have the same drag coefficient as in the y-direction. The linear damping is assumed to be 1% of the critical damping, using the spring stiffness of the cable at 400 m depth.

The rotational damping is assumed to be a nonlinear drag force. In Berg [2012] a rotational drag coefficient of 1.0 is suggested as a typical value for an ROV. The Xmas tree and an ROV has a lot of structural similarities, both having a a complex structure inside a rectangular frame. The rotational drag coefficients are therefore set to 1.0

This leads to the following damping matrices:

$$\boldsymbol{D}_l = \begin{bmatrix} 640 & 0 & 0 & 0 & 0 & 0 \\ 0 & 1336 & 0 & 0 & 0 & 0 \\ 0 & 0 & 5635 & 0 & 0 & 0 \\ 0 & 0 & 0 & 0 & 0 & 0 \\ 0 & 0 & 0 & 0 & 0 & 0 \\ 0 & 0 & 0 & 0 & 0 & 0 \end{bmatrix} \tag{2.41}$$

$$\boldsymbol{D}_{nl} = \begin{bmatrix} 2807 & 0 & 0 & 0 & 0 & 0 \\ 0 & 5861 & 0 & 0 & 0 & 0 \\ 0 & 0 & 5398 & 0 & 0 & 0 \\ 0 & 0 & 0 & 2575 & 0 & 0 \\ 0 & 0 & 0 & 0 & 6956 & 0 \\ 0 & 0 & 0 & 0 & 0 & 7554 \end{bmatrix} \tag{2.42}$$

In this analysis we disregard the off-diagonal elements of these matrices. This is due to lack of time and information about these. These terms should however be identified in order to refine this model.

2.3.5 The Experimental Scale Model

In order to test the control system using the ROVs owned by NTNU it is necessary to make a scaled experimental model of the Xmas tree. This was done in two steps, first by simply scaling the input parameters to full scale model by a scaling factor λ. The inputs factors used to calculate all model parameters of the Xmas tree is the height, width and length as well as the mass of the XT. These factors was

scaled according to the following equations:

$$H_{ms} = \lambda H_{fs} \tag{2.43a}$$
$$W_{ms} = \lambda W_{fs} \tag{2.43b}$$
$$L_{ms} = \lambda L_{fs} \tag{2.43c}$$
$$\boldsymbol{M}_{ms} = \lambda^3 M_{fs} \tag{2.43d}$$

In these equations the subscript ms stands for model scale, while fs stands for full scale. This model was used in the design phase of the experimental model in order to find the appropriate sizes. The finished design had a scaling factor of approximately $\frac{1}{3.5}$.

When the design of the experimental model was finished a new model was made. Now we knew the actual mass, volume and outer dimensions of the XT, so a more detailed simulation model could be made. The unknown hydrodynamical parameters was estimated using the same equations as for the full scale model.

2.3.6 Xmas Tree Process Plant Model

By summing up the above derivations we get the following process plant model for the Xmas tree:

$$\dot{\boldsymbol{\eta}} = \boldsymbol{J}_{\Theta}(\boldsymbol{\eta})\boldsymbol{\nu} \tag{2.44a}$$
$$\begin{aligned}\boldsymbol{M}_{RB}\dot{\boldsymbol{\nu}} + \boldsymbol{C}^*_{RB}(\boldsymbol{\nu})\boldsymbol{\nu} + \boldsymbol{M}_A\dot{\boldsymbol{\nu}}_r + \boldsymbol{C}^*_A(\boldsymbol{\nu}_r)\boldsymbol{\nu}_r + \\ \boldsymbol{D}_L\boldsymbol{\nu}_r + \boldsymbol{D}_{NL}(\boldsymbol{\nu}_r)\boldsymbol{\nu}_r + \boldsymbol{g}(\eta) + \boldsymbol{G}_{wire} = \boldsymbol{\tau}_{ext}\end{aligned} \tag{2.44b}$$

2.4 System Model

The system model is a model of how the connected system with the ROV and the behaves during the installation of a Xmas tree. Because the control objective is to position the Xmas tree, we specify the origin of the body-frame of the system model as the geometrical centre of the Xmas tree.

In the following the superscript denotes the reference frame where s is the system body-frame, r is the ROV body-frame and n is the NED-frame. The subscript relates the matrix to the object, where R is the ROV, and X is the Xmas tree. No subscript is used for the system matrices.

2.4.1 Interaction Forces

In order for the ROV to be able to control the position of the Xmas tree it will need to be physically connected. We assume that the ROV is able of making a physical

connection to the Xmas tree that will not change over time, meaning e.g that the grip will not slip. How this connection is done is not elaborated in this thesis. In the connection between the Xmas tree and the ROV a set of interaction forces will act. The force vectors acting on the two objects will be of the same magnitude, but have the opposite direction according to Newtons 3rd law of motion. This interaction force is modeled as a stiff spring with equilibrium point in the centre of the ROV, when no forces act between the objects. The physical interpretation of this spring is the structural stiffness in the connection arm.

The equilibrium centre of the ROV can then be specified with a vector from the origin, called $\boldsymbol{r}_R^s$. So the equilibrium position of the ROV in the NED-frame can be found by:

$$\boldsymbol{\eta}_{eq,R} = \boldsymbol{\eta} + \boldsymbol{J}(\boldsymbol{\eta})\boldsymbol{r}_R^s \tag{2.45}$$

Then the interaction force vector acting on the ROV, specified in the body-frame of the ROV will be:

$$\boldsymbol{\tau}_{i,R} = \boldsymbol{J}^{-1}(\boldsymbol{\eta}_R)(\boldsymbol{\eta}_{eq,R} - \boldsymbol{\eta}_R)K \tag{2.46}$$

Where K is the spring stiffness matrix. By using the system transformation matrix specified in [Fossen, 2011, ch. 7.5] we can find the interaction force on the Xmas tree in its own body frame:

$$\boldsymbol{\tau}_{i,X} = -\boldsymbol{H}^T(\boldsymbol{r}_R^b)\boldsymbol{J}(\boldsymbol{r}_R^b)\boldsymbol{\tau}_{i,R} \tag{2.47}$$

$\boldsymbol{J}(\boldsymbol{r}_R^b)$ is the rotation matrix from the ROV BODY frame into the XT BODY frame.

2.4.2 Control Plant Model

The control plant model is a simplified model that contains the most important aspect of the process plant model, and is used as a basis for model based controllers and for analytical stability analysis, such as Lyapunov stability (Sørensen [2013a]). The control plant model is defined in the *working space* of the vehicle, or system in our case. The working space is a reduced space in which the control objective is defined (Fossen [2011]). The working space of our system is the horizontal plane, considering surge, sway and yaw. The depth is controlled by the length of the wire. Both the Xmas tree and the ROV are stable in both pitch and roll, and we assume that the connected system is the same.

In order to simplify our system model, we collect the Rigid body terms and the hydrodynamical terms into common matrices. Further we assume that the connection between the two objects is rigid. These assumptions makes it possible to transform the equations of motion for the ROV, specified in its body frame, to the

system body frame using the transformation matrix [Fossen, 2011, ch. 7.5]:

$$\begin{aligned}
\boldsymbol{M}_R^s &= \boldsymbol{H}^T(\boldsymbol{r}_R^s)\boldsymbol{J}(\boldsymbol{r}_R^b)\boldsymbol{M}_R^r\boldsymbol{H}(\boldsymbol{r}_{\boldsymbol{R}}^{\boldsymbol{s}}) \\
\boldsymbol{C}_R^s(\boldsymbol{\nu}) &= \boldsymbol{H}^T(\boldsymbol{r}_R^s)\boldsymbol{J}(\boldsymbol{r}_R^b)\boldsymbol{C}_R^r(\boldsymbol{\nu})\boldsymbol{H}(\boldsymbol{r}_{\boldsymbol{R}}^{\boldsymbol{s}}) \\
\boldsymbol{D}_R^s(\boldsymbol{\nu}) &= \boldsymbol{H}^T(\boldsymbol{r}_R^s)\boldsymbol{J}(\boldsymbol{r}_R^b)\boldsymbol{D}_R^r(\boldsymbol{\nu})\boldsymbol{H}(\boldsymbol{r}_{\boldsymbol{R}}^{\boldsymbol{s}}) \\
\boldsymbol{g}_R^s &= \boldsymbol{H}^T(\boldsymbol{r}_R^s)\boldsymbol{J}(\boldsymbol{r}_R^b)\boldsymbol{g}_R^r \\
\boldsymbol{\tau}_{ctrl,R}^s &= \boldsymbol{H}^T(\boldsymbol{r}_R^s)\boldsymbol{J}(\boldsymbol{r}_R^b)\boldsymbol{\tau}_{ctrl,R}^r
\end{aligned}$$

where

$$\begin{aligned}
\boldsymbol{M}_R^r &= \boldsymbol{M}_{RB,R}^r + \boldsymbol{M}_{A,R}^r \\
\boldsymbol{C}_R^r(\boldsymbol{\nu}) &= \boldsymbol{C}_{RB,R}^r(\boldsymbol{\nu}) + \boldsymbol{C}_{A,R}^r(\boldsymbol{\nu}) \\
\boldsymbol{D}_R^r(\boldsymbol{\nu}) &= \boldsymbol{D}_{NL,R}^r(\boldsymbol{\nu}) + \boldsymbol{D}_{L,R}^r
\end{aligned}$$

Using this transformation we get the following control plant model for the system:

$$\dot{\boldsymbol{\eta}} = \boldsymbol{J}_\Theta(\boldsymbol{\eta})\boldsymbol{\nu} \tag{2.48a}$$

$$\dot{\boldsymbol{b}} = -\boldsymbol{T}_b^{-1}\boldsymbol{b} + \boldsymbol{E}_b\boldsymbol{w} \tag{2.48b}$$

$$\begin{aligned}
&\boldsymbol{M}\dot{\boldsymbol{\nu}} + \boldsymbol{C}(\boldsymbol{\nu})\boldsymbol{\nu} \\
&+\boldsymbol{D}(\boldsymbol{\nu})\boldsymbol{\nu}_r + \boldsymbol{G}_{wire}(\eta) = \boldsymbol{\tau}_{ctrl} + \boldsymbol{J}^{-1}(\boldsymbol{\eta})\boldsymbol{b}
\end{aligned} \tag{2.48c}$$

where

$$\begin{aligned}
\boldsymbol{M} &= \boldsymbol{M}_{RB,X}^s + \boldsymbol{M}_{A,X}^s + \boldsymbol{M}_R^s \\
\boldsymbol{C} &= \boldsymbol{C}_{RB,X}^s(\boldsymbol{\nu}) + \boldsymbol{C}_{A,X}^s(\boldsymbol{\nu}) + \boldsymbol{C}_R^s(\boldsymbol{\nu}) \\
\boldsymbol{D} &= \boldsymbol{D}_{NL,X}^s(\boldsymbol{\nu}) + \boldsymbol{D}_{L,X}^s + \boldsymbol{D}_R^s(\boldsymbol{\nu})
\end{aligned}$$

The bias vector $\boldsymbol{b}$ accounts for currents and modeling errors. The bias modeled as a first order Markov process with $\boldsymbol{T}_b$ as a diagonal matrix of time constants, a scaling matrix $\boldsymbol{E}_b$ and a zero mean gaussian noise vector $\boldsymbol{w}$. The bias vector is specified in the NED-frame, as its main purpose is to model the current. It will therefore be rotated into the system frame.

2.5 Environmental Loads

The models and simulations in the scope of this thesis are considered to be deeply submerged. This means that they are below the wave zone, and will not experience any wind forces. This means that the only environmental load experienced by the system is a current load. The current loads will vary both with time and place. This section will investigate the main components that cause currents. Then a model of the current will be presented.

According to Encyclopedia Britannica Online [2013a] an ocean current is *a stream made up of horizontal and vertical components of the circulation system of ocean waters that is produced by gravity, wind friction and water density variation in different parts of the ocean.* The general circulation of water in the ocean follows a specific pattern, much like in the atmosphere. This pattern can be seen in figure 2.4. This general circulation pattern is defined by the average movement of seawater in the ocean. Superimposed of this pattern there are oscillations of tides and waves. The wave motion is regarded a high frequency motion, and will not be further discussed in this thesis.

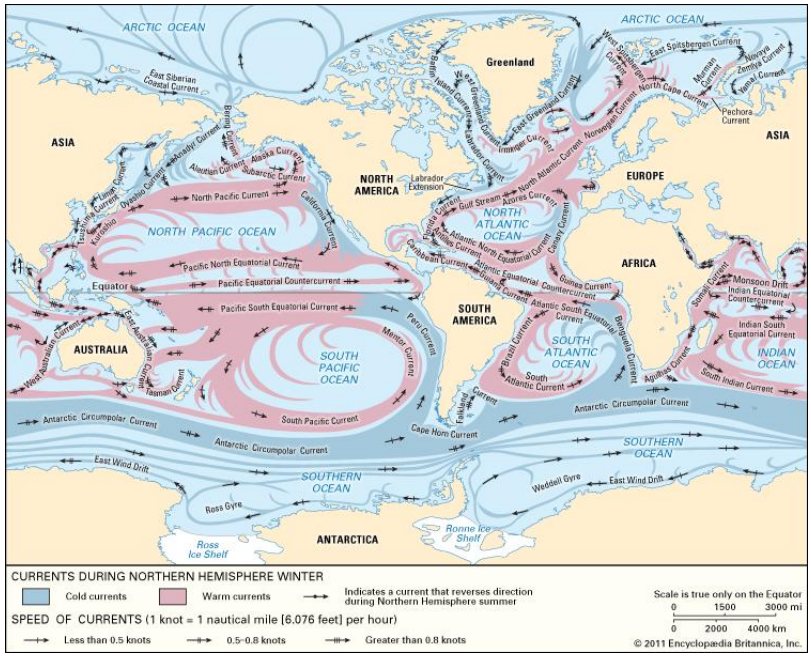

Figure 2.4: Ocean Current circulation system, courtesy of Encyclopedia Britannica

The main ocean circulation system derives its energy from two sources that define two circulation types. This is the wind-driven circulation and the thermohaline circulation, which is driven by horizontal differences in water density mainly due to temperature and salinity differences. In addition the Coriolis effect deflects the movements causing the circular patterns seen in figure 2.4. The wind-driven circulation is strongest in the surface layer, and is by Faltinsen [1990] modeled with a linearly decreasing speed down to a certain depth. The layer where the wind current is acting is called the Ekman layer. This layer extends to a depth of about 100 m, according to Encyclopedia Britannica Online [2013a]. The surface current speed generated by the wind can be set to 2 % of the wind speed (Faltinsen [1990]).

The thermohaline circulation system is a much more sluggish system, with a typical water velocity of 1 cm/s (Encyclopedia Britannica Online [2013a]). Unlike the wind driven system it reaches the whole way down to the seafloor, and is often refereed to s the deep or abyssal ocean circulation. The main water transport due to the thermohaline circulation system can be seen in figure 2.5.

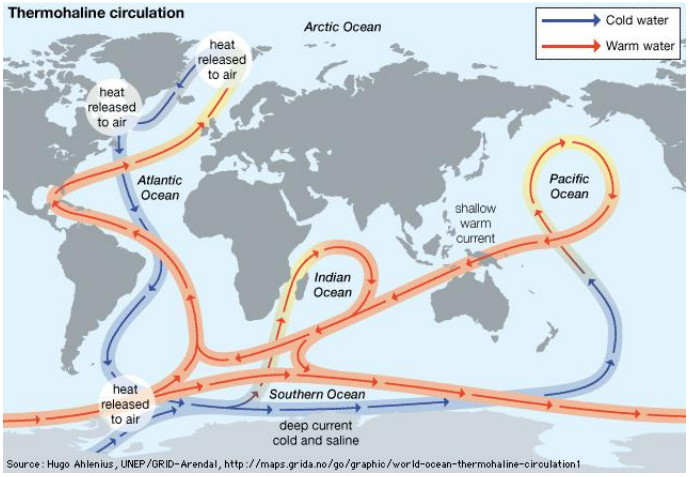

Figure 2.5: The thermohaline circulation system, courtesy of Encyclopedia Britannica

The tide motion is a motion that is cased by the gravitational forces exerted on the earth by astronomical bodies. The largest effects observed on the earth is due to the moon and the sun. The tide currents has an average period of 12 hours and 25 minutes according to Encyclopedia Britannica Online [2013b]. When the tidal motions run into shallow water the energy accumulates and the rise and fall is accumulated. Because of this the strength of the tidal currents depends of the depth and shape of the sea bottom, called the bathymetry as well as the shape of the coastline. This also means that areas situated a long distance from the coastline or with a flat sea bottom the tidal currents are small. Because of this the strength of the tidal currents are difficult to predict. They range from zero to over 10 m/s in Saltstraumen, the worlds strongest tidal current situated near the city Bodø.

2.5.1 Current Model

The current model is going to represent environmental loads that is likely to occur on both the ROV and the Xmas tree during the installation process. In section 2.3.3 we see that the local horizontal dynamics of the Xmas tree due to the wireline is unaffected by the drag forces along the line. It is also assumed that the ROV

is deployed with a TMS system that will eliminate most of the cable drag forces acting on the ROV. It is therefore considered most important to derive a model for how the currents act at the depth of the ROV and Xmas tree and not so important to find a design current profile for the whole water column. We do also assume that the vertical current velocity can be neglected since the operations are performed near the seafloor.

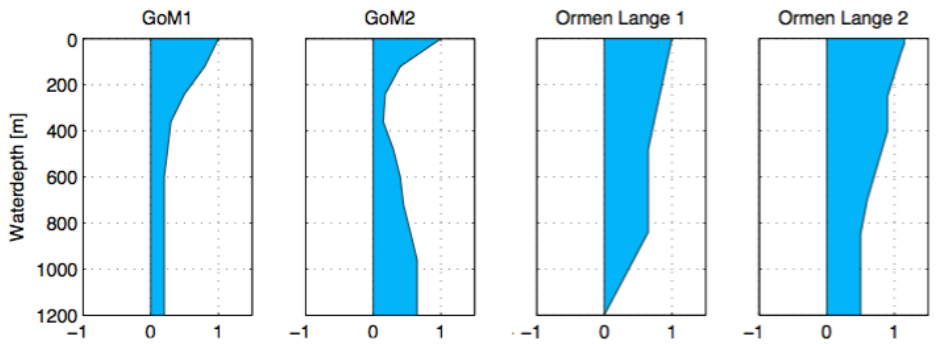

Figure 2.6: Current profiles for the gulf of Mexico and the Ormen Lange field, courtesy of Rustad [2007]

In Rustad [2007] we find design current profiles for the Ormen Lange Field and for the Gulf of Mexico. These profiles can be seen in figure 2.6. These are current profiles with one year return period. This means that the current velocities seen in these probably are higher than what one can expect during installation. Using this as a background we can conclude that the highest probable current speed experienced near the seabed during installation is 0.5 m/s. During the simulation different current speeds will be used in order to test the performance of the system.

The current will probably have some variations, both in direction and speed. To account for this the current velocity and directions is modeled as a limited random walk process according to the following equations:

$$\dot{V}_c = w_1, \quad V_{c,min} < V_c(t) < V_{c,max} \tag{2.49}$$

$$\dot{\beta}_c = w_2, \quad \beta_{c,min} < \beta_c(t) < \beta_{c,max} \tag{2.50}$$

where w_1 and w_2 is Gaussian white noise. Using this equations the current will follow the following equation in the NED-frame:

$$\begin{aligned} \nu_c, NED &= \begin{bmatrix} u_c & v_c & 0 & 0 & 0 & 0 \end{bmatrix}^T \\ &= \begin{bmatrix} V_c(t) \cdot cos(\beta_c(t)) & V_c(t) \cdot sin(\beta_c(t)) & 0 & 0 & 0 & 0 \end{bmatrix} \end{aligned} \tag{2.51}$$

This velocity needs to be rotated into the body frame of the system before its is used to calculate forces.

2.5.2 Wave Model

Subsea Xmas trees are sometimes installed on smaller depths where one may experience wave induced motions. In order to study the effect the control system has on these motions a wave model has to be implemented. According to Faltinsen [1990] and Fossen [2011] we can model the wave forces using a wave spectrum ($S(\omega)$). From the wave spectrum we get the following relation for the wave amplitude of wave component k:

$$\frac{1}{2}A_k^2 = S(\omega)\Delta\omega \tag{2.52}$$

When we have the amplitude of the wave component it is possible to find its speed in the horizontal direction by using the relation:

$$u_k = \omega A_k e^{kz} sin(\omega_k + \epsilon_k) \tag{2.53}$$

We can then sum all wave components to find the total horizontal speed:

$$u = \sum_{k=1}^{n} u_k \tag{2.54}$$

We can then find the wave current speed in the NED frame by using the following relation where β is the angle between the NED frame and the wave direction:

$$u_{NED} = ucos(\beta) \tag{2.55}$$
$$v_{NED} = usin(\beta) \tag{2.56}$$
$$\tag{2.57}$$

The ITTC wave spectra is used for the simulations with waves.

2.6 Measurements

The control system need input from sensors in order to know where the Xmas tree is, and how far away it is from its desired position in order to do feedback control. The ROV does typically have some sensors for sensing position, heading, depth, and speed. The problem with sensor-measurements is that they often are noisy and they may be biased, in addition one may have more than one sensor measuring the same thing. In order to get useful information it is common practice to use signal processing together with a state estimator to get more precise and trustworthy information from sensors. A typical information flow set-up can be seen in figure 2.7, this is the set-up for NTNUs ROV Minerva. In this section we are studying how measurements are typically made, and treated in a control system. In the last subsection of this chapter a simulation for measurements is presented.

2.6.1 Hydro-acoustic Positioning System

In subsea applications the most common way to get position measurements is to use a hydro-acoustic positioning system. A hydro-acoustic positioning is based upon the basic triangulation principles, and works by measuring the time it takes for a sound to propagate to a specific place and back. This is then used to calculate the position (Christ and Wernli [2007]). There are two dominating methods for calculating the position of Submersibles, namely Ultra Short Base Line (USBL) or Long Base Line (LBL) systems (Ludvigsen [2010]).

The USBL system uses two main devices to measure the position of the ROV. This is an *interrogator* and a *transponder*. The interrogators is a combined transmitter receiver device that sends out an interrogation signal on one frequency and receives a reply on a second frequency. This device is typically mounted on the ship, while the transponder is monted on the ROV. The transponder device is also a combined transmitter receiver device, but the transponder sends out the transponder signal on receipt of an interrogation signal from the interrogator (Christ and Wernli [2007]). See figure 2.8 for the system set up. The distance between the ROV and the interrogator, often called the range are calculated by measuring the time of flight for the signal, and the bearing angle of the returning signal is calculated from phase measurements on the interrogator element . This is then used to calculate the position of the ROV. The accuracy of such system is typically between 0.4 m and 0.1 m in range and 3.0° and 0.12° in bearing . The HiPAP USBL positioning system installed on NTNUs research vessel Gunnerus has a propagated accuracy in position measurement of 0.85 m when the ROV is at 200 m depth. When depth increases this method becomes more inaccurate, and the update frequency of the measurements goes down. However this system is much more flexible than the LBL system (Ludvigsen [2010]).

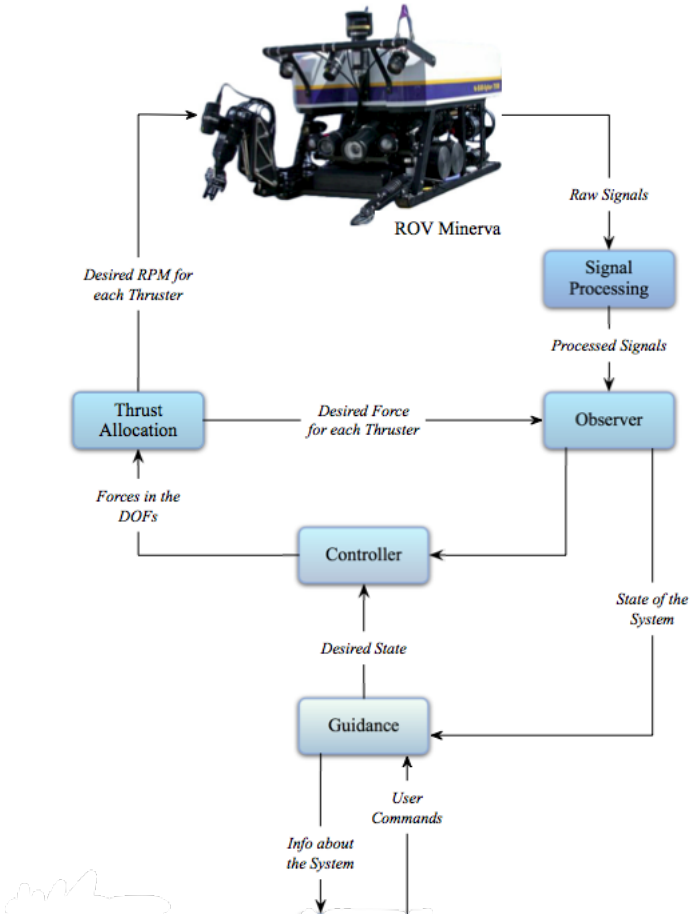

Figure 2.7: Information flow in the control system of ROV Minerva, from Candeloro [2011]

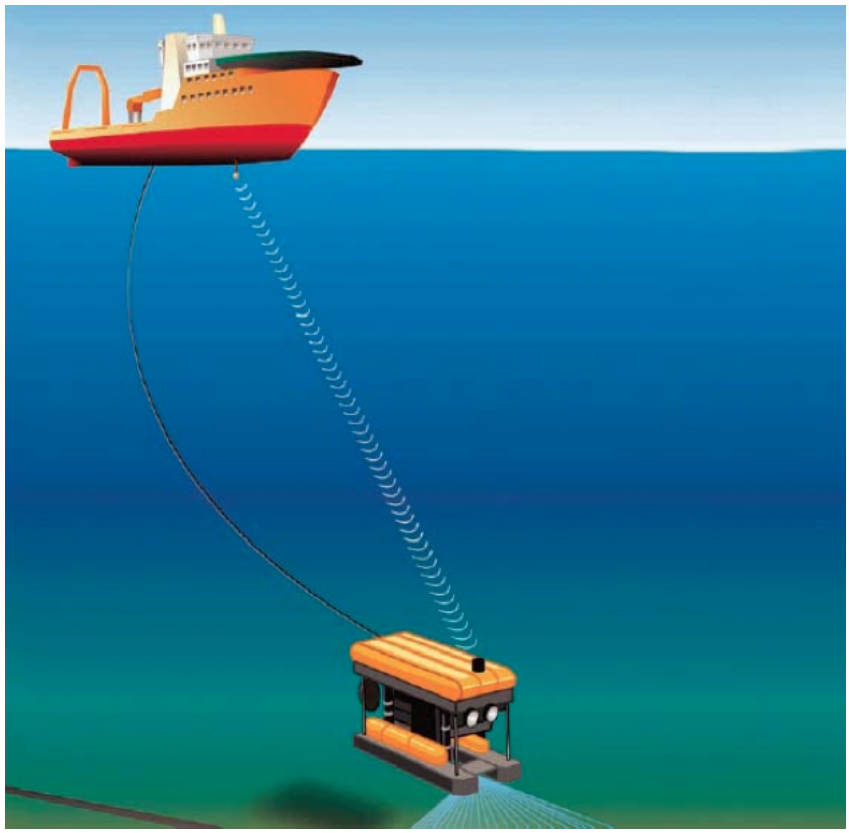

Figure 2.8: Ultra Short Baseline acoustic positioning system, courtesy of Kongsberg Maritime

A LBL system consist of one or more interrogators, and a set of either transponders or *pingers*. A pinger is a device that continuously sends out an acoustic pulse on a particular frequency (Christ and Wernli [2007]). In this system the interrogator is typically mounted at the ROV, and the interrogator then uses either the response from the transponders, or the signals from the pingers to calculate the distance to each device. The devices are typically mounted on the seafloor, and the position of these are known. The vessel with the interrogator then use triangulation to calculate its position. The accuracy of the LBL system is often much better than for a USBL system, and the accuracy is not dependent of the depth. The system is however less flexible because the transponders or pingers need to be positioned at the seabed before it starts to work (Ludvigsen [2010]). See figure 2.9 for the system set up.

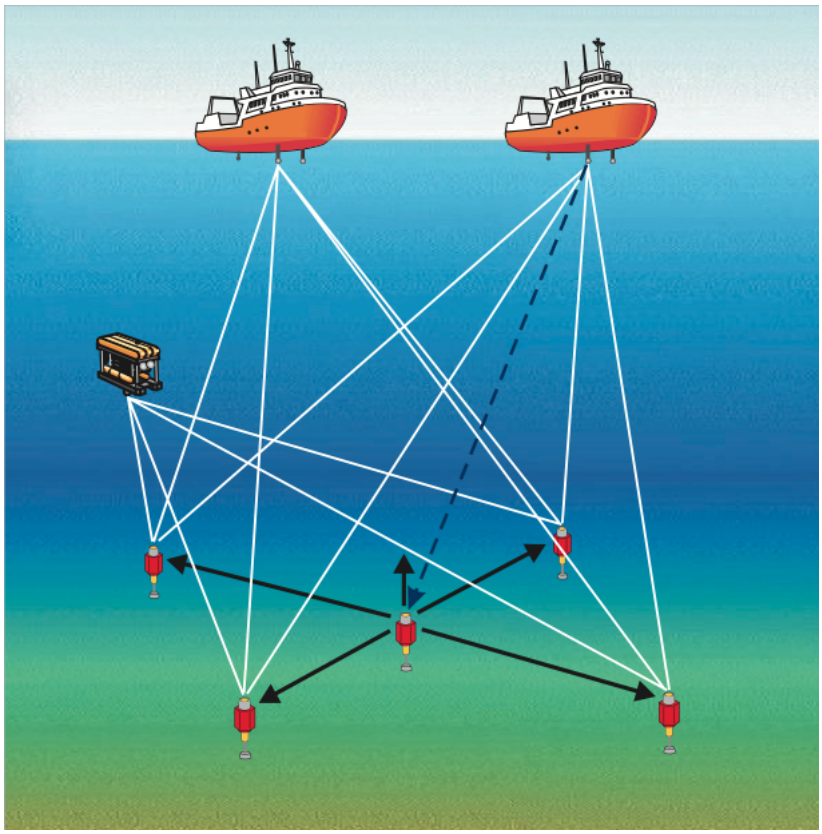

Figure 2.9: Long Baseline acoustic positioning system, courtesy of Kongsberg Maritime

Due to better accuracy and a higher update frequency an LBL system is considered best for the problem investigated in this thesis. The transponders or pingers could be mounted on structures in the subsea field. This will probably be beneficial for other operations as well as there is a lot of work that is performed with ROV in the installation phase of a subsea field.

2.6.2 ROV Sensors

ROVs typically comes with a sensor suite consisting of:

- Flux Gate Compass
- Depth sensor (Pressure gauge)
- Doppler Velocity Log

- Sonar
- Gyroscope
- Accelerometers

The flux gate compass is measuring the direction of the horizontal component of the earths magnetic field, making it able to sense the heading of the ROV. The depth sensor is measuring the hydrostatic pressure, so the depth of the ROV can be calculated if the atmospheric pressure at the sea surface is known. The doppler velocity log measures the frequency change in acoustic pings that are sent out and uses this to calculate the speed in x-,y- and z-direction. The sonar is sending out sound and is registering the echoes in order to detect objects in the water. The gyroscope is using the principles of angular momentum to measure the attitude of the vehicle. The accelerometer is measuring acceleration in the 3 linear degrees of freedom.

In addition to these the ROV typically carries some variety of a hydroacoustic positioning system. Either a interrogator in a LBL system or a transponder for use with a USBL system. It should not be necessary to put more sensors in the ROV for this system to function properly. The ROV should ideally be a standard ROV, so the system can be used independently of the vessel.

If the position and motions of the ROV is known this information could be used to find the position and motions of the Xmas tree by using kinematic relations.

2.6.3 Signal Processing

When we install sensors in our system we need to know that we can trust them, and we need to be able to extract the information from the electrical signals they give us. The sensors are the way computers sense the world. The signals obtained directly from a sensor are often noisy and biased. It is also possible that the sensor is unhealthy and do not give us correct information at all. It is therefore important to process the signals before they are fed into a control loop. If an unhealthy, noisy or biased signal is fed into a simulation or a controller this might give unwanted effects on the system. There are two main aspects to consider when we talk about sensor signal processing:

- *Signal quality checking:*
  Each sensor signal has to be checked for errors subject to certain criteria before it is sent to the control system for processing.
- *Handling of multiple signals:*
  If several sensors provide measurements of the same state variable, weighing and voting mechanisms must be introduced.

Signal Quality Checking

The signal shown in figure 2.10 has four failures that can be detected by a signal processing unit. A wild point is detected by comparing a signal reading to the last reading. If the difference between these readings is larger than a predefined threshold the wild-point reading will be rejected. If the system detects a lot of wild points this might indicate that the sensor is faulty or unhealthy.

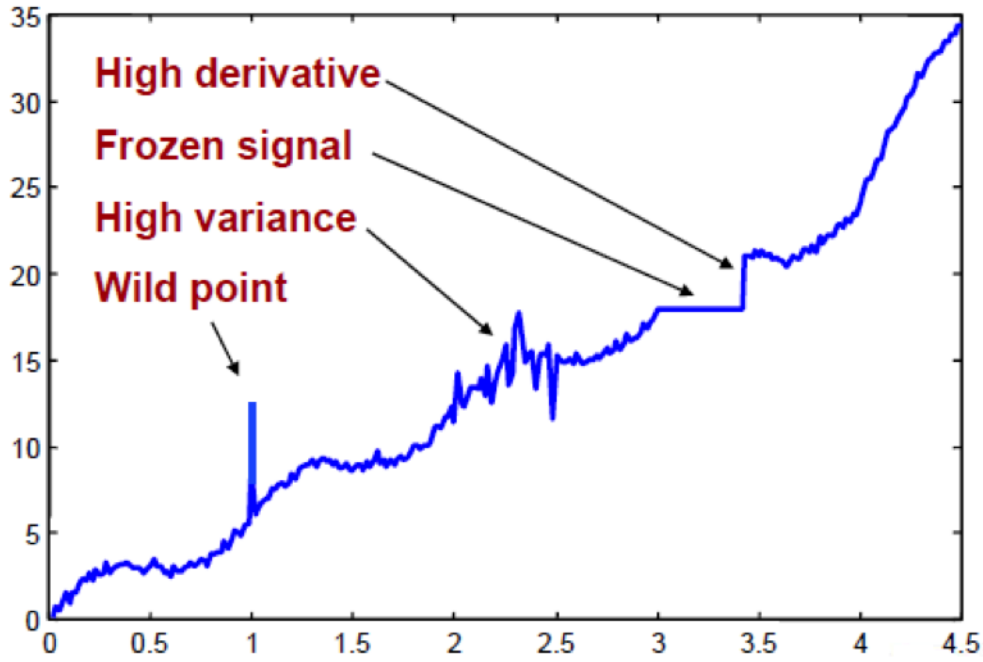

Figure 2.10: Typical signal failures, courtesy of Sørensen [2013a]

A high variance of a signal may indicate sensor failure or an inaccurate measurement, and a very low variance might indicate a frozen signal. The variance is a statistical parameter that indicates how much a series of numbers are varying. In a signal processor the variance is calculated on-line for the n last sensor readings, where n is a preset number. We can change n in order to tune our signal processor.

A range check can also be used to decide whether a signal is healthy or not. A lot of measurements can only be within a certain range. An example is that a compass will always show between 0° and 360°. If the signal is outside the predefined range this indicate that the sensor is faulty.

Multiple Signals Handling

When we have several signals measuring the same thing we actually get more information about the sensors. This information can, if it is used properly give us more accurate information about the process we are measuring. There is however some challenges in synchronizing these signals.

When we have several sensors measuring the same thing we often just want to feed one value into our control system. This value can be an average of the signals, the median or a weighted average where the weight is based on the signal health or accuracy. If we have more than two sensor readings on the same process we can use a technique called voting. Voting is used for detecting if a sensor is drifting. Voting is basically to check if one sensor value is far away from the other sensor values. If so this sensor need to be discarded or recalibrated.

If a sensor is discarded or lost we will experience a sudden jump in the value that is sent to the control system. This should be avoided because the control system might interpret this jump as a sudden change in the system that will need to be corrected. It is therefore smart to put a low-pass filter on the signal to make the transition smooth. This can be seen in figure 2.11. When we are adding more sensors the transition is smooth without a filter.

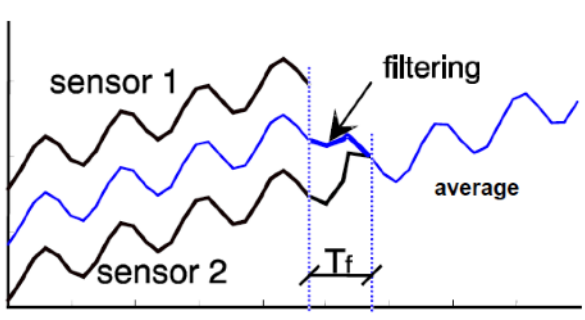

Figure 2.11: Fusing of two sensor outputs, courtesy of Sørensen [2013b]

When the control system described in this thesis is implemented in experimental scale the signal processing is already implemented. This control system will use this signal processing as is, and this subject is therefore not treated more extensively in this thesis. A reference is made to Tolpinrud [2012] and Kirkeby [2010] for a closer description of the existing control system.

2.6.4 Signal Modelling

In order to test and tune the state estimator described in Section 3.1 we need to simulate the measurements that are taken. This is done by adding a white noise to

the signal, and then sample it using a zero order hold element. The block diagram of this process can be seen in Figure 2.12. The power of the noise and the sampling rate is adjusted for each signal in order to get a realistic output.

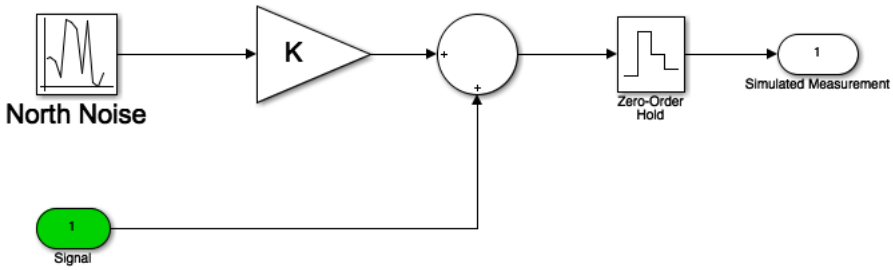

Figure 2.12: Sensor modelling

Chapter 3

Control Design

This chapter is treating the design of the control system. The control system proposed is a hybrid control system where several controller-observer pairs work together in order to control the ROV both when it is connected to a Xmas tree and when it is not. In this chapter the development of an extended Kalman filter, a nonlinear PID controller and a corresponding reference model is described. In addition the thrust allocation and hybrid setup is studied.

3.1 State Estimator

A state estimator or an observer is an algorithm that compares measurements to a model of the measured system in order to get a signal with higher quality. A state observer for marine applications has three main objectives:

- Reconstruct unmeasured states based on the available outputs, including *dead-reckoning*
- Estimate the environmental disturbances acting on the system
- Perform filtering of the measured signals

(Candeloro [2011])

The estimates from the state observer is used in the control system of the marine vessel. The estimates of the environmental disturbances and the signal filtering functions will typically make the control system more effective and economical. This is because these functions typically filter out noise and high frequency motions that the control system cannot counteract, and it should therefore not try to do so. The result is that less energy is used, and there is less wear and tear on the components in the system.

An observer typically consists of two parts, a predictor and a corrector, see figure 3.1. The predictor uses a model and the commanded control input to predict the behavior of the system. Some measurements can be used in the predictor, such as orientation. Then the corrector corrects the state that is estimated by the predictor by using the available measurements.

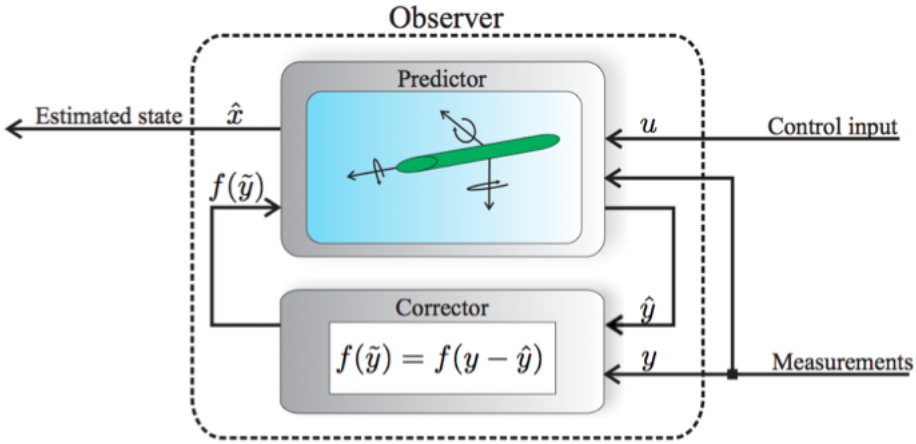

Figure 3.1: Typical observer modules, the predictor and the corrector. From Refsnes [2008]

The main differences between different kinds of observers is the difference in how the predictor and corrector works together. In the linear deterministic observer by Luenberger [1964] the corrector is added with a fixed gain, while in the Kalman filter the optimal feedback is determined by stochastic considerations [Kalman [1960]]. Adaptive and passive observers have also been developed for marine applications. A reference is made to Fossen [2011] for a more extensive treatment of this subject.

In this masters thesis an Extended Kalman Filter (EKF) is implemented in order to estimate the position of the Xmas tree using the measurements from the ROV.

3.1.1 Extended Kalman Filter

The EKF is an extension of the regular discrete Kalman filter that is used for nonlinear systems. The EKF linearizes the nonlinear model in each iteration. The EKF algorithm can be found in Table 3.1, where the discrete quantities

$\mathcal{F}(\boldsymbol{x}(k), \boldsymbol{u}(k)), \boldsymbol{\Theta}(k)$ and $\boldsymbol{\Gamma}(k)$ is found using *forward euler* integration:

$$\mathcal{F}(\boldsymbol{x}(k), \boldsymbol{u}(k)) \approx \hat{\boldsymbol{x}}(k) + h[\boldsymbol{f}(\hat{\boldsymbol{x}}(k)) + \boldsymbol{B}\boldsymbol{u}(k)] \tag{3.1}$$

$$\boldsymbol{\Theta}(k) \approx \boldsymbol{I} + \frac{\partial \boldsymbol{f}(\hat{\boldsymbol{x}}(k))}{\partial \boldsymbol{x}(k)}\bigg|_{\boldsymbol{x}(k)=\hat{\boldsymbol{x}}(k)} \tag{3.2}$$

$$\boldsymbol{\Gamma}(k) \approx h\boldsymbol{E} \tag{3.3}$$

In these equations $\boldsymbol{f}(\hat{\boldsymbol{x}}(k), \boldsymbol{u}(k))$ represents the control plant model in 2.48, where $\boldsymbol{x} = [\boldsymbol{\eta}, \boldsymbol{\nu}, \boldsymbol{b}]^T$. This model however has its origin in the centre of the Xmas tree, but the measurements that is received from the ROV is given in its local origin. These measurements are therefore translated into the correct reference frame using the following equations:

$$\boldsymbol{\eta} = \boldsymbol{\eta}_{ROV} - \boldsymbol{J}(\hat{\boldsymbol{\eta}})\boldsymbol{r} \tag{3.4}$$

$$\boldsymbol{\nu} = \boldsymbol{H^{-1}}(\boldsymbol{r})\boldsymbol{J}(\boldsymbol{r})\boldsymbol{\nu}_{ROV} \tag{3.5}$$

$$\boldsymbol{u} = \boldsymbol{H^{T}}(\boldsymbol{r})\boldsymbol{J}(\boldsymbol{r})\boldsymbol{u}_{ROV} \tag{3.6}$$

Where $\boldsymbol{r}$ is the vector specifying the position and attitude of the ROV in the Xmas tree BODY-frame,$\boldsymbol{J}(\hat{\eta})$ is the rotation matrix between the BODY-frame of the Xmas tree and NED, $\boldsymbol{J}(\boldsymbol{r})$ is the rotation matrix rotating from the ROV BODY-frame into the Xmas tree-BODY frame and $\boldsymbol{H}$ is the translation matrix.

Table 3.1: Algorithm of the EKF

Design matrices	$\boldsymbol{Q}(k) = \boldsymbol{Q}^T(k) > 0$ $\boldsymbol{R}(k) = \boldsymbol{R}^T(k) > 0$
Initial conditions	$\bar{\boldsymbol{x}}(0) = \boldsymbol{x}_0$ $\bar{\boldsymbol{P}}(0) = E[(\boldsymbol{x}(0) - \hat{\boldsymbol{x}}(0))(\boldsymbol{x}(0) - \hat{\boldsymbol{x}}(0))^T] = \boldsymbol{P_0}$
Kalman gain matrix	$\boldsymbol{K}(k) = \hat{\boldsymbol{P}}(k)\boldsymbol{H}^T(k)[\boldsymbol{H}(k)\bar{\boldsymbol{P}}(k)\boldsymbol{H}^T(k) + \boldsymbol{R(k)}]^{-1}$
State estimate update	$\hat{\boldsymbol{x}}(k) = \bar{\boldsymbol{x}}(k) + \boldsymbol{K}(k)[y(k) - \boldsymbol{H}(k)\bar{\boldsymbol{x}}(k)]$
Error covariance update	$\hat{\boldsymbol{P}}(k) = [\boldsymbol{I} - \boldsymbol{K}(k)\boldsymbol{H}(k)]\bar{\boldsymbol{P}}(k)[\boldsymbol{I} - \boldsymbol{K}(k)\boldsymbol{H}(k)]^T$ $+\boldsymbol{K}(k)\boldsymbol{R}(k)\boldsymbol{K}^T(k)$ $\hat{\boldsymbol{P}}(k) = \hat{\boldsymbol{P}}(k)^T > 0$
State estimate propagation	$\bar{\boldsymbol{x}}(k+1) = \mathcal{F}(\hat{\boldsymbol{x}}(k), \boldsymbol{u}(k))$
Error covariance propagation	$\bar{\boldsymbol{P}}(k+1) = \boldsymbol{\Phi}(k)\hat{\boldsymbol{P}}(k)\boldsymbol{\Phi}^T(k) + \boldsymbol{\Gamma}(k)\boldsymbol{Q}(k)\boldsymbol{\Gamma}^T(k)$

3.2 Controller

To obtain position tracking for the Xmas tree system a nonlinear PID controller with acceleration feedback is proposed. This controller is known to be quite robust

because of the integral action. This is important because of the uncertainties in the Xmas tree model. In addition this kind of controller has a simple implementation and the tuning process is well known.

The control objective of the controller can be specified mathematically as:

$$\boldsymbol{\eta} \to \boldsymbol{\eta}_d, \boldsymbol{\nu} \to \mathbf{0}$$

3.2.1 Control Strategy

Two control strategies were considered for this control system. The first strategy is position based, while the other is force based.

In the position based control strategy we look at the desired position of the Xmas tree, and then use this position together with information about the relative position between the ROV and the XT to calculate a desired position of the ROV. Then it is possible to use the existing control system in the ROV to position the Xmas tree. The existing control system will then probably need some tuning to achieve good performance.

The force based strategy is to use the position of the Xmas tree as input to the controller. The controller will then make a desired force vector to be applied to the Xmas tree. The force is produced by the ROV. In order to use the existing thrust allocation scheme in the existing control system of the ROV, the force vector needs to be translated into the body frame of the ROV. This is done by using the inverse of 2.47:

$$\boldsymbol{\tau}^r_{ctrl,R} = \boldsymbol{J}^{-1}(\boldsymbol{r}^b_R)\boldsymbol{H}^{-T}(\boldsymbol{r}^s_R)\boldsymbol{\tau}_{ctrl} \tag{3.7}$$

Where $\boldsymbol{\tau}_{ctrl}$ is the desired force vector applied to the Xmas tree. This is the vector that is the output of the PID-controller.

The force based control strategy is chosen as the preferred strategy in this thesis. This is because it is believed that this strategy will make a more robust system as the motions of the XT is controlled in a more direct way than with the position based strategy.

3.2.2 Control Algorithm

The control law of a MIMO-nonlinear PID Controller in 3 DOFs can be written as:

$$\boldsymbol{\tau}_{ctrl} = \boldsymbol{R}^T_\psi(\psi)\boldsymbol{\tau}_{PID} \tag{3.8}$$

where

$$\boldsymbol{\tau}_{PID} = -\boldsymbol{K}_p\tilde{\boldsymbol{\eta}} - \boldsymbol{K}_s\dot{\boldsymbol{\eta}} - \int_0^t \tilde{\boldsymbol{\eta}}(\tau)d\tau \tag{3.9}$$

Where $\tilde{\boldsymbol{\eta}} = \boldsymbol{\eta} - \boldsymbol{\eta}_d$. This controller is inspired by a 6 DOF version of the same controller found in Fossen [2011]

3.2.3 Stability

Assume that

$$\int_0^t \tilde{\boldsymbol{\eta}}(\tau)d\tau = \boldsymbol{b}$$

So the integrator perfectly compensates the bias and constant environmental forces. This yields the following closed loop system:

$$\boldsymbol{M}\dot{\boldsymbol{\nu}} + [\boldsymbol{C}(\boldsymbol{\nu}) + \boldsymbol{D}(\boldsymbol{\nu}) + \boldsymbol{K}_d^*(\boldsymbol{\eta})]\,\boldsymbol{\nu} + \boldsymbol{R}_\psi^T(\psi)\boldsymbol{K}_p\tilde{\boldsymbol{\eta}} = \boldsymbol{w} \tag{3.10}$$

Where

$$\boldsymbol{K}_d^*(\boldsymbol{\eta}) = \boldsymbol{R}_\psi^T(\boldsymbol{\psi})\boldsymbol{K}_d\boldsymbol{R}_\psi(\boldsymbol{\psi}) \tag{3.11}$$

In the following stability analysis it is assumed that the regulation from $\boldsymbol{\eta}$ to $\boldsymbol{\eta}_d$ is constant, meaning that $\dot{\boldsymbol{\eta}}_d = 0$. A Lyapunov function candidate for the system is:

$$V = \frac{1}{2}\boldsymbol{\nu}^T\boldsymbol{M}\boldsymbol{\nu} + \frac{1}{2}\tilde{\boldsymbol{\eta}}^T\boldsymbol{K}_p\tilde{\boldsymbol{\eta}} \tag{3.12}$$

Where $\boldsymbol{M} = \boldsymbol{M}^T > 0$ and $\boldsymbol{K}_p = \boldsymbol{K}_p^T > 0$.

By differentiation of $\boldsymbol{\nu}$ and $\tilde{\boldsymbol{\eta}}$ in 3.12 with respect to time we get:

$$\begin{aligned}\dot{V} =& \boldsymbol{\nu}^T\boldsymbol{M}\dot{\boldsymbol{\nu}} + \dot{\boldsymbol{\eta}}^T\boldsymbol{M}\tilde{\boldsymbol{\eta}} \\ =& \boldsymbol{\nu}^T(\boldsymbol{M}\dot{\boldsymbol{\nu}} + \boldsymbol{R}_\psi^T(\psi)\boldsymbol{K}_p\tilde{\boldsymbol{\eta}})\end{aligned} \tag{3.13}$$

By using that $\dot{\boldsymbol{\eta}}_d = 0$ and $\dot{\tilde{\boldsymbol{\eta}}} = \dot{\boldsymbol{\eta}} - \dot{\boldsymbol{\eta}}_d$ we get $\dot{\tilde{\boldsymbol{\eta}}} = \dot{\boldsymbol{\eta}}$. Further we use that $\dot{\boldsymbol{\eta}}^T = \boldsymbol{\nu}^{\boldsymbol{T}}\boldsymbol{R}_\psi^T$. We now substitute 3.10 into 3.13. This gives us:

$$\begin{aligned}\dot{V} &= \boldsymbol{\nu}^T(\boldsymbol{w} - [\boldsymbol{C}(\boldsymbol{\nu}) + \boldsymbol{D}(\boldsymbol{\nu}) + \boldsymbol{K}_d^*(\boldsymbol{\eta})]\,\boldsymbol{\nu}) \\ &= \boldsymbol{\nu}^T\boldsymbol{w} - \boldsymbol{\nu}^T\,[\boldsymbol{C}(\boldsymbol{\nu}) + \boldsymbol{D}(\boldsymbol{\nu})]\,\boldsymbol{\nu})\end{aligned} \tag{3.14}$$

We get this by using property 7.2 from Fossen [2011], which states that the Coriolis and centripetal matrix always can be parametrized such that it is skew symmetric.

In the case where the disturbance $\boldsymbol{w} = 0$ we can use *Krasovskii-LaSalle's Theorem* to prove that the system is *Globally Asymptotically Stable* (GAS):

We have V:$\mathbb{R}^n \to \mathbb{R}_+$, a continuously differentiable positive definite function such that:

$$\begin{aligned}&V(\boldsymbol{\nu}, \tilde{\boldsymbol{\eta}}) \to \boldsymbol{\infty} \text{ as } ||\boldsymbol{\nu}|| \text{ and } ||\tilde{\boldsymbol{\eta}}|| \to \boldsymbol{\infty} \\ &\dot{V}(\boldsymbol{\nu}, \tilde{\boldsymbol{\eta}}) \leq 0, \forall(\boldsymbol{\nu}, \tilde{\boldsymbol{\eta}})\end{aligned}$$

We then let Ω be the set of all points where $\dot{V}(\boldsymbol{\nu}, \tilde{\boldsymbol{\eta}}) = 0$, that is:

$$\Omega = \{\boldsymbol{\nu}, \tilde{\boldsymbol{\eta}} \in \mathbb{R}^n | \dot{V}(\boldsymbol{\nu}, \tilde{\boldsymbol{\eta}}) = 0\} \tag{3.15}$$

This set is found from:

$$\dot{V}(\boldsymbol{\nu}, \tilde{\boldsymbol{\eta}}) = \boldsymbol{\nu}^T \left[\boldsymbol{C}(\boldsymbol{\nu}) + \boldsymbol{K}_d^*(\boldsymbol{\eta})\right] \boldsymbol{\nu} \equiv 0 \tag{3.16}$$

which is true for $\boldsymbol{\nu} = \mathbf{0}$. Therefore

$$\Omega = \{(\boldsymbol{\nu}, \tilde{\boldsymbol{\eta}}) : \boldsymbol{\nu} = \mathbf{0})\} \tag{3.17}$$

When $\boldsymbol{\nu} \equiv \mathbf{0}$ we get that

$$\boldsymbol{M}\dot{\boldsymbol{\nu}} = -\boldsymbol{R}_{\psi}^T(\psi)\boldsymbol{K}_p\tilde{\boldsymbol{\eta}} \tag{3.18}$$

This expression is nonzero as long as $\tilde{\boldsymbol{\eta}} \neq \mathbf{0}$, meaning that the system will have its only equilibrium-point in $(\boldsymbol{\nu}, \tilde{\boldsymbol{\eta}}) = (\mathbf{0}, \mathbf{0})$. This equilibrium point is then the largest invariant set M in Ω and this equilibrium point is then according to *Krasovskii-LaSalle's Theorem* GAS. For proof see LaSalle [1966].

In the case where $\boldsymbol{w} \neq 0$, but is constant the PD-Controller will make the system converge to a circle about the origin $(\boldsymbol{\nu}, \tilde{\boldsymbol{\eta}}) = (\mathbf{0}, \mathbf{0})$. The radius of the circle is decided by the size of the disturbance. We say that the system has the property uniform ultimate boundness (UUB). In this case it can be proved that if one include the integral action the system is Locally Asymptotically Stable (LAS). See Arimoto and Miyazaki [1984]

3.2.4 Anti Wind-up Strategy

A controller with integral action controlling an actuator that can become saturated can cause undesirable effects. These effects can occur if the error between the set-point and the actual position is large over time. This may cause the integrator to integrate up to a very large value. Because this value is higher than the saturation value of the actuator it will not actually help to correct the error. When the error finally is reduced it might take considerable time to discharge it. During this discharge period one typically experienced an overshoot, because the integrator continues to push in the same direction until its discharged. This effect is called integrator wind-up Åstrøm and Wittenmark [1996].

In order to avoid integrator wind-up a anti wind-up strategy is employed. The strategy chosen is to saturate the output from the integrator. Then we take the value surpassing this saturation limit and subtract is from the error signal going

into the integrator. However the actuators in this system is situated on the ROV, but the control vector is calculated in the body-frame of the system. In other words will the saturation apply to the translated force vector. We therefore translate the integral part of the force vector into the body-frame of the ROV, and apply a saturation function on this signal. The surpassing value will then need to be translated back to the body-frame of the system before it is subtracted from the error signal. The saturation limit for the integral part of the controller is set to 90% of the maximal thruster output. This is to have some reserves for dynamic control. A block diagram of the anti wind-up function can be seen in figure 3.2. Mathematically the integral action term of the controller can be expressed by:

$$\boldsymbol{\tau_i} = (\boldsymbol{K_i} - \boldsymbol{H}(\boldsymbol{r}_S^r) sat(\boldsymbol{H}_R^s \boldsymbol{\tau}_i)) \int_0^T \tilde{\boldsymbol{\eta}}(t) dt \tag{3.19}$$

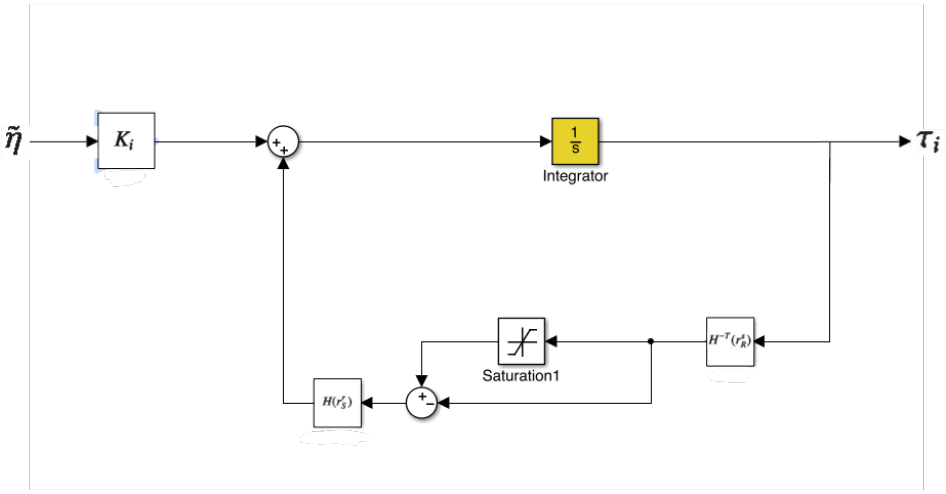

Figure 3.2: A block diagram for anti wind-up structure

3.2.5 Thrust Allocation

The nonlinear PID-controller is making a desired force vector. This force vector is being generated from the thrusters on the ROV. The mapping between this desired thrust vector and the set-point in rpm for each thruster is called thrust allocation. In this section two different ways of allocating the thrust is shown.

Standard Thrust Allocation

The thrust is calculated using 2.13. If we take the inverse of this relation we get:

$$\boldsymbol{u} = \boldsymbol{T}^{\dagger} \boldsymbol{K}_T^{-1} \boldsymbol{\tau} \tag{3.20}$$

where $\boldsymbol{T}^{\dagger}$ is the *Moore-Penrose pseudoinverse* of T and $u_i = n_i|n_i|$ is a vector containing the signed square of the rotational speed of every thruster. The reason the pseudoinverse is used is because the thrust configuration matrix, T is not square, and it is therefore not possible to find the regular inverse of it. The pseudoinverse is calculated using the following equation:

$$\boldsymbol{T}^{\dagger} = \boldsymbol{T}^{T}(\boldsymbol{T}\boldsymbol{T}^{T})^{-1} \tag{3.21}$$

The desired speed for the thrusters can then be calculated by taking the signed square-root of each element in $\boldsymbol{u}$:

$$n_i = sign(u_i)\sqrt{|u_i|} \tag{3.22}$$

The rotational is speed is however limited to a maximum of 1500 rpm.

Recursive nullspace-based control allocation with strict prioritization

Simulations as well as experience using ROV Minerva with the existing control system has shown that the standard thrust allocation may cause problems when the control system is asking for more thrust than Minerva can deliver [Kirkeby [2010]]. For this system an example of this can be found in Figures 4.14 and 4.15. A solution to this problem is to use a smarter way of allocating thrust where one prioritize between the different directions of motion. One such way is presented in Skjetne and Kjerstad [2013].

This way of allocating the thrust is implemented with a [yaw, sway, surge] prioritisation, meaning yaw has highest priority while surge has lowest. It has proved to make the system much more robust. This is because the actual thrust output is more predictable with this type of allocation. Figures 3.3 and 3.4 is showing a comparison between this and the standard allocation.

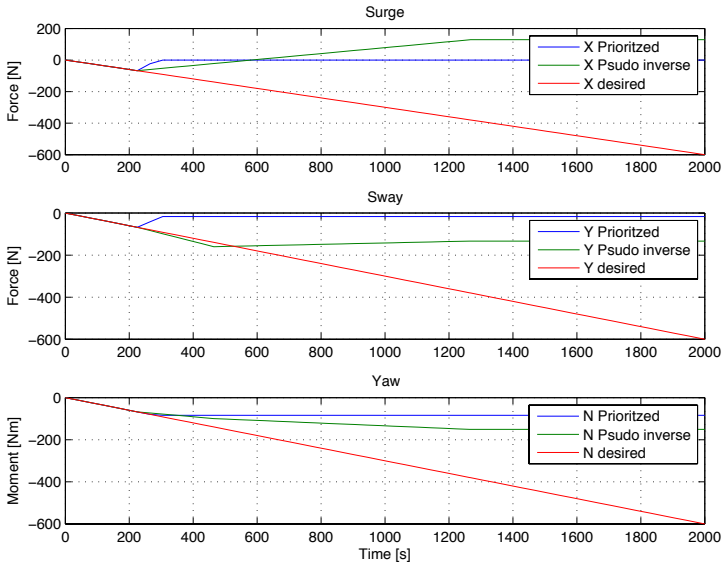

Figure 3.3: Thrust comparison between standard and prioritized thrust allocation for positive thrust values

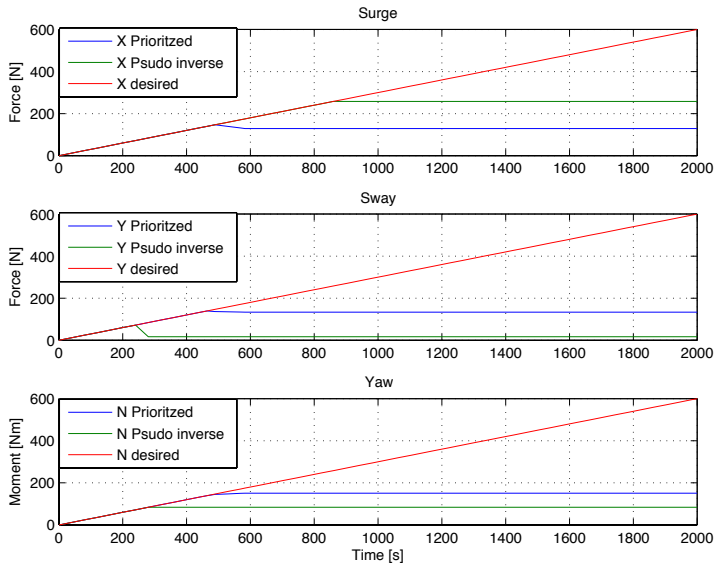

Figure 3.4: Thrust comparison between standard and prioritized thrust allocation for negative thrust values

3.3 Reference Model

The task of the reference model is to make smooth and feasible trajectories that is within the bandwidth of the controller, meaning that it is capable of following the output reference from this model. In this thesis the reference model has not much attention, and a simple 1st order low-pass filter with saturated input is used to generate feasible references. The saturation is representing the maximum speed of the system, and in this way ensuring that the reference is not changing to fast. A block diagram of the reference model can be found in Figure 3.5.

This reference model is inspired by the synthetic reference model presented in de A. Fernandes et al. [2012], however the version presented here is simplified. While the reference model in de A. Fernandes et al. [2012] is generating a reference where both the maximum acceleration and speed is taken into account, the model presented here only take the maximum speed into account. It is assumed that this control system would benefit from using the more sophisticated reference model, and this could be a point for further work.

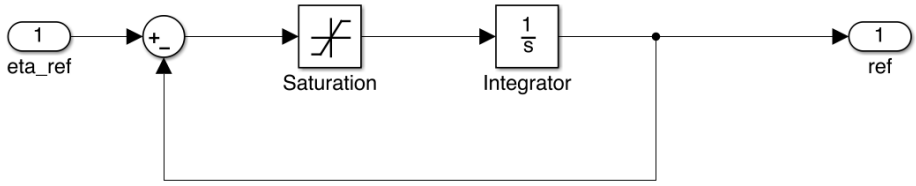

Figure 3.5: block diagram of the reference filter

3.4 Supervisory Switching Control

The control system that is developed in this chapter will probably not be capable of controlling the ROV when it is not connected to a Xmas tree, or the performance will at least be poor. This is mainly due to the extreme differences in mass and damping, as well as the fact that the control vector is calculated in the Xmas tree reference frame when the Xmas tree controller is used. In addition the heave motion would need to be controlled when there is no Xmas tree connected.

It is desirable to have a control system that is capable of controlling the ROV in all operation situations, therefore a supervisory switching control system (SSC) is proposed. This system integrates both the controller and observer described in this chapter and one or possibly more controllers for controlling the ROV when it is not connected to the Xmas tree. A block diagram of this system can be seen in Figure 3.6. The switching between the different controller sets can either be done automatic or by human interaction. In the experimental setup described in Chapter 5 it is done by human interaction. This system is inspired by the systems presented in Nguyen et al. [2009] and Nguyen et al. [2007].

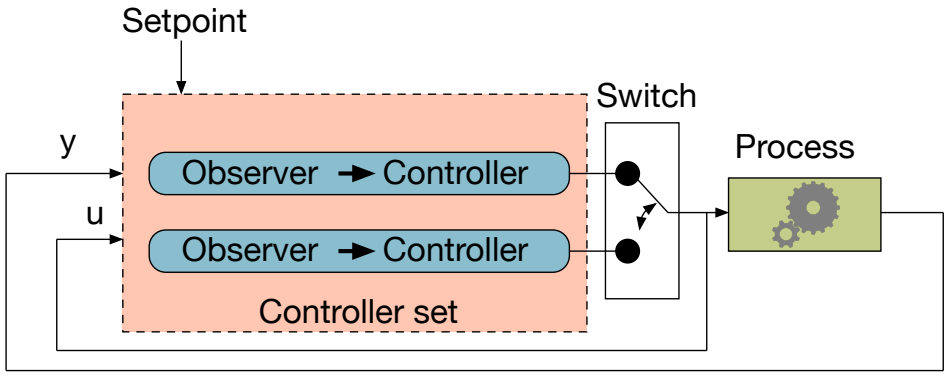

Figure 3.6: Supervisory Switching Control System

Chapter 4

Simulations

In the first period of working with this thesis the main area of focus was to simulate and model the control system in full scale. It was verified during these simulations that it was feasible to use an ROV to position Xmas trees. It was then decided that the control system should be tested using ROV Minerva and a scaled model. The focus was then shifted towards preparing this test by studying the experimental system through simulations. Because of this shift in focus both full scale and experimental scale simulations are presented in this chapter.

Through the full scale simulations we are studying the model and the feasibility of the control system. In addition we are looking at how well the control system is suppressing wave induced motions of the Xmas tree. On the other hand the simulations done using the experimental scale model is studying aspects that are important for the sea trials. This is how the system reacts to sensor feedback instead of perfect feedback, aspects regarding the thrust allocation of Minerva and how robust the system is to modelling errors.

The simulations presented here are simulated using the Matlab Simulink software. The simulation is done using the process plant model described in Section 2.4. This model is parametrized using different parameters according to what we want to show with the simulations. There are two set of parameters for the ROV used, one that is modelling a large working class ROV used in the full scale simulations, and another set of parameters that are modelling ROV Minerva. These are used in the experimental scale simulations. For the Xmas tree there is also two set of parameters. The first set is a set of parameters developed to model a real Xmas tree. This set are equipped with a scaling factor so they can be scaled to fit our simulation needs. The last variation of parameters is a set that is modelling the Xmas tree model made for the experimental testing of the control system. All parameters can be found in Appendix B.

All simulations are performed with a uniform current of $0.1m/s$ through the whole

water column. The current direction is 225°, meaning it is going in the South-West direction. The lifting wire is piercing the water surface at position $[1, 1]([N, E])$.

4.1 Full Scale Simulations

As the goal of this masters thesis is to design a control system that makes an ROV capable of governing the position and orientation of a Subsea Xmas tree during installation, a set of simulations using a model of the full scale model is done. The main goal of these simulations is to verify the feasibility of such a system as well as to verify and test the controller algorithms. An important aspect is also to study the system to learn more about the responses it has to disturbances and the control system.

The simulations presented here has three purposes. The first simulations is performed without any an activated control system to check if the system model is behaving as expected. The second is a set of simulations that is verifying that our control strategy works as we want, and the last simulations is studying if the control system is capable of suppressing wave induced motions of the Xmas tree.

4.1.1 Model Behavior

In this sections two simulations is shown where we look at the uncontrolled system. The first simulation is a simulation where only the Xmas tree model is included, while the second includes the ROV as well. In both of these simulations the Xmas tree is initialized at position $[1, 1, 400]([N, E, D])$. In the simulation containing the ROV, it is connected to the XT with an offset of $-2m$ in the x-direction. In other words the ROV is placed $2m$ behind the XT, with the same heading.

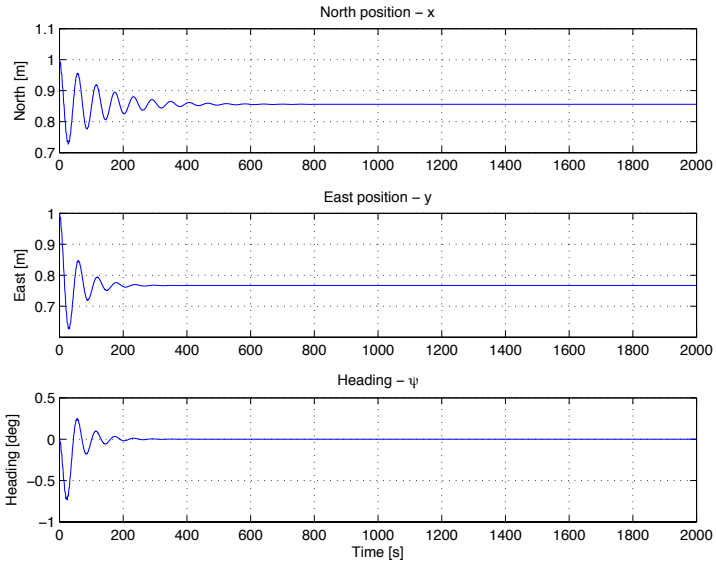

Figure 4.1: Positions of Xmas tree without control

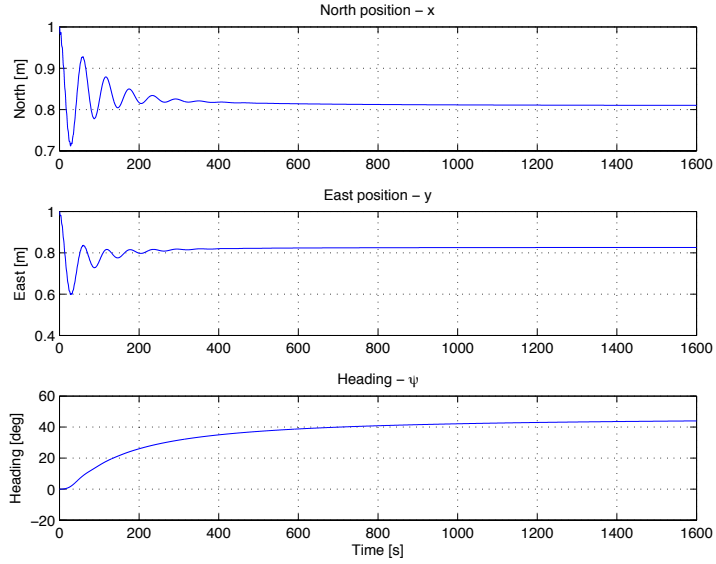

Figure 4.2: Positions of Xmas tree and ROV interconnected without control

In figure 4.1 we can see the positions of the XT while it is uncontrolled, and in figure 4.2 we see the same with the ROV connected to the XT. In the beginning of the simulations we can see that the XT is moving in the current direction for a short while, and oscillates for some time around its equilibrium position before it is coming to rest. We see that in the simulation containing only the XT the heading angle is not changing noteworthy during the simulation, while in the connected system rotates 45° so the system is heading directly towards the current.

4.1.2 Control Concept Verification

In this section the results of three simulations are shown. These are showing that our control system is actually working. The control system is working with *perfect feedback* meaning that it uses the actual position of the Xmas tree to calculate the control output.

The first simulation is showing the system performing a 360° rotation first in the positive direction(clockwise CW) ,then in the negative direction (counterclockwise (CCW). This simulation is shown in Figure 4.3, 4.4 and 4.5. In the two last simulations the XT is rotated 90°, then moved in a $2m$ x $2m$ square pattern. In the two first simulations the Xmas tree is at initialized at position $[1, 1, 400]([N, E, D])$, while in the last it is initialized at $[1, 1, 100]$. The last simulation is to show the effect of the depth for the control system. The ROV is connected to the XT with an offset of $-2m$ in the x-direction. The results from the first of these simulations is shown in 4.6, 4.7 and 4.8 while the second is shown in in Figure 4.9, 4.10 and 4.11.

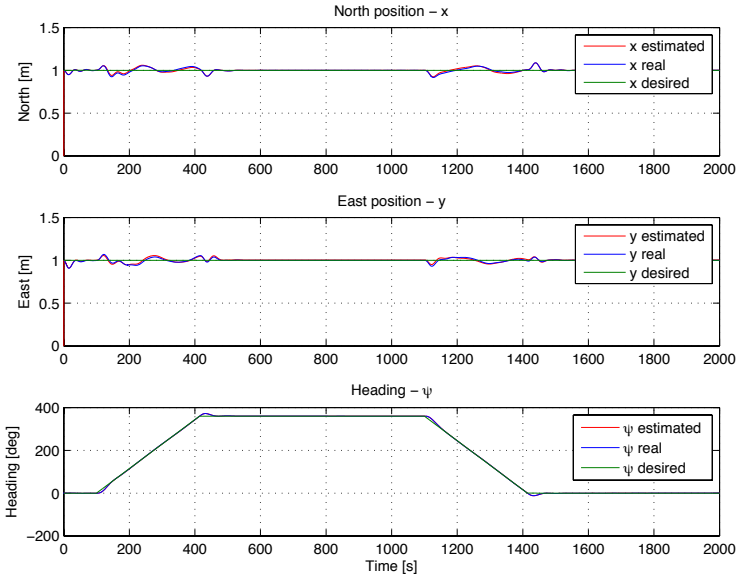

Figure 4.3: Position plots of Xmas tree during rotation

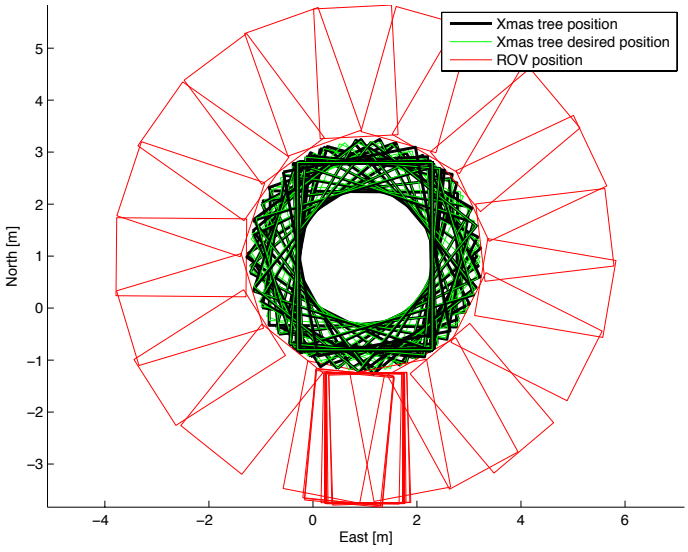

Figure 4.4: North East position of ROV and Xmas tree during rotation

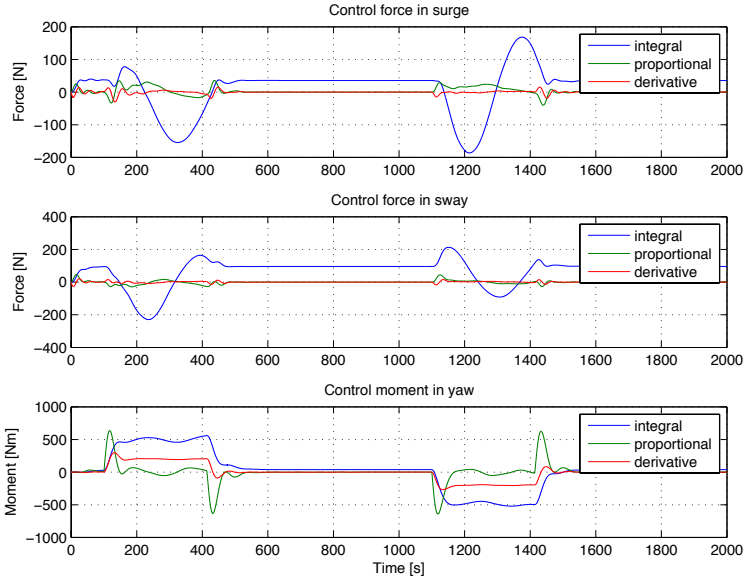

Figure 4.5: The commanded control forces during a rotation move

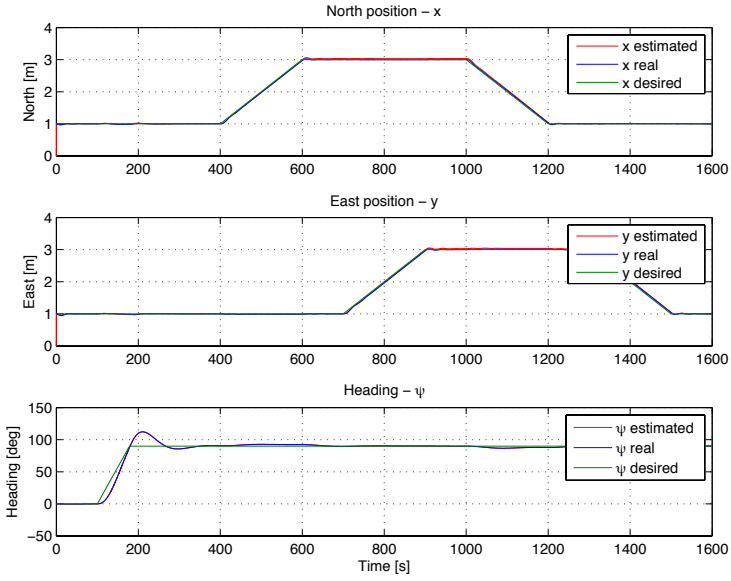

Figure 4.6: Position plots of Xmas tree during a square move at 400 m

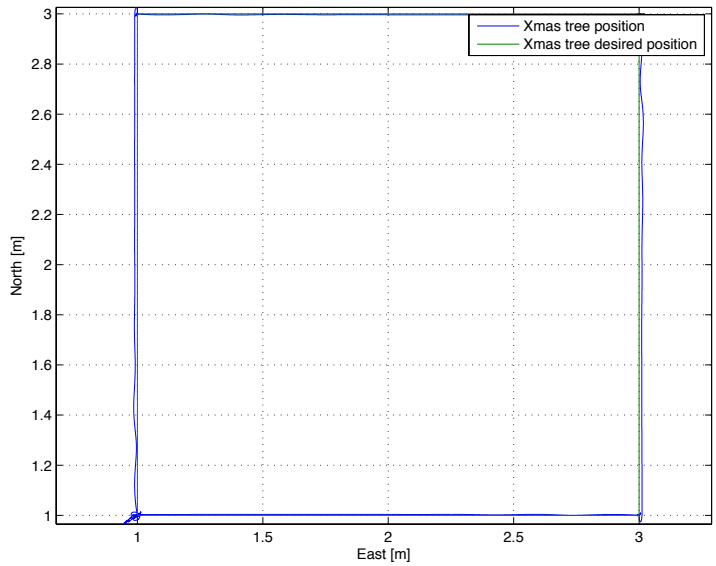

Figure 4.7: North East position of Xmas tree during a square move at 400m

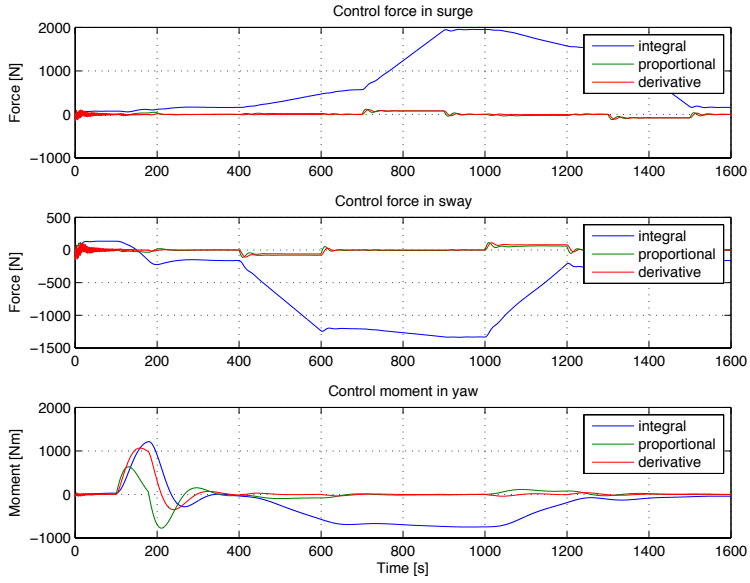

Figure 4.8: The commanded control forces during a square move at 400m depth

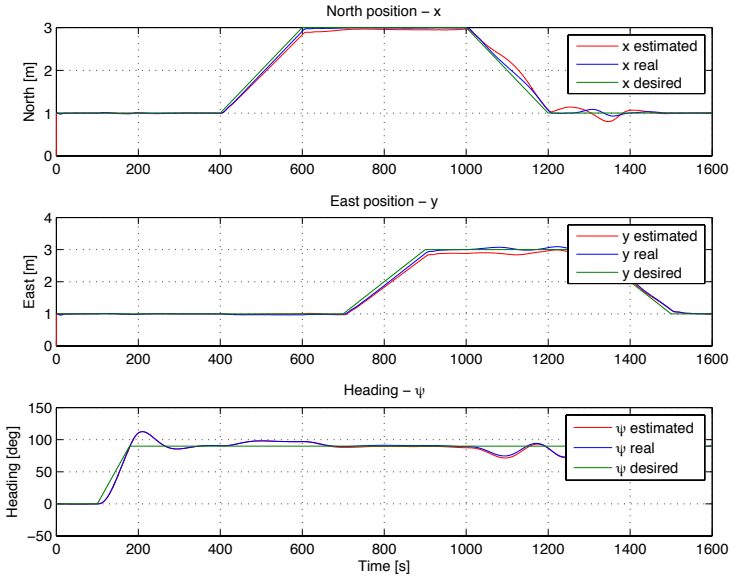

Figure 4.9: Position plots of Xmas tree during a square move at 100 m depth

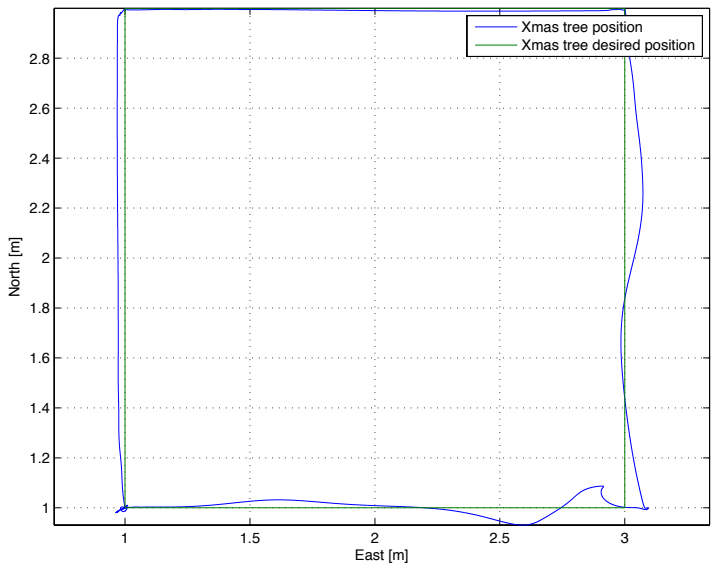

Figure 4.10: North East position of Xmas tree during a square move at 100m depth

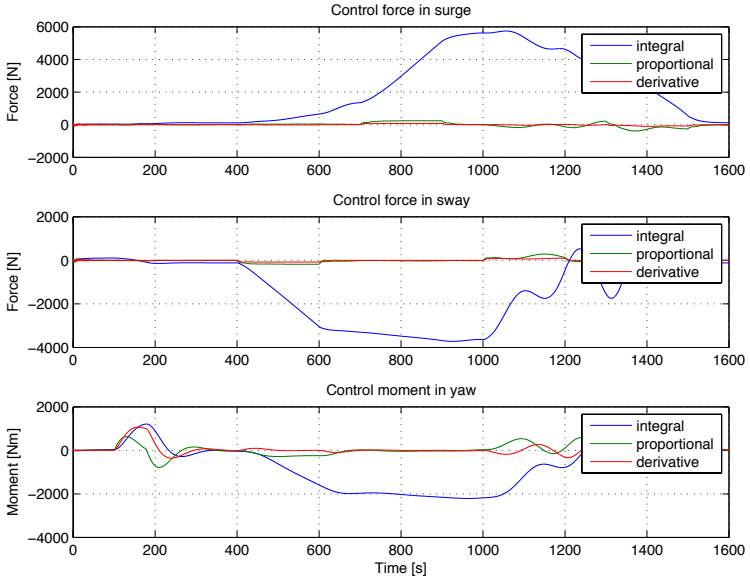

Figure 4.11: The commanded control forces during a square move at 100m depth

In all these simulations we see that the XT is following the reference quite good. We do also see that it is struggling a bit more to keep the correct position in the shallower water in the third simulation.

4.1.3 Suppression of Wave Disturbances

In this section we are studying the effect of the control system on the wave induced motions on the submerged XT. This is done by first running a simulation with wave currents and the control system turned off. Then the control system was activated and another simulation was conducted.

These simulations were conducted without any current, and with the XT at a depth of $100m$

In order to compare the motions of the uncontrolled XT to the controlled ones the Root Mean Square (RMS) value was used. For the uncontrolled simulation the RMS-value was calculated according to the following formula:

$$RMS_{uncontrolled} = \sqrt{\frac{1}{n}\sum_{i=1}^{n}(\eta(i) - \bar{\eta})^2} \tag{4.1}$$

Where n is the number of position measurements, $\eta(i)$ is the i-th measurement and $\bar{\eta}$ is the mean value of the position, and $\eta \in [N, E, \psi]$.

Similarily the RMS value for the controlled case is calculated according to:

$$RMS_{controlled} = \sqrt{\frac{1}{n}\sum_{i=1}^{n}(\eta(i) - \eta_d)^2} \tag{4.2}$$

where η_d is the desired position.

This was done for four different sea states. The result from these simulations are shown in Table 4.1. in this table T is the peak period of the sea state, while H_s is the significant wave height.

Table 4.1: Results for four simulations at different sea states

	RMS North [m]	RMS East [m]	RMS Heading [degrees]
$T = 10$, $H_s = 8$			
Uncontrolled	0.0024	0.0017	0.0343
Controlled	0.0027	0.0014	0.0051
$T = 20$, $H_s = 8$			
Uncontrolled	0.1706	0.0690	0.8785
Controlled	0.1311	0.0587	0.1221
$T = 30$, $H_s = 8$			
Uncontrolled	0.7521	0.3549	3.0110
Controlled	0.2263	0.1244	0.2386
$T = 30$, $H_s = 12$			
Uncontrolled	1.3373	0.6012	3.7956
Controlled	0.4351	0.2244	0.4640

4.2 Experimental Scale Simulations

The simulations shown in this section was conducted as a preparation for the experimental testing. The simulations in this section is showing the how the additions that were made for the control system to work during the experimental testing. The first section shows a simulation showing the performance of the control system when using sensor feedback and an observer for the control input. The second section is showing the advantages of using a thrust allocation that is prioritizing the yaw-motion, while the last section shows two simulations that were done before the sea trials. They were done in order to check how robust the control system is against modelling errors.

4.2.1 Sensor Feedback

The simulation in this section is showing the performance of the simulated system when the sensors of the ROV are modelled and used as feedback for the controller. The measurements are sent through the observer that are described in Section 3.1. The simulation is conducted at a depth of 400 m, and using the parameters for the experimental scale Xmas tree model and ROV Minerva. The simulation results can be seen in Figure 4.12 and 4.13.

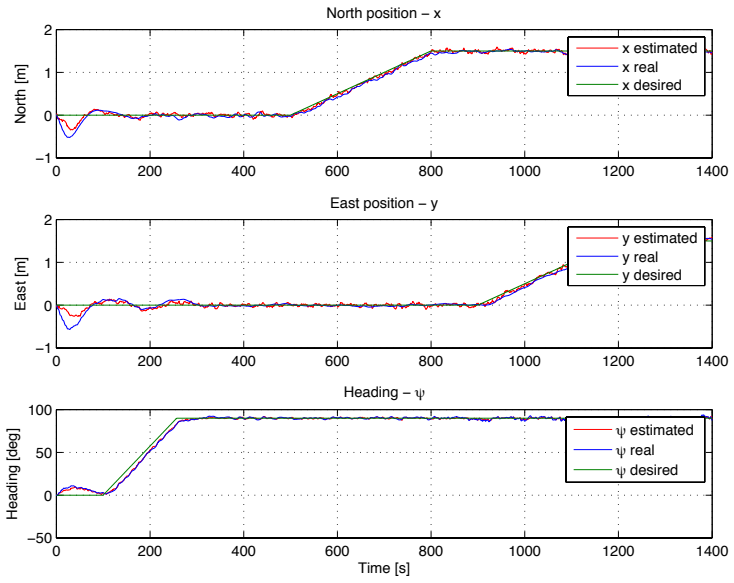

Figure 4.12: Position plots of Xmas tree during a square move with sensor feedback

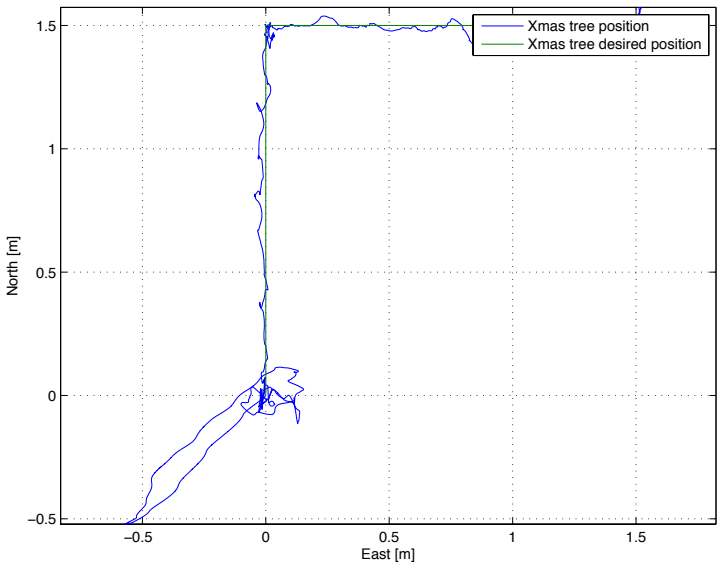

Figure 4.13: North East position of Xmas tree during a square move with sensor feedback

4.2.2 Thrust Allocation

In this section the difference between two different thrust allocation schemes is shown. To make the difference easy to see we try to make an impossible move. The move we are trying to make the control system to conduct is a step 5 m north and 5 m east, with a heading of 90°. The first simulation, that can be seen in Figure 4.14 and 4.15 is showing the move with the standard thrust allocation. The second simulation in Figure 4.16 and 4.17 is showing the same move done with prioritized and constrained thrust allocation. Both these allocation methods is described in Section 3.2.5.

The simulation is performed with the experimental scale model and ROV Minerva. The system is initialized at $[1, 1, 400]([N, E, D])$.

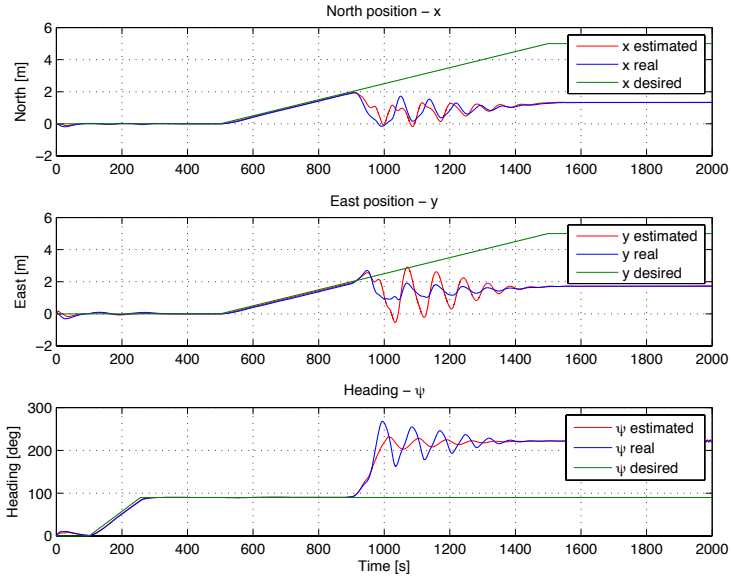

Figure 4.14: Position plot of simulation using standard thrust allocation

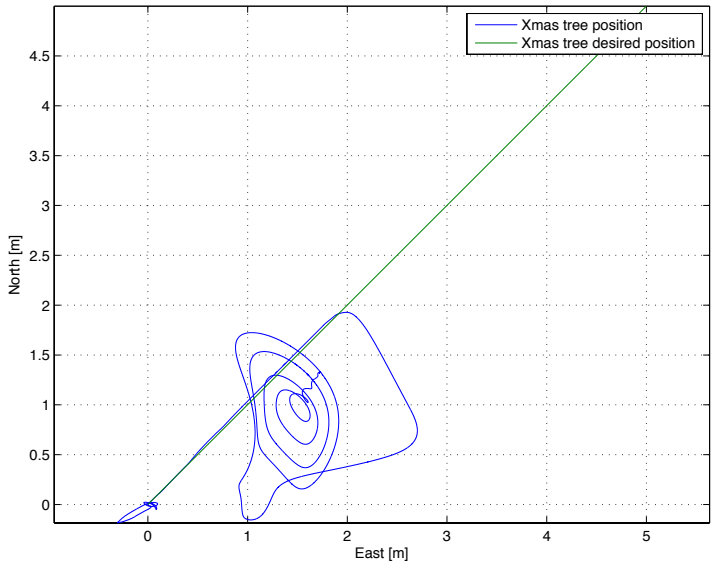

Figure 4.15: North East plot of simulation using standard thrust allocation

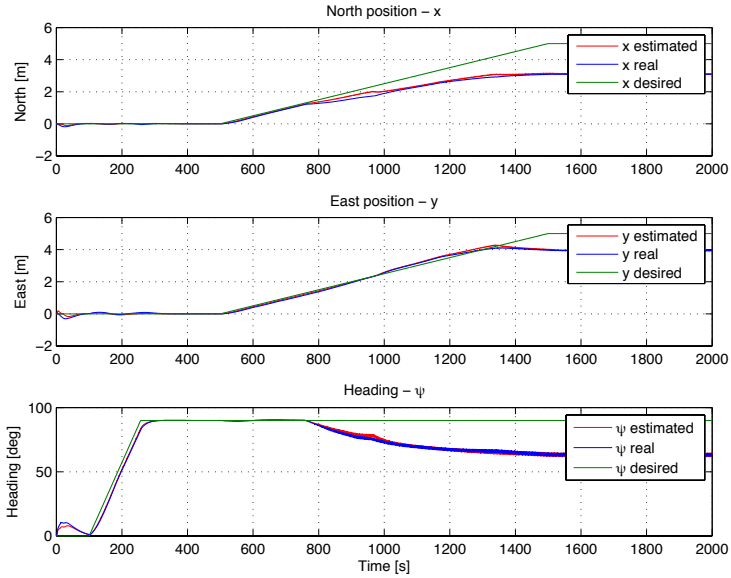

Figure 4.16: Position plot of simulation using prioritized thrust allocation

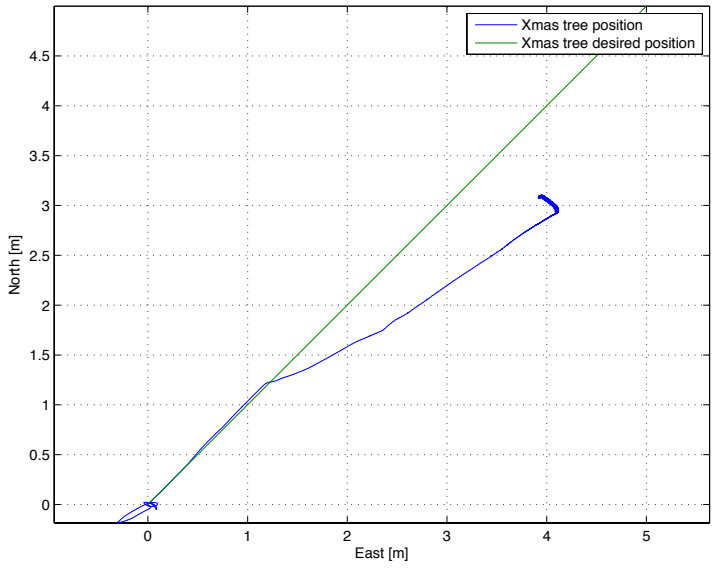

Figure 4.17: North East plot of simulation using prioritized thrust allocation

4.2.3 Robustness

In this section a series simulations is conducted with parameter variations are conducted. This is to study how robust the system is to errors in the modelling. during this simulation the control system was not changed in any way, but the simulation model was. The parameters that are varied is the mass and the submerged weight of the Xmas tree. These two parameters are chosen because it is assumed that these have the most impact on the motions of the Xmas tree, the submerged weight indirectly through being the cause of the restoring force, and the mass because of it represent the inertial forces. It shall be noted that even if these parameters are closely related in real life they can be varied independently in the simulation.

To compare the results the RMS value from Equation 4.2 is used. The results of this simulation can be seen in Table 4.2. In addition two plots from the simulation with a submerged weight that is 50% decreased is shown in Figure 4.18 and 4.19, that being the case with the highest RMS-values.

Table 4.2: Results for simulations with parameter variation

Parameter	Change	RMS North [m]	RMS East [m]	RMS Heading [degrees]
	-	0.0694	0.0626	2.7807
Mass	-20%	0.0677	0.0667	2.7479
Mass	+20%	0.0745	0.0714	2.8414
Weight	-20%	0.0792	0.0739	2.8560
Weight	+20%	0.0631	0.0643	2.8292
Mass	-50%	0.0626	0.0598	2.6573
Mass	+50%	0.0764	0.0732	2.9294
Weight	-50%	0.0943	0.0859	2.9439
Weight	+50%	0.0605	0.0613	3.0356

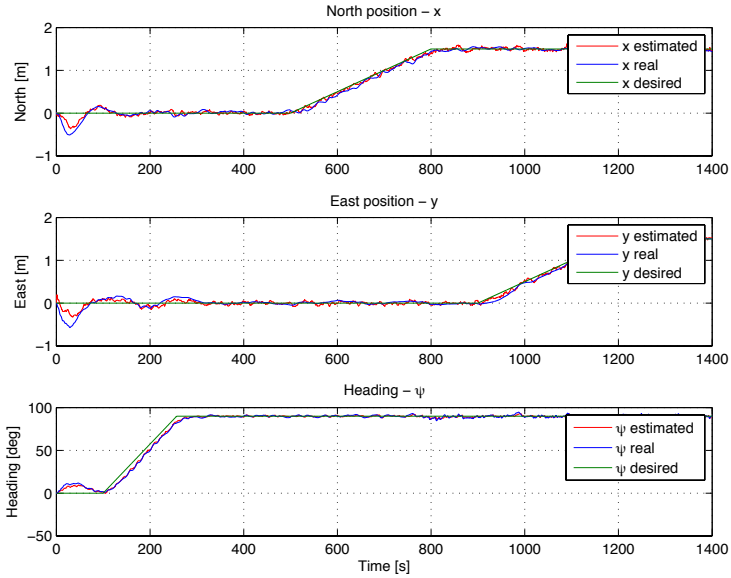

Figure 4.18: Position plot showing simulation with 50% decreased submerged weight

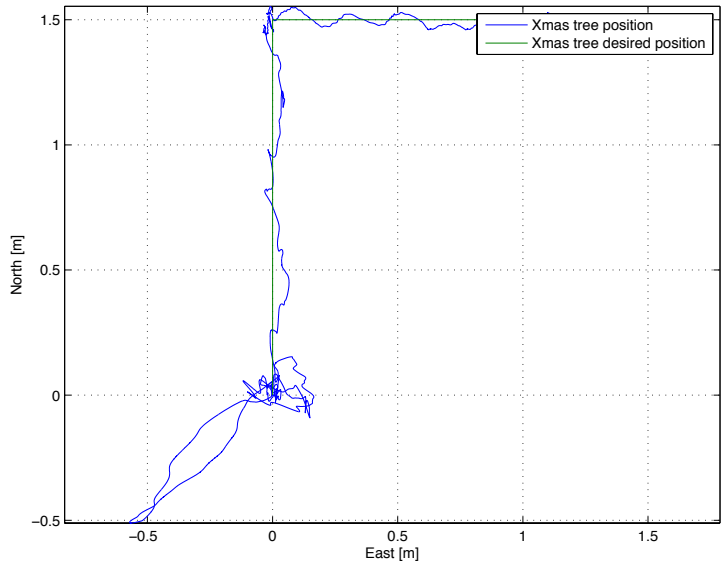

Figure 4.19: North East plot showing simulation with 50% decreased submerged weight

4.2.4 HIL-simulation

In the earlier phases of the project the control system and simulation model was implemented in Matlab Simulink, but in order for the control system to be tested with ROV Minerva the control system needed to be reimplemented in National Instruments LabView. LabView is a graphical programming language were NTNU AUR-lab already has an implementation of a control system for its ROVs. This control system is made to be a framework for experimenting and prototyping with different parts of the control system, making it easy to exchange smaller parts of the control system for testing and verification. The modularity of the control system is achieved by using *Object Oriented Programming (OOP)*. This modularity makes the job of implementing the new parts of this control system a manageable job. The development of this control system is described in Dukan et al. [2011], Berg [2012] and Tolpinrud [2012]. The LabView implementation of the control system can be found in Appendix F.1.

A *Hardware In the Loop simulator (HIL-simulator)* has been made to make it possible to test the control system without actually being aboard Gunnerus with the ROV in the water. This HIL-simulator consists of a compact-RIO, (an IO-interface module made to work with LabView) and a computer running a simulation model of the ROV. The compact-RIO is identically configured as the Compact-RIO aboard Gunnerus. The simulation model is simulating sensors on the ROV and outputting these to the IO-module. One can then connect the control system to the IO-module to run it, and verify its functionality. The testing process is illustrated in Figure 4.20.

In order to make it possible to run HIL-simulations to test the control system implementation in this thesis the simulation model described in Chapter 2 had to implemented in the existing HIL-simulator. This was done by exchanging the existing model of the ROV in the simulator with the Xmas tree model. Then the output of this model was translated to the body frame of the ROV in order for the simulator to simulate the sensor measurements on the ROV.

The possibility of HIL-testing of the control system makes the time needed for testing aboard the ship less. This is because one can test most of the functionality before going to the ship. The HIL-testing decreases the risk of damaging the equipment during testing, as most errors are corrected before the program is put in control of the real hardware.

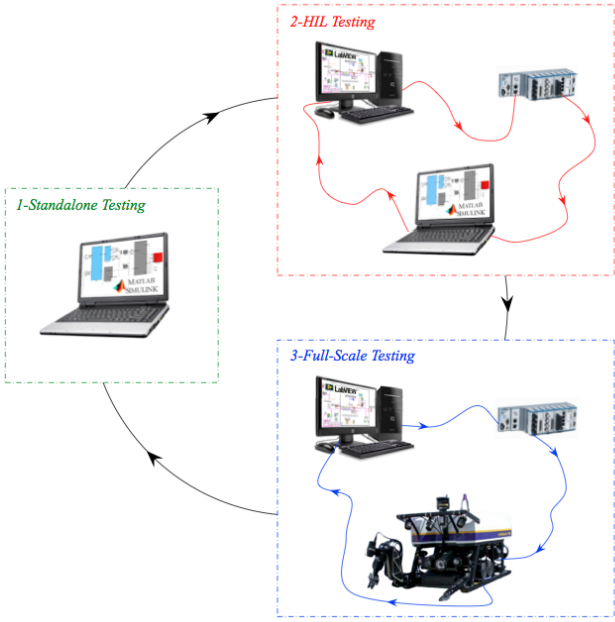

Figure 4.20: Testing procedure for control system, courtesy of Candeloro [2011]

The purpose of these simulations was to verify that the control system was working as expected after it was reimplemented in LabView. In the first simulation shown in this section the ROV is trying to keep the Xmas tree on the same position, without any rotation. The results from this simulation is shown in Figures 4.21 4.22 and 4.23.

The second simulation is showing a rotation move, where the XT model are rotated first 180° and then an additional 180° in the same direction. The result from this simulation is shown in Figure 4.24 and 4.25.

The third simulation is showing the XT model being moved in a square pattern of 1 m x 1 m. The result from this simulation is shown in 4.26 and 4.27.

All simulation are conducted at 200 m depth with a small current of 0.014 m/s going in the north-east direction with a heading of 45°. The position plots where the north, east and heading is plotted against time is showing three lines. The blue line is showing the desired position, the green is the measurement and the red is the estimated value. In the velocity plot and in the plot of the horizontal plane the blue line is showing the measured value while the green is showing the estimated one.

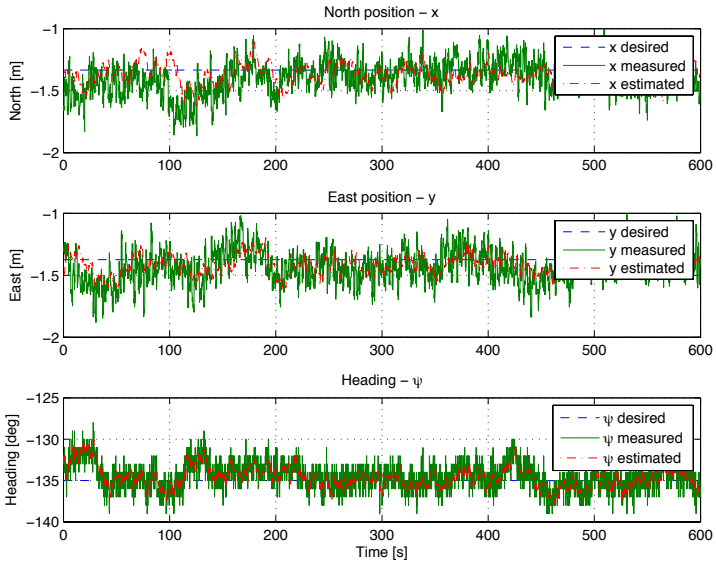

Figure 4.21: Plot showing north east and heading during HIL-simulation of stationkeeping

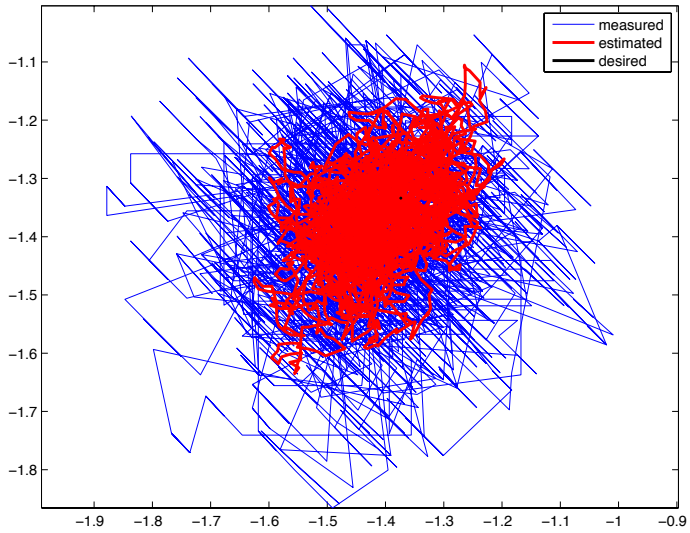

Figure 4.22: Plot showing he horizontal plane during HIL-simulation of station-keeping

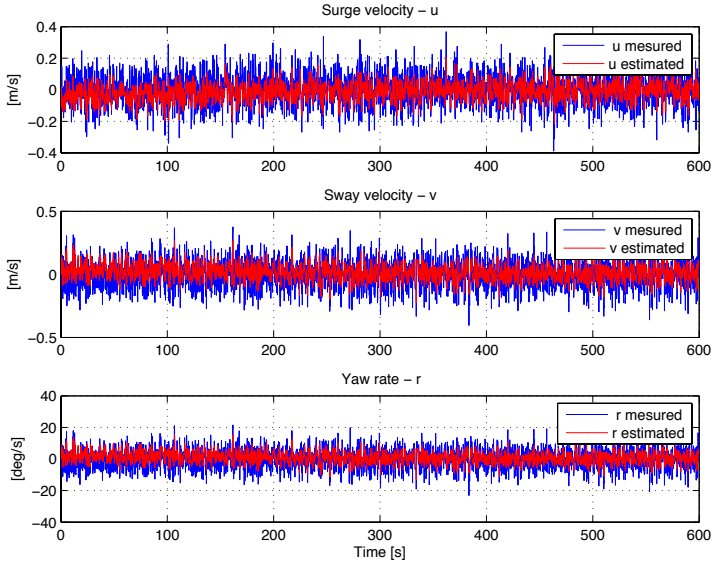

Figure 4.23: Plot showing the velocities during HIL-simulation of stationkeeping

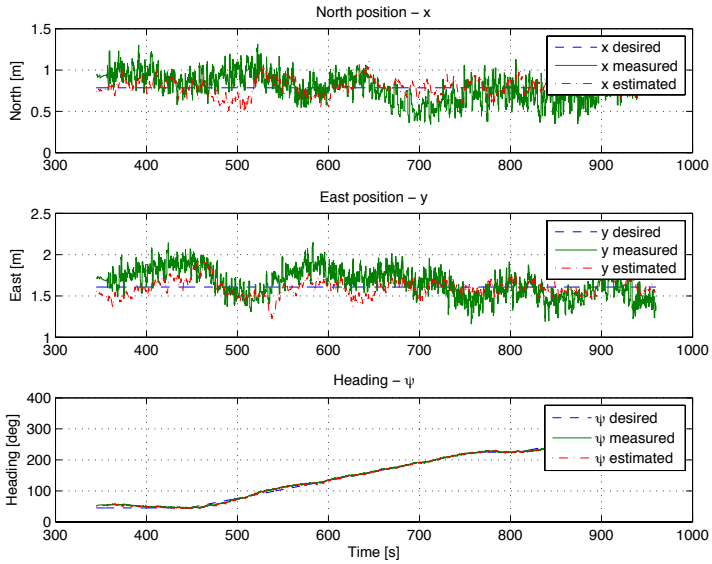

Figure 4.24: Plot showing north east and heading during HIL-simulation of a rotation move

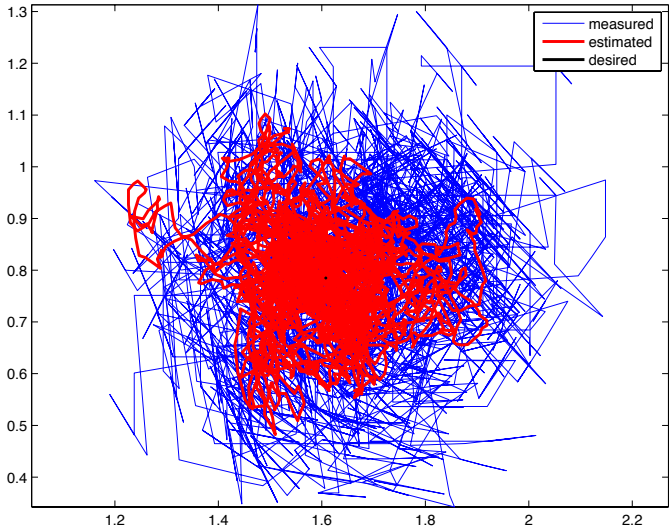

Figure 4.25: Plot showing he horizontal plane during HIL-simulation of a rotation move

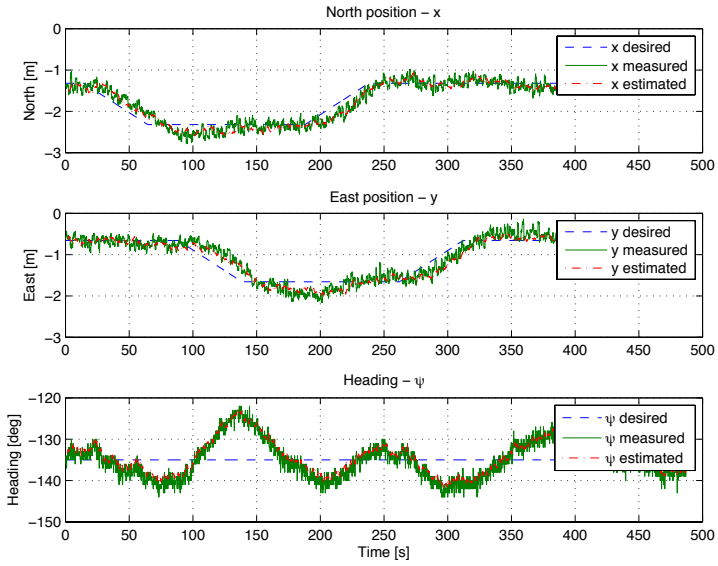

Figure 4.26: Plot showing north east and heading during HIL-simulation of a square move

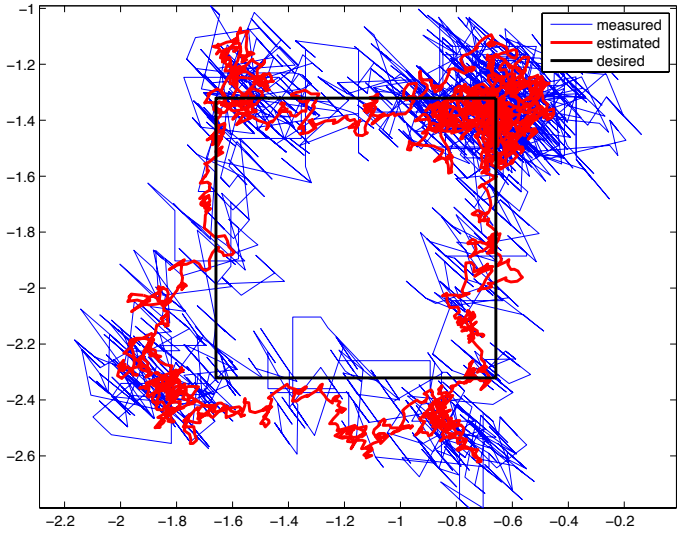

Figure 4.27: Plot showing he horizontal plane during HIL-simulation of a square move

Chapter 5

Experimental Testing

The control system was tested using an experimental setup and ROV Minerva in the Trondheim Fjord the 12. and 13. of May 2014. The tests were performed from the research vessel R/V Gunnerus. This chapter will explain the experimental setup, the control system implementation, the test plan and the results obtained in the tests.

The whole first day aboard Gunnerus was used to rig the experimental set-up, and to fix problems with the ROV. This gave us a little under a half a day with actual testing of the system, and there was little time to make improvements and modifications to the system.

5.1 Experimental Setup

In order to test if the control system proposed acually was capable of controlling the position of a Subsea tree an experimental setup was made. The idea was to use NTNUs ROV Minerva. This is a relatively small ROV so a scaled subsea tree model was designed. In addition a docking frame to land the subsea tree model on and a interface frame to transfer the force from Minerva to the module was designed.

In order to run the control system on Minerva it had to be reimplemented in *LabView*, a programming language that is commonly used for data acquisition, instrument control, and industrial automation. A Control system to control ROV Minerva was already developed in this programming language, and a lot of this code could be reused in this control system.

5.1.1 Subsea Tree Model

The subsea tree model had to fulfill the following requirements:

- Similar Hydrodynamical behavior as a real subsea tree
- The weight of the model should accommodate the force capacity of Minerva
- It needs a way to connect to the ROV, and to be docked at the seafloor.

In order to design a model with the same hydrodynamical properties as a real subsea tree the design found in Berg [2012] was used as a starting point. In the masters thesis of Berg tree different model designs for testing the hydrodynamical properties of a subsea tree is proposed. This was also used as a background in the modelling work done for simulating this control system. So the model denoted as model B in Kjemperud [2011] was scaled up. The objective was to end up with a model that had a submerged weight of about $5000N$ ($\approx 500kg$). Then two guidepost was added to the model in order for the ROV to dock onto the module to control its motions. Two funnels was placed on the bottom plate for the module to dock into guideposts on the docking frame. The design was then adapted to fit standard dimensions of steel plates and pipes to keep the production and material costs at a reasonable level. The design drawing and the finished module can be seen in Figure 5.1. After all modifications the module ended up with a steel weight of about 880 kg which led to a submerged weight of about 800 kg. This was a little heavier than the goal but it was assumed that ROV Minerva would still be capable of moving the module. The reason for the difference between the design weight and actual weight was because the finished design was with open pipes, while the initial design had closed pipes. Closed pipes would have given the model more buoyancy so the submerged weight had become lower.

The module needed some arrangement in order to be lifted and lowered down to the seafloor. As seen in Figure 2.2, real XTs are lowered down using a wire attached to one single point. It was considered to use this solution in the experimental setup, but if the module was not balanced about this point it could lead to problems, both with the docking and with connecting the ROV interface. In order to avoid these problems the module was fitted with 4 attachment points for lifting equipment, one in each corner. This way we knew that the module was going to hang straight.

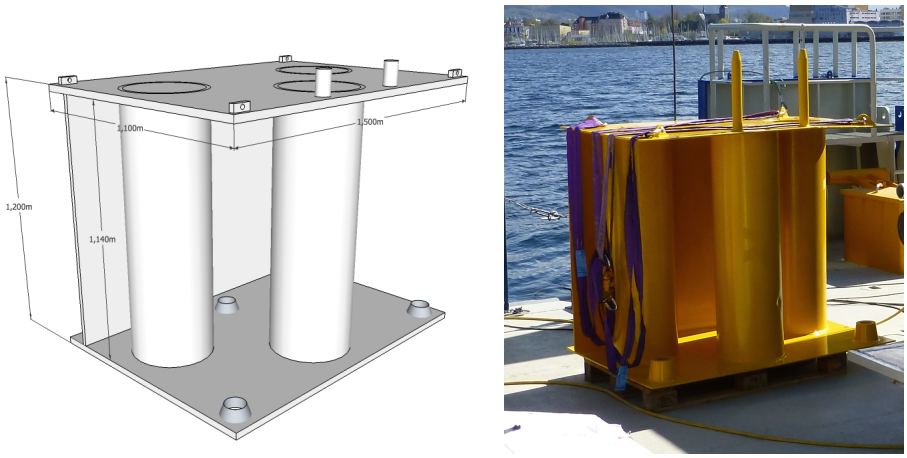

Design drawing Finished module

Figure 5.1: The subsea tree model

5.1.2 Auxiliary Equipment

The experimental setup consists of two auxiliary units in addition to the subsea tree module. This is a docking frame, and an interface module for connecting the ROV to the XT-module. The function of the docking frame is to be a fixed point on the seafloor to land the XT-module on. This was done by designing a frame with two guideposts. These two guidepost were meant to fit the into the funnels in the bottom plate of the XT-module. The frame was made by welding two beams together to form a cross. The plan was to mount an acoustic transponder to this frame in order to get a position reference for the control system. This acoustic transponder was placed inside a floating collar, and the floating collar was tied to the frame using a rope. The frame can be seen in Figure 5.2.

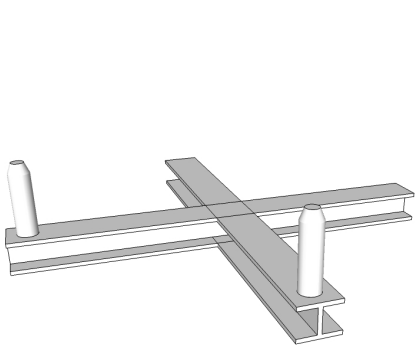

Design drawing

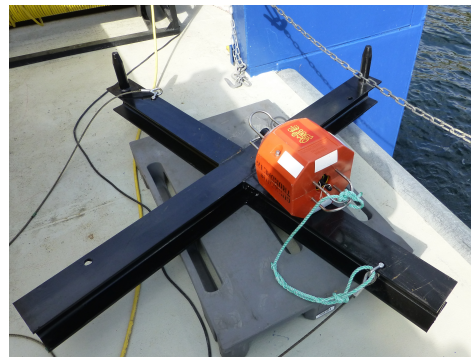

Finished docking frame

Figure 5.2: The docking frame

An interface between the ROV and the module was made by designing a frame that was attached to the ROV. The possibility of using the arm on the ROV instead of this interface was considered. This was however quickly turned down because the interface needed to be able of transferring moment, and we were uncertain if the arm was strong enough to transfer the amount of force needed to position the XT.

The frame was designed with two funnels that was supposed to fit on the guideposts on the top of the subsea module. It had to be strong enough to transfer the force from the ROV, but also lightweight so the ROV could keep its positive buoyant force even with it mounted. The frame was therefore made in aluminum. The frame can be seen in Figure 5.3.

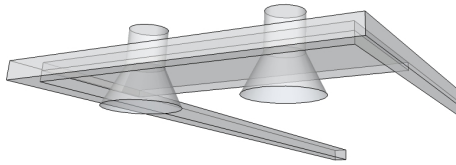

Design drawing

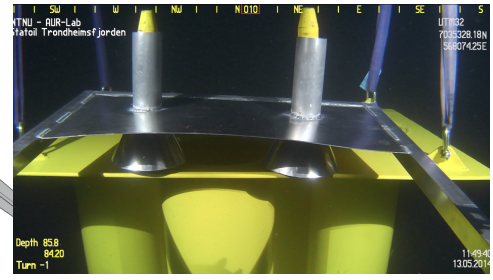

Finished interface frame in use

Figure 5.3: The interface frame

These modules together with ROV Minerva constitutes the physical part of the experimental setup. Figure 5.4 shows how the assembly was meant to fit together.

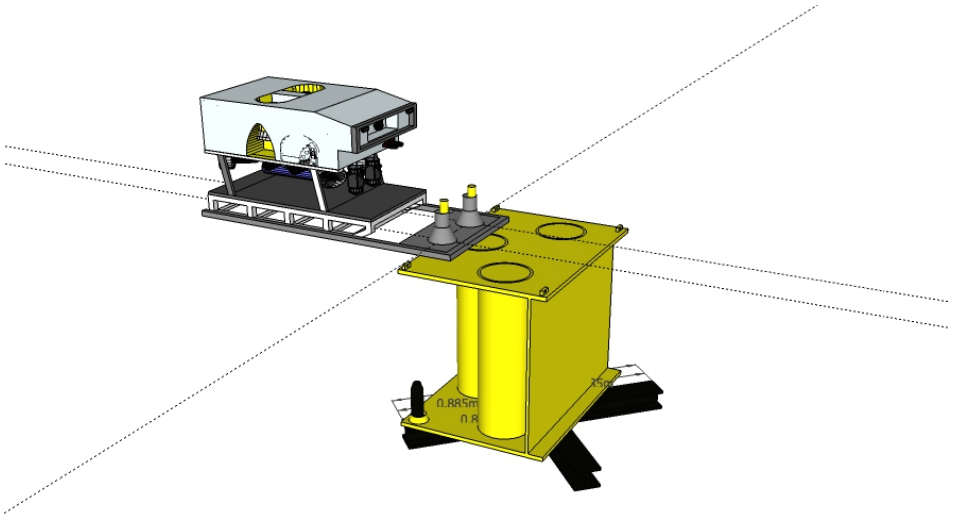

Figure 5.4: Illustration of the complete experimental set-up

5.1.3 Control System Implementation and Testing

While most of the simulation was run using a Matlab Simulink implementation of the control system, the testing with ROV Minerva had do be done using a LabView implementation of the control system. The LabView implementation used a lot of the code that was already implemented in the existing control system for ROV Minerva, including the signal processing and communication modules. In this implementation the hybrid control structure described in Section 3.4 was also implemented by running the existing DP-controller for Minerva alongside the Xmas tree controller. The testing procedure and results of this system is described in section 4.2.4.

5.1.4 Operation Manual

Prior to the testing an operation manual was made. The plan included all steps of the operation, and all the equipment needed during the operation. The manual was made so all the people that was involved in the operation would know what was going to happen, and so we could prepare and assess the risks involved in the operation. The plan was sent out to the crew on Gunnerus before the tests, and were discussed on the test day. This plan can be found in Appendix C.

The plan for testing of the actual control system was that the ROV should be connected to the XT module by manually controlling it. When the connection was done the control system should be activated. Then the intention was to perform

some motion tests, to check if the ROV was capable of actually control the position and orientation of the Xmas tree. When these tests had successfully been carried out the intention was to move on and attempt to dock the XT module on the bottom assembly.

There was some considerations to take into account when deciding the depth the testing should be performed at. In order to accommodate the low thrust capacity of Minerva the tests should be performed as deep as possible. This is because the restoring force stiffness is get lower at larger depth. This can bee seen in Figure 5.5. On the other hand the accuracy of the acoustic position measurements is decreased as the depth gets larger Ludvigsen [2010]. With this in mind it was decided that a depth of about 200m would be best. At this depth the horizontal stiffness curve seems to have flattened out, and the accuracy of the position measurement is assumed to be adequate for this tests.

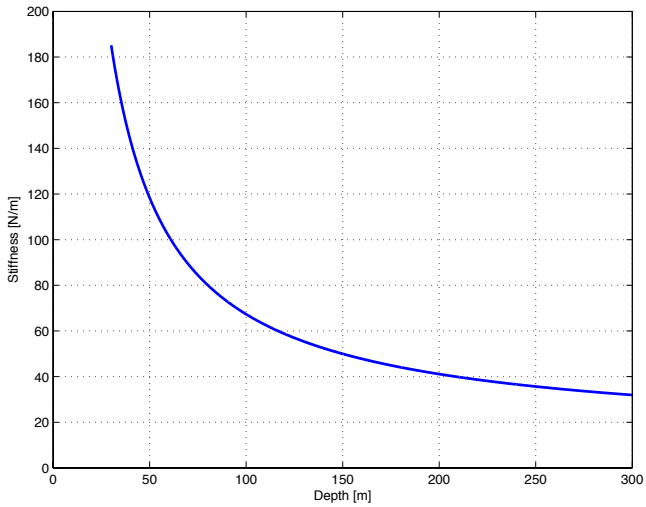

Figure 5.5: Horisontal stiffness plottet against depth of module

5.2 Results and Observations

This section will present both the results and what was done during the testing. This is done to set the results in a context.

5.2.1 Setup

The first day aboard Gunnerus was started with a *toolbox talk*. This is a session where the whole crew of the the ship is going through the upcoming operation. During this talk it was revealed that the Doppler velocity log (DVL) on Minerva did not work. It was believed that it was faulty due to a broken cable. The Doppler velocity log is an instruments that measures the speed of the ROV. Due to the slow update times of the acoustic positioning system it is considered a crucial part of the control system, as it gives the control system the ability to update the position in between the position updates. It was estimated that it would take over 24 hours to fix the cable in a permanent way, due to curing time. A possibility was however to make a temporary cable, using a vulcanizing rubber tape. The ROV-engineer believed that this cable would fail if used on larger depths than 100 m. In addition the captain of the ship did not know of any place where the seafloor was flat enough to place the XT-module at 200m depth. he did however know of a place with 100m depth or around 400m. A decision was then made to perform the tests at 100 m depth, using this temporary cable. The concern about performing the tests at such a small depth was that the restoring forces of the module would be to large for the ROV to handle.

The rest of the talk went on without detecting any major flaws in the plan, so the ship went out on the fjord to find a good spot. On the deck the assembly of the interface frame and the bottom assembly started. It was soon discovered that the design of the frame could have been better, as there were some instruments that interfered with the intended placement. This was however solved, but for further use the interface frame should be redesigned to fit the ROV better. When the interface frame was mounted the operation of placing the bottom assembly on the seafloor was carried out. It was performed as planned.

Then another error in the experiment setup was discovered: The lifting slings attached to the XT-module was in conflict with the interface frame of the ROV, making the connection between the ROV and the XT module impossible. This could be solved by using a spreader bar, but we did not have that aboard the ship. It was then decided to go to shore to make a spreader bar, and try again the following day.

When the second day of testing started most of the practical problems with the experimental setup was sorted out, and just a couple of hours after we left the dock the XT-module was in the water an the ROV was launched. The process of

connecting the ROV to the XT-module proved to a bit difficult as the XT-module was spinning, but after some attempts the connection was made.

5.2.2 Observer

With the connection done the control system was started up. The first impression when the control system was put in charge over the system was that it did not work at all. The interconnected ROV and XT-module system started spinning, and moving back and fourth. All observers and controllers was reset and it was left for a short period of time to see if it was stabilizing. It was not, but it was observed that the position estimates from the observer was very bad. A plot showing the estimation can be seen in Figure 5.6.

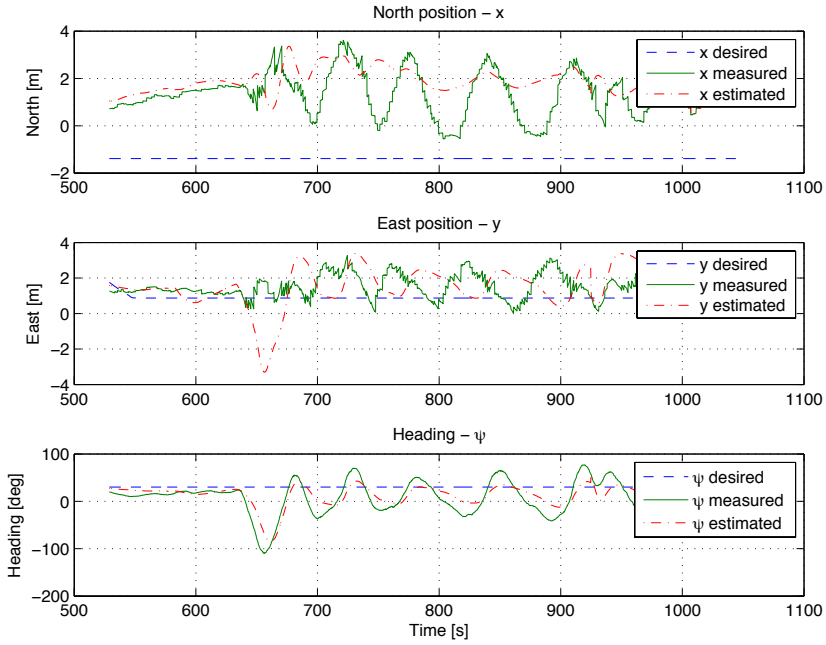

Figure 5.6: Plot showing the performance of the observer

It was obvious that the observer could not be used with this performance. A attempt was therefore made to use the standard kalman filter that was developed for use with Minervas regular control system. It was first run *offline*, meaning that the control loop was not running and Minerva was manually controlled. A plot showing the positions during this test is shown in figure 5.7. During the

offline period the observer performed pretty good. But when the control system was started (at time 800 in the plot) the observer started to overestimate the motions caused by the thrusters of the ROV, so the system started oscillating. The conclusion was that neither this observer could be used, nor the observer designed for use with the Xmas tree.

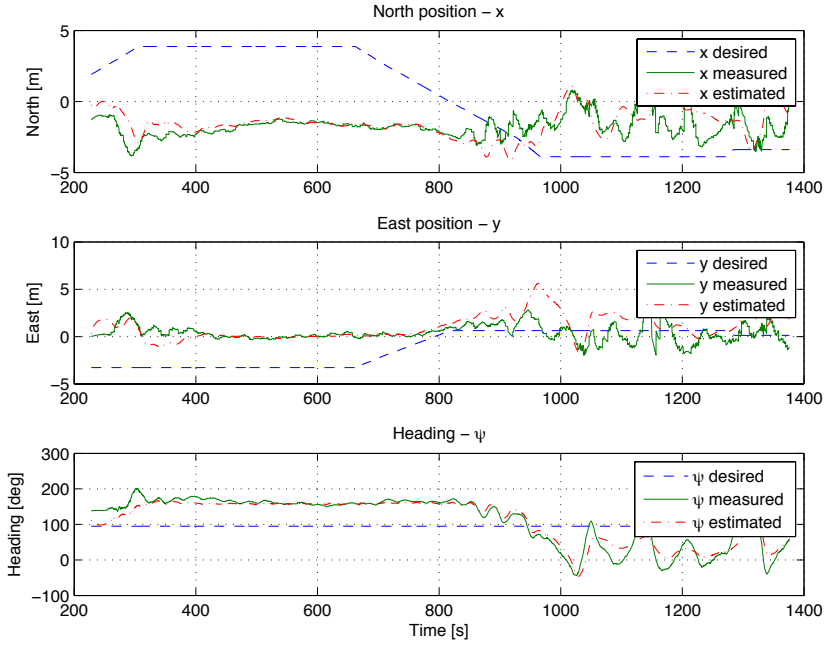

Figure 5.7: Plot showing the performance of the observer

The observer was therefore bypassed, so the controller got unfiltered state measurements. This seemed to improve the situation, and the system started stabilizing. At the time it was assumed that the cause of the bad behavior of the observer was an error in the estimation of the restoring force for the module or a something wrong with the mass matrix. Debugging of the observer was not started because of the limited time left for testing. Instead the motion tests were started with raw measurements as input to the control system.

5.2.3 Controller

During these motion tests the controller was struggling to control the positions of the XT module, but it seemed to manage to control the position in the horizontal

plane to some extent, but not the heading of the system. This seemed strange as the heading was very easy to control manually, before the control system was activated. After some discussion a theory was launched that the module was pushed so far out of its equilibrium that there was no more thrust capacity left for controlling the heading. This was a phenomenon that earlier had been seen during simulations. To verify this theory the controller gains for surge and sway was set to zero, making a controller that only controlled the heading.

Heading Controller

The performance of the heading controller is shown i Figure 5.8. It is seen that this controller is very much capable of controlling the heading for the system. This strengthened the theory that is was a lack of thrust capacity that led to the lacking performance for the heading control earlier.

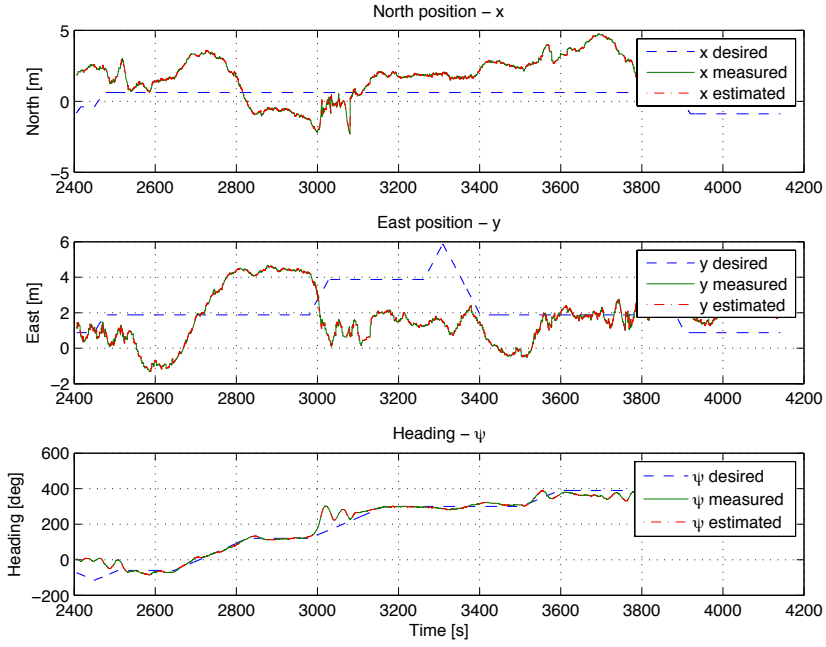

Figure 5.8: Plot showing the performance of the heading controller

3-DOF controller

With the results from the heading controller test in mind we reactivated the the 3-DOF controller. When it was reactivated we made sure that the setpoint was close to the equilibrium point of the system. This way we made sure the Minerva had some room for action, and should then be capable of moving the XT-model according to the setpoints given. A short test was done where we did some short moves in North and East direction as well as in heading. This went ok, so it was decided to move on to make a docking attempt.

The plan for the docking attempt was to keep an eye on how much force the ROV used in the different directions. This way we would know if we started to move far out of the equilibrium position. If this was detected the captain of the ship was asked to move the ship a bit, so the equilibrium point would move a bit closer to the setpoint, making the job easier for the ROV.

Figures 5.2, 5.10 and 5.11 shows different parameters that was recorded during the docking attempt. Figure 5.9 shows the desired and measured positions of the XT-model. Figure 5.10 shows the commanded thrust force that was the output from the controller, while Figure 5.11 is showing the depth of the ROV during the operation.

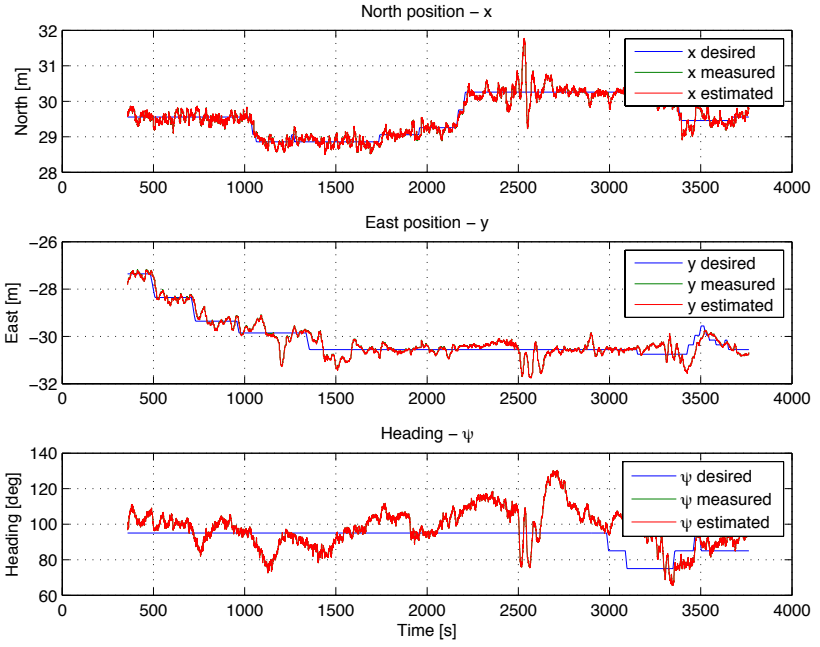

Figure 5.9: Plot showing the docking North east and ψ during docking

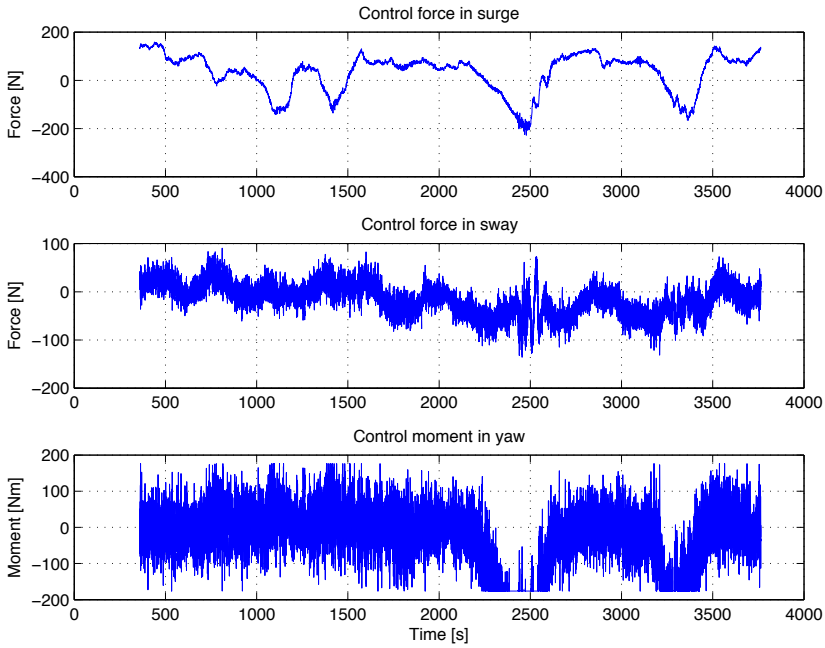

Figure 5.10: Plot showing the commanded thrust force during docking

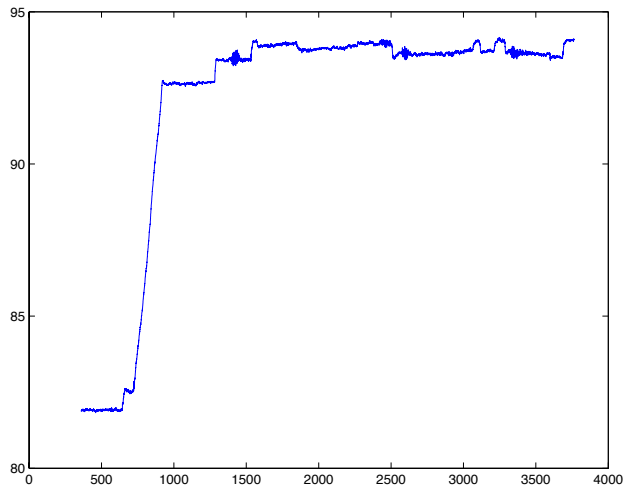

Figure 5.11: Plot showing the depth during docking

As seen in Figure 5.11 the XT-model was first lowered from a depth of about 82 m to 93 m. At 93 m depth, the bottom frame was spotted trough the camera on the ROV. The lowering was therefore stopped, and the aligning of the model was started. This was done by using the visual input from the camera to estimate how much we needed to move in order to be aligned with the docking frame. After a while we believed that we had a pretty good alignment and started to lower the model even further. The model was now so close to the bottom that it started to whirl up the bottom, so the view was clouded. This made it hard to do the last fine tuning of the alignment, so it was decided to wait a while and see if the view became better. At time 2500 s in the plot the module hit the docking frame accidentally, due to slip in the winch. The module was then hoisted up 1 m. This caused the disturbances seen in Figure 5.9 at this time. At time 3000 s the last fine tuning before docking was initiated. At time 3650 s a docking attempt was made. The result can be seen in Figure 5.12.

In figure 5.9 it is seen that the module is held pretty close to the setpoint both in the North and East direction, while the performance is not quite as good in heading. When looking at Figure 5.10 it is possible to observe the effect of moving the the ship to make the job easier for the ROV. As the heading was about 90° the surge force of the ROV was working in the east direction. It is seen that in the beginning of plot the setpoint is moved towards the west, and we see that the surge force of Minerva is decreasing towards $-200N$ (right after 1000 s). This is the maximum negative Minerva is capable of producing, so we decided to move the ship. And after a short while the commanded force is slightly positive, making more rom for action.

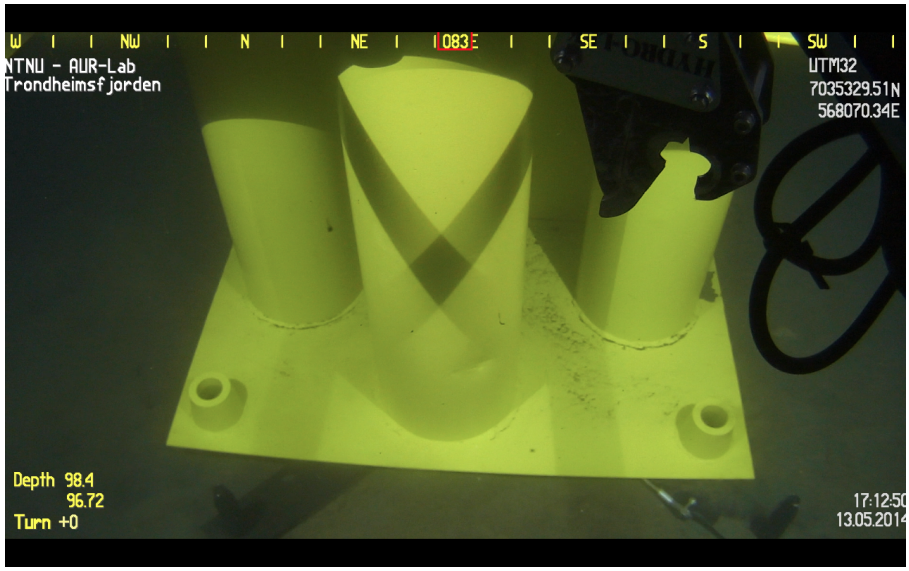

Figure 5.12: Picture showing the end position of the Xmas tree

Chapter 6

Discussion

In this chapter we are going to take closer look at the results that are presented in Chapter 4 Simulations and in Chapter 5 Experimental Testing. The result from the two chapters are first studied separately. In the last section we compare the simulation results to the results obtained at sea.

6.1 Simulation Results

In this section we are studying the results from the simulations that are presented in Chapter 4. Both simulations of the full scale system and the experimental scale are presented.

6.1.1 Full Scale Simulations

The presented simulations done with the full scale model was trying to study three aspects of the presented material in this thesis. That is the validity of the simulation model, the feasibility of using the proposed control system for governing the movement of a Xmas tree and how well this control system is capable of suppressing the wave induced motions of a Xmas tree that is installed in shallower waters. In addition we are going to discuss how the depth affects the performance of the system.

Model Validity

In Figure 4.2 a simulation done using just the model of the Xmas tree is shown. In this simulation we see that when the simulation starts the XT starts to move a

bit with the current (in N- and E-direction), then oscillates a bit around the equilibrium point before it comes to rest. This is the exact response that is inuitively expected from a 3d pendulum in a fluid. If we take a look at the equilibrium point of the Xmas tree, we see that this is at a distance $d = \sqrt{(0.12m)^2 + (0.22m)^2} = 0.25m$ away from where the lifting wire is piercing the surface. In Figure 6.1 a the wire position is plotted against depth when lifting an object with the same weight, drag coefficient and projected area as the XT has in x-direction in a current of 0.1 m/s. The wire position is calculated with the method shown in section 5.3 in Nielsen [2007]. These results are in accordance with each other. The difference is attributed to the fact that the XT in not facing directly towards the current in the simulation.

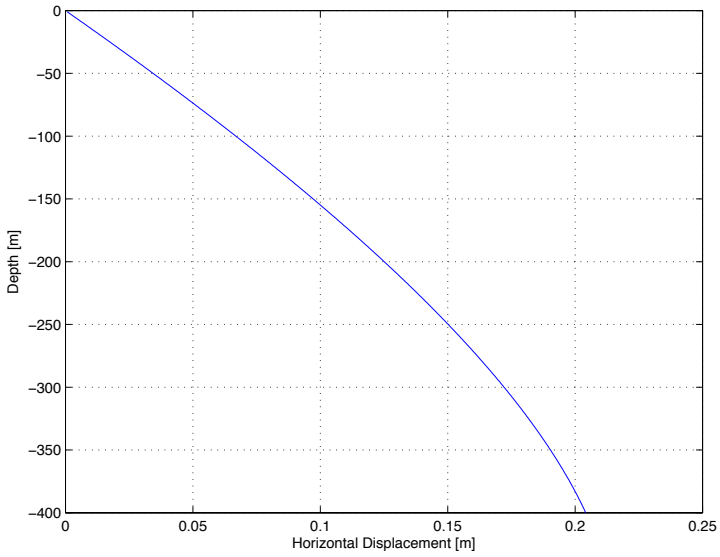

Figure 6.1: Figure showing lifting wire horizontal displacement at different depths when lifting XT

If we take look at the yaw plat in the same figure we notice that the XT does not change heading. The current is coming in with a heading of 270° and we would expect that the Xmas tree would rotate in yaw during these conditions. The reason it does not do that is because the damping matrices are diagonal and without coupling terms. In this system we would expect couplings between surge and yaw, and sway and yaw. These coupling effects are not modelled due to lack of information about the hydrodynamical properties of the Xmas tree. It is however assumed that these coupling forces are small, and that they safely can be neglected in this model.

In figure 4.1 the ROV is connected to the Xmas tree, but the control system is not activated. In this case we see that the Xmas tree is pushed a bit further downstream than without the ROV, and that the heading is changing so the XT is facing the current head on. We see that the inclusion of the ROV in the model adds the coupled forces we were missing in the Xmas tree model. The fact that this system is pushed a bit further downstream than the XT alone is natural as the drag forces are also working on the ROV in addition to the XT. However in reality the XT would cause a shadowing effect for the ROV when the ROV is situated downstream. This effect is not modelled. As this effect is getting larger and larger with higher water speed, we can conclude that if the model are going to be used in high water velocities this should be included. It is however assumed that this effect can be neglected at the water velocities that are relevant for installation of XTs.

Control System

In Section 4.1.2 the result from three simulations are shown. These simulations were run to check if the ROV using the control system was capable of governing the motions of a Xmas tree. The ROV passed the tests and we can conclude that it is in fact capable of controlling the Xmas tree. However as mentioned in Section 2.2 will need a decent thrust capacity to do so. In the first stages of the work with this thesis a model of NTNUs ROV SF30k was used, this ROV was capable of controlling the motions of the XT to some extent, but only when placed in the ideal positions where it could work directly towards the current or with no current present. It was however discovered that other commercial working class ROVs had a lot more power, so the thrust capacity of the model was scaled up to the level of these. This improved the situation considerably and we had showed that this is a feasable solution for installing Xmas trees.

The Effect of Depth

If we compare the results from the second and third simulation that is discussed in the previous section, shown respectively in Figure 4.6, 4.7, and4.8 and in Figure 4.9, 4.10 4.11, we can see how the depth of the Xmas tree affects the performance of the control system. In the simulation that is done at 400 m depth we see that the XT is following the reference almost perfectly, while at 100 m depth it struggles to keep the XT exactly on the reference while moving. When we look at the figures that is showing the controller output force we see that the commanded force is a lot larger in the shallower simulation. This is not surprising when we look at Figure 6.2 that is showing how the restoring stiffness are developing through different depths. We see that the stiffness is about three times larger at 100 m depth than at 400 m. This means that this system will be performing better the deeper the Xmas tree is placed, and that the thrust capacity of the ROV is a more important parameters for shallower installations.

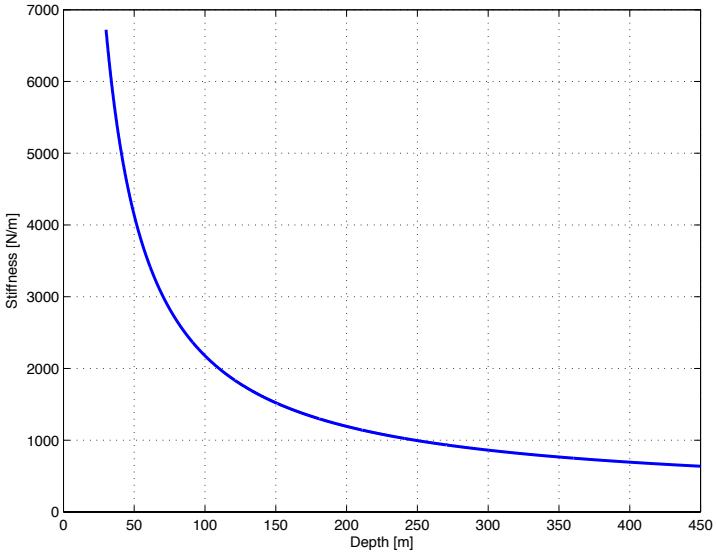

Figure 6.2: Figure showing the horizontal stiffness vs depth for the full scale XT

Waves

In Table 4.1 we can see how well the control system is capable of suppressing the wave induced motions on the XT. This is to investigate to investigate how the control system handles these motions, and if this system can expand the weather window for the installation operation. The model used in the simulations are a very simplified model and do not consider a series of effects that is assumed to have impact on the real response of the XT in waves. In order to get a more realistic simulation of this we would need to know more about the ship wave response, the dynamic properties of the lifting wire and how the vertical motions of the Xmas tree are coupled with horizontal forces. Even if the simulations are simplified they say something about how well the control system is to suppress the oscillations that is caused by the waves.

The simulation is conducted with four different sea states at 100 m depth. In general we can see that the wave induced motions are quite small at the sea states with the lowest peak periods, while at the sea state with peak periods of 30 s the waves are actually causing a significant response of the XT. When comparing the controlled and uncontrolled value we see that the control system is suppressing the wave motions quite good. It is assumed that the system can suppress wave motions even better if acceleration feedback is added to the controller. However if a Xmas tree installation are to be performed during the sea states studied here it will be

the motion damping systems on the installation vessel that is the dimensioning factor for the operation.

6.1.2 Experimental Scale Simulations

The simulations done with the experimental scale model is studying the properties and performance of the experimental setup. In Section 4.2 four simulation cases is presented. The first case is looking at how a noisy and sampled sensor feedback affects the performance of the system, the second is studying the thrust allocation of ROV Minerva, the third is looking at the robustness of the system while the last is the results from the HIL-simulations done to test the reimplemented control system that was actually used during the experimental testing.

Sensor Feedback

In Figure 4.12 and 4.13 the results from a simulation where both the measurements and the observer is included in the model. It should be noted that this simulation was performed with the Minerva model as the ROV, and due to its limited thrust capacity the tuning of the controller is less aggressive than the tuning for the larger ROV showed in the previous simulations. This results in a small transient in the beginning of the simulation where the ROV need some time to compensate for the current.

The first thing this simulation shows is that the control system is capable of controlling the position of the XT-model. The Xmas tree is following the reference signal quite good. The second thing it shows is that the EKF is working as intended. Unlike the previous simulations we are using the observer as feedback and the sensor noise and sampling is turned on. When we take a look at the red lines in Figure 4.12 we observe that the estimated position is following the real position (in blue) very well. On the first row in Table 4.2 this simulation is used as a performance reference, and we see that the RMS value of the position error in the north and east directions is about 6-7 cm, while the value for heading is about 3°. This is considered to be quite good.

Thrust Allocation

The limited thrust capacity of the ROV Minerva combined with the thrust allocation that was implemented proved to be a problem when we wanted the ROV to control the motions of the XT model. The Control system needed all the thrust available, and the thrust allocation appeared to behave rather unpredictable when the commanded thrust was close to the limits of what Minerva could deliver. This can be observed in Figures 4.14 and 4.15 showing a simulation where the ROV is asked to make an impossible move, and in Figure 3.4 and 3.3 that is showing

the commanded thrust vs allocated thrust for both the standard thrust allocation and a prioritized one. When we look at the simulation results we see that the first thing that happens is that the system is not capable of keeping the desired heading. Its heading changes from 90° to 225°, so it is facing the same direction as the current. When this happens the position in north and east direction is lost as well.

As a response to this problem a prioritized thrust allocation was implemented. This thrust allocation is prioritizing thrust in yaw so the Xmas tree will not loose the heading. This thrust allocation is also constrained so the commanded thrust in one direction only causes a force in this direction, and do not allocates thrust in extra directions to fullfill the thrust demand in the commanded direction. This for instance can happen if a large yaw moment is commanded, then the two horizontal thrusters are run opposite ways to create a moment, but due to the flow conditions around the propellers they will produce more thrust in the forward direction, than backwards. So when the backward propeller hits its saturation limit the standard thrust allocation will further increase the speed on the forward going propeller. This will result in a larger yaw moment, but in addition we get a force in surge as well. With the constrained thrust allocation this will not happen.

In this thesis it was early decided that the existing thrust allocation in the ROV should be used. This was a way of limiting the scope of the thesis. However when the thrust allocation was studied in more detail it was discovered that this might not be the best idea. A good example of this is the use of the lateral thruster on Minerva. This thruster is placed in front of the centre of gravity on the ROV. When a positive yaw moment is commanded this thruster is creating a positive force in sway, causing a positive moment on Minerva. If we however take a step back and consider the complete system we will notice that the the lateral thruster is behind the CG of the system, so when this thruster is producing a positive force, the effect of the system will be that this thruster individually is producing a negative yaw moment. This negative moment is neutralized by the positive moment made by the other thrusters, but on a system level we clearly see that this way is not optimal.

One way of solving this challenge is to redesign the whole thrust allocation. Another one is to make a more sophisticated way of translating the desired force vector from the origin of the XT to the ROV. This could be implemented as a sort of preallocation. This subject is however not treated further in this thesis but is included in the recommendations for further work.

Robustness and HIL-simulation

Table 4.2 shows the RMS values of the position and heading errors during a set of simulations with parameter variation. These simulations were done in order to study how robust the system was to modelling errors. This is an important test to do before the testing as we are not capable to model the system perfectly. In this

way we make sure that modelling errors do not have large impacts on the behavior of the system during tests, so we get the results we want.

If we take a look at the values in this table we see that all the north and east error values are below 10 cm, while the largest value in heading is 3°. This is quite good considered the magnitude of the parameter errors. When we look at Figure 4.18 and 4.19 showing the simulation with the worst performance we observe that the control system still manages to move the model along the desired pattern. The performance decrease is mainly attributed to the observer as this seems to give a somewhat biased position estimate during the moves of the Xmas tree so the controller believe it is on position while it is actually not. The controller does not have any model parameters and is creating the desired force vector only based on measurements. It is assumed that this gives better robustness against modelling errors than a controller using model based feedforward.

In Section 4.2.4 the results from a set of simulations that are conducted using the HIL-simulator is done. This simulator let us test actual control system on the same hardware that is used aboard the ship. The main purpose of doing these simulations is to verify that there are no bugs in the control system, as well as tuning the system roughly.

In the section the result from three simulation scenarios are shown, that is stationkeeping, rotation and a square move. All the scenarios are showing that the control system is working as expected, but there are some need for tuning.

In the first simulation that were done using the HIL-simulator the tuning parameters was the same as the ones that gave good performance in the Matlab Simulink simulations. The result of this simulation can bee seen in Figure D.5 and D.6 in Appendix D. In this simulation the output from the extended kalman filter is quite smooth, but there is a delay. This time delay caused the system to oscillate. The covariance matrices of the filter was therefore tuned in order to get a faster response. The response in the simulations presented in Section 4.2.4 is faster, and we see that the oscillations are gone. But the estimates are quite noisy, and this makes the job hard for the controller.

At the time these simulations where done the HIL-simulator did not include simulations of all the sensors that Minerva are equipped with, and the the output noise from the sensors that are simulated are not exactly the same as the real ones. Due to this fact no more time was spent trying to tune the system, as this probably had to be repeated when the system was connected to the real ROV. The tuning was therefore postponed. It should be noted that a fellow student is currently working on improving the HIL-simulator, so it will be more realistic.

6.2 Experimental Results

In this section the results from the experimental testing that are presented in Chapter 5 are discussed. The testing was performed using ROV Minerva and a scaled model of a Xmas tree that was lowered from R/V Gunnerus. During the two days aboard Gunnerus some problems emerged. Some of these problems was fixed and some was not. Anyhow a lot of lessons were learned during these days.

6.2.1 Finding the Error in the Control System

Shortly after the testing was finished the hunt for the error that caused the problems with the observer started. This error is described in Section 5.2.2. After some time trawling through the code of the control system an error was found. The error was in the $\boldsymbol{r}$ vector that specifies the distance between the origin of the Xmas tree to the centre of the ROV. This length was measured aboard the ship, after the interface frame was mounted to the ROV. Then it was entered into the control system, and when this was done it was entered with the wrong sign. This meant that the control system believed that the XT-model was situated behind the ROV, while in reality it was in front.

When this error was discovered a simulation was set up in order to investigate what kind of effects this error would have, and if this error could explain the responses that were seen during the testing. The result from this simulation is shown in Appendix E.

In figure E.1 the result from the first one of these simulations is shown. If we compare this plot to the plot showing the observer response during testing found in Figure 5.6 we see that the response is very similar. It was then concluded that this was in fact the error that caused the problems with the state estimation.

We therefore moved on to investigating the effect this error had for the controller, as the same parameter is used here to translate the desired force vector from the XT to the body frame of the ROV. During the testing we did not have any trouble controlling the north and east position of the XT model as long as the heading was close to the set-point, but the controller did however struggle a lot when the heading was changed. Considering what the error was, this corresponds well to what our intuition tells us. A simulation was therefore run where we tried to rotate the Xmas tree 180°. The result from this simulation can be seen in Figure E.2, E.3 and E.4. We see that insted ov the ROV moving around the Xmas tree as intended, the ROV moves the tree around itself, an at the same time it is moving around the point where it thinks the Xmas tree is. In this simulation the Initial position of the Xmas tree was very near the equilibrium point. Because of this the control system actually managed to follow the desired heading quite good, but it is not hard to see that this can cause the control system to struggle a bit to make changes in the heading.

6.2.2 Experimental Setup

There are room for improving the experimental setup that was used in the testing. In this section we are going to point out a couple of changes that could be done to make the setup even better.

The first thing is the design of the guideposts on the docking frame. These should been made a lot longer, and they should have been painted in a color that was easy to see even when it is dark. Now they are painted black, and was therefore quite hard to spot at the seabed. In addition the subsea module was whirling up particles from to bottom that made the situation even more difficult. This could have been avoided if the guideposts were longer.

In addition to the poor visibility during the last part of the docking attempt it was quite difficult to decide if the model was aligned properly using only the views from the cameras mounted on the ROV. A camera placed outside the module with a live feed to the control room would make this a lot easier. This camera could either be placed over the module looking down, or on the seabed looking at it from the side. If this is combined with some sort of alignment marks it would be a lot easier to verify the alignment before the module is lowered down the last part. In addition it would be a clear advantage if the alignment funnels had a larger diameter, making more room for error.

The last thing in the setup that would benfit from a design change is the interface frame on the ROV. The frame did its job as intended, but it was a little wobbly. It would certainly benefited from having a stiffer design.

6.2.3 Experimental Results

Even though we ran into some problems during the experimental testing we managed to verify that some parts of the designed control system was working. We did not get to test the observer properly due to the error that is described in Section 6.2.1, and due to the same error the controller did work completely as intended.

We did however manage to control the heading quite good using the decoupled heading controller described in Section 5.2.3. This can be seen when looking at the plots in Figure 5.8. Even if this controller is not fulfilling the whole control objective, this result shows that the ROV is in fact capable of controlling the heading of the whole system, using the control strategy that is proposed. The error in the control system did not apply to this controller as it do not care about the north and east positions. Therefore it is not trying to move the XT the extra distance that is seen in figure E.3.

During the last part of the experimental testing the 3-DOF controller was tested, and used during a docking attempt of the XT-model. In this phase of the testing most of the position changes was done in the north and east direction, and the

changes in heading was small. As the error in the control system was most evident during changes in heading, the error was not so apparent in this phase. And as we might expect, when we look at Figure 5.9 we see that the controller is actually working, even though its performance is degraded due to the missing observer.

So to summarize the experimental results we are confident that the control strategy proposed in this thesis is actually working, and that the control system will be capable of performing at the same level as it does in simulations in full scale, when the error is corrected and it is tuned properly.

6.3 Additional Comments

A secondary objective of the testing was to get indications on how realistic the simulation model is compared to the real system. Due to the problems that were encountered during the testing this was not an easy task. It might however seem like the restoring forces was a bit bigger than what the model predicted, even though the tests was conducted in shallower waters than planned. This might be because of a heavier model than expected, or may be actually be attributed to the problems with the control system. This suspicion was raised when the commanded control force was monitored during the docking attempt when the controller seemed to reach saturation after quite short moves.

Chapter 7

Conclusions and Further Work

7.1 Conclusions

A new installation method for subsea Xmas trees is emerging. This method is using a single wire to lower the Xmas tree, and no guidewires. In order to align the Xmas tree to existing interfacing structures on the seabed, an ROV is used for positioning. The control of this ROV is manual today but it is evident that it would be advantageous to automate this. This thesis has investigated such an automated system and proposed a design. The design is tested through simulations and during experiments on a downscaled model and NTNUs ROV Minerva.

A model has been developed in order to simulate the motions of the Xmas tree while an ROV its trying to control its position and orientation. The model is composed out of a standalone ROV-model, a standalone model of a Xmas tree that hangs in a wire and a model of the interaction forces between these. In addition environmental models and sensor signal modelling is added to the model. This model is then used to simulate the controlled system, both in full scale and in experimental scale.

A hybrid control system is proposed where several controllers are available in order to control the ROV both while it is positioning a Xmas tree, and while doing other tasks. A controller that is capable of governing the motions of the Xmas tree has been designed. This controller is intended to be a subset of the hybrid controller. The control design consists of a state observer, a reference model and the controller itself.

The control system was studied through simulations done in Matlab Simulink. The system was simulated both in full scale and in experimental scale. The control

system showed very good performance in simulations.

In order test the system an experimental setup was designed and produced. The setup consists of a scaled model of a subsea xmas tree, a docking frame and a interface frame that connects the ROV to the Xmas tree model. The control system was reimplemented in LabView in order to be used during testing in the Trondheim fjord.

During the experimental testing some problems was encountered. The main problem was an error in the control system that made it impossible to use the observer, and degraded the performance of the controller. Despite this error that was discovered after the testing, we managed to get some promising results from the testing and was able to position the Xmas tree model only about 20 cm from its target.

As this error is now discovered and corrected further testing should be done in order to verify the functionality of the system.

7.2 Recomendations for Further Work

Even if a lot of work with this control system has already been done, the bulk is still ahead if this is going to be used in full scale. This section will therefore focus on the work that can be done within the NTNU cummunity and in AUR-lab. This will represent the first step towards a full scale implementation.

7.2.1 Testing

First of all the system needs more testing, and in order to have a greater chance of succeed with this testing one should consider some changes is the experimental setup. The first test revealed some weaknesses with the current setup, and these should be quite easy to fix. This includes extending the guideposts on the bottom assembly and painting them in a color that is easily visible in the dark, enlarge the alignment funnels on the bottom of the XT-model and using extra cameras in order to verify the alignment of the module.

More testing is needed to test if the control system is actually working when the error that caused problems during the testing in this thesis has been corrected. Proper tuning of the system should also be conducted during this testing. In addition test using NTNUs larger ROV SF30k may be considered.

7.2.2 Added Mass and Damping Refinement of the Mathematical Model

The mathematical model of the Xmas tree is also an important subject for further work. The model that is developed in this thesis is modelling the main phys-

ical properties of the Xmas tree model, but there is a need for refinement and verification of the model.

Two approaches is suggested for refining the model. The first one is to use the physical model that was made for the experimental testing to perform experiments. Experiments that will make it possible to calculate the hydrodynamical properties of the model like added mass and the drag forces include towing tests of the module and oscillation tests. In a free oscillation test it is possible to decide the added mass by looking at the frequency of the oscillations, and the damping may be calculated by looking at the decay rate of the oscillations. Such a test may be performed while the Xmas tree model is hanging in a wire. It could then be pulled out of equilibrium to start an oscillation similar to the one seen in 4.1. A alternative strategy for experimental testing is *adaptive estimation*. In this approach one can either let an adaptive estimation algorithm run offline, or as a part of the control system like its done in Skjetne et al. [2004].

It is also possible to to set up experiments in the towing tanks at MARINTEK using the XT-model. This is also suggested by Kjemperud [2011]. Such tests can be used to decide the damping terms, as well as added mass of the Xmas-tree model.

The other approach is the same as is used for deciding the hydrodynamical properties for ROV SF30k in Berg [2012]. Here the geometry of the ROV is simplified in a 3d model in order to make it feasible to run this model through the 3d potential theory program WAMIT. This code is capable of calculating both 3-dimensional added mass and potential damping terms. It was the intention in Kjemperud [2011] to do this, but it was not conducted do to problems in the setup of the simulation. If this approach is used, the physical model that was made in this thesis might be used for verification using the experimental methods above.

7.2.3 Thrust Allocation

As discussed in earlier sections of this thesis the way the thrust is allocated in the control system presented in this thesis is not optimal. Further investigation in how to make this better should be done.

7.2.4 Additional Sensors

In order to get a good estimate of the Xmas tree position it is proposed to add extra sensors during the installation process. If possible they should be installed on the running tool, which is the physical interface between the wire and the Xmas tree. This way the mounting of these extra sensors will not impose extra work during the installation process.

The most important state to measure is the position of the Xmas tree. This should therefore be measured by adding an acoustic interrogator to the running tool. In order to get an even more accurate positioning reference it is proposed to add one or more video cameras and use computer vision techniques to get an additional position reference. The use of video cameras as a position reference is described in Xu and Negahdaripour [1999] and Caccia [2006]. It is today common to use alignment marks on the Xmas tree and the interfacing structure to confirm that the Xmas tree is properly aligned before it is lowered down the last part. If these alignment marks are made visible to the computer vision cameras it should be possible to use them as a relative reference that will make the position estimate more precise. Such alignment marks can be seen in figure 7.1. A computer vision system will have a higher update frequency than the hydroacoustic positioning reference, and it will therefore be easier to detect smaller changes in the position of the Xmas tree.

Figure 7.1: Alignment marks on Xmas tree and subsea structure

In addition to the hydroacoustics and the computer vision it is a possibility of

installing a set of accelerometers and/or a gyroscope on the running tool. This will help the state estimator but more importantly it will add fault-tolerance to the system by making so called *inertial navigation* possible. Inertial navigation is to use accelerometer measurements to estimate velocity and position based on an internal model. This will make the system more fault tolerant by making an alternative position reference in the case where no position measurement is available.

Bibliography

S. Arimoto and F. Miyazaki. Stability and robustness of pid feedback control for robot manipulators of sensory capability. In M. Brady and R. Paul, editors, *Proceedings of the 1st International Symposium on Robotics Research*, pages 783–799. MIT Press, 1984.

Karl Johan Åstrøm and Bjørn Wittenmark. *Computer-Controlled Systems: Theory and Design*. 1996.

Viktor Berg. Development and commissioning of a dp system for rov sf 30k. Master's thesis, Department of Marine Technology, Norwegian University of Science and Technology. Trondheim, Norway, 2012.

Massimo Caccia. Laser-triangulation optical-correlation sensor for rov slow motion estimation. *Journal of Oceanic Engineering, IEEE*, 31:711–727, July 2006.

Mauro Candeloro. Design of observers for dp and tracking of rov "minerva" with experimental results. Master's thesis, Department of Marine technology, Norwegian University of Science and Technology. Trondheim, Norway, 2011.

R. Christ and R. Wernli. *The rov manual - a user guide for observation-class remotely operated vehicles*. Elsevier, 2007.

Daniel de A. Fernandes, Fredrik Dukan, and Asgeir J. Sørensen. Reference model for high performance and low energy consumption motions. *Navigation, Guidance and Control of Underwater Vehicles*, 3(1), 2012.

DNV. Recomended practice dnv-rp-c205, environmental conditions and environmental loads, October 2010.

Fredrik Dukan, Martin Ludvigsen, and Asgeir J. Sørensen. Dynamic positioning system for a small size rov with experimental results. *OCEANS, 2011 IEEE - Spain*, pages 1–10, 2011.

Encyclopedia Britannica Online. Ocean current, December 2013a. URL `http://global.britannica.com/EBchecked/topic/424354/ocean-current`.

Encyclopedia Britannica Online. Tides, December 2013b. URL `http://global.britannica.com/EBchecked/topic/595148/tide`.

Odd Magnus Faltinsen. *Sea Loads on Ships and Offshore Structures*. Cambridge University Press, 1990.

FMC Technologies. Product datasheet, scilling robotics hd rov, 2014.

Forum Energy Technologies. Product datasheet, perry xlr 125 work class rov, 2014.

Thor Inge Fossen. *Nonlinear Modeling and Control of Underwater Vehicles*. PhD thesis, Department of Engineering Cybernetics, Norwegian University of Science and Technology. Trondheim, Norway, 1991.

Thor Inge Fossen. *Handbook of Marine Craft Hydrodynamics and Motion Control*. John Wiley & Sons, Ltd, 2011.

Eirik Hexeberg Henriksen. Offshore installation of xmas tree using rov. Project Thesis, Department of Marine Technology, Norwegian University of Science and Technology. Trondheim, Norway, 2013.

Jennifer Pallanich Hull. Mariner energy saves time, money with new approach to tree installation. *Offshore Magazine*, 64(2), 2004.

Rudolf Emil Kalman. A new approach to linear filtering and prediction problems. *Journal of Basic Engineering*, pages 35–45, 1960.

Marianne Kirkeby. Comparison of controllers for dynamic positioning and tracking of rov minerva. Master's thesis, Department of Marine technology, Norwegian University of Science and Technology. Trondheim, Norway, 2010.

Stig Kjemperud. Hydrodynamic coefficients for wellhead structures. Master's thesis, Department of Marine Technology, Norwegian University of Science and Technology. Trondheim, Norway, 2011.

J. P. LaSalle. Stability theory for ordinary differential equations. *Journal of Differential Equations*, pages 57–65, 1966.

Martin Ludvigsen. *An ROV toolbox for optical and acoustical seabed investigations*. PhD thesis, Department of Marine technology, Norwegian University of Science and Technology. Trondheim, Norway, 2010.

David Luenberger. Observing the state of a linear system. *IEEE Transactions on Military Electronics*, pages 74–80, April 1964.

Timofey Mukha. Modeling large equipment behavior in the sea splash- zone using methods of computational fluid dynamics. Master's thesis, Department of Applied Mechanics, Division of Fluid Dynamics, Chalmers University of Technology. Gothenburg, Sweden, 2012.

Dong T. Nguyen, Asgeir J. Sørensen, and S. T. Quek. Design of high level hybrid controller fo dynamic positioning from calm to extreme sea conditions. *Automatica* **43***(5)*, pages 768–785, 2007.

Dong T. Nguyen, Arild H. Sørbø, and Asgeir J. Sørensen. Modelling and control for dynamic positioned vessels in level ice. *8th IFAC Conference on Manoeuvring and Control of Marine Craft*, pages 229–236, 2009.

Finn Gunnar Nielsen. *Lecture Notes in Marine Operations.* Department of Marine Technology, Norwegian University of Science and Technology. Trondheim, Norway, 2007.

Jon Erling Gorset Refsnes. *Nonlinear Model-Based Control of Slender Body AUVs.* PhD thesis, Department of Marine technology, Norwegian University of Science and Technology. Trondheim, Norway, 2008.

Anne Marthine Rustad. *Modeling and Control of Top Tensioned Risers.* PhD thesis, Department of Marine Technology, Norwegian University of Science and Technology. Trondheim, Norway, 2007.

Roger Skjetne and Øivind Kåre Kjerstad. Recursive nullspace-based control allocation with strict prioritization for marine craft. *9th IFAC Conference on Control Applications in Marine Systems*, pages 49–54, 2013.

Roger Skjetne, ÃŸyvind N. Smogeli, and Thor I. Fossen. A nonlinear ship manoeuvering model: Identification and adaptive control with experiments for a model ship. *Modelling, Identification and Control*, 25(1), 2004.

Asgeir J. Sørensen. *Lecture Notes, Marine cybernetics: Modelling and Control.* Department of Marine Technology, Norwegian University of Science and Technology. Trondheim, Norway, 2013a.

Asgeir J. Sørensen. Lecture slides, tmr4240 - marine control systems. 2013b.

Sverre Steen. *Lecture Notes, Experimental Methods in Marine Hydrodynamics.* Department of Marine Technology, Norwegian University of Science and Technology. Trondheim, Norway, 2007.

Subsea 7. Vessel infosheet, skandi seven, 2014.

Espen M. Tolpinrud. Development and implementation of computer-based control system for rov with experimental results. Master's thesis, Department of Marine Technology, Norwegian University of Science and Technology. Trondheim, Norway, 2012.

H. H. Vanderveldt, B. S. Chung, and W. T. Reader. Some dynamic properties of axially loaded wire ropes. *Experimental Mechanics*, 13(1), 1973.

X. Xu and S. Negahdaripour. Automatic optical station keeping and navigation of an rov: Sea trial experiment. In *PProc. Marine Technology Society (MTS)/IEEE OCEANS*, volume 1, pages 71–76, 1999.

Martin Yarrow. Monohull deployment cuts time and cost of ormen lange tree installations. *Offshore Magazine*, 69(11), 2009.

Appendix A

Drawings of the Xmas tree

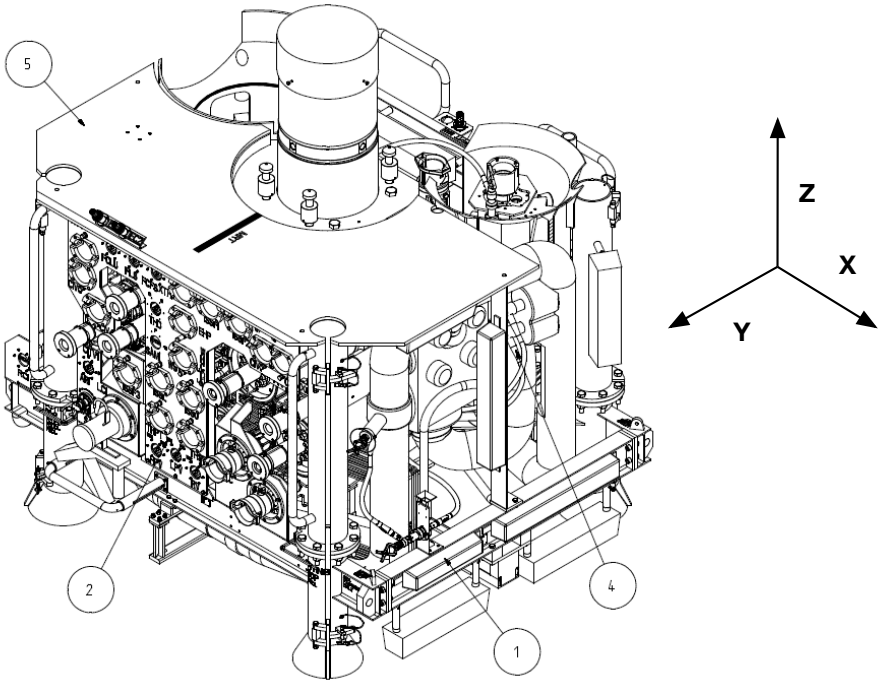

Figure A.1: Xmas tree with axes

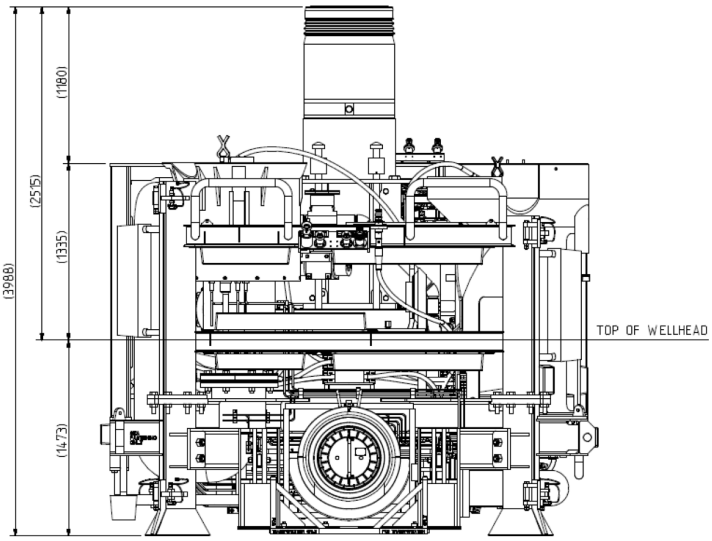

Figure A.2: Xmas tree seen from the side

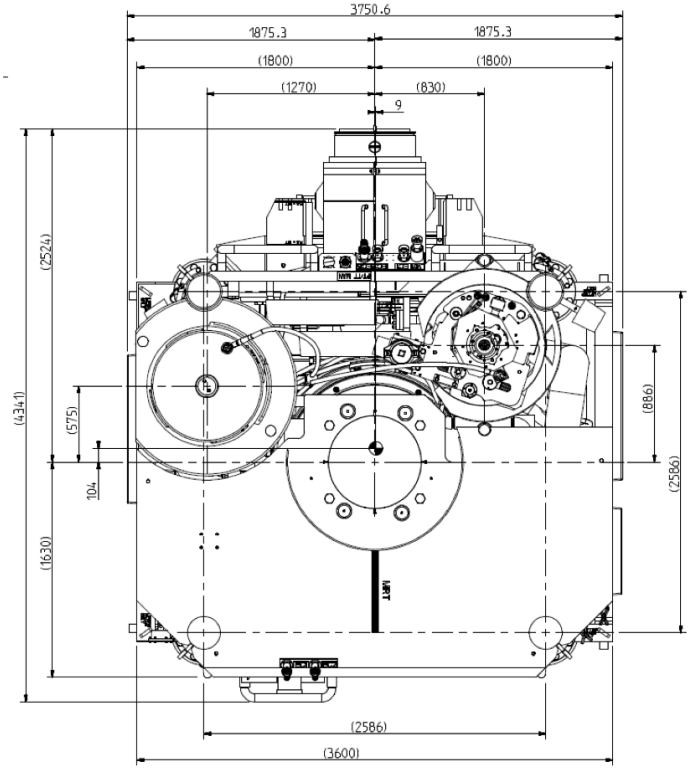

Figure A.3: Xmas tree seen from the top

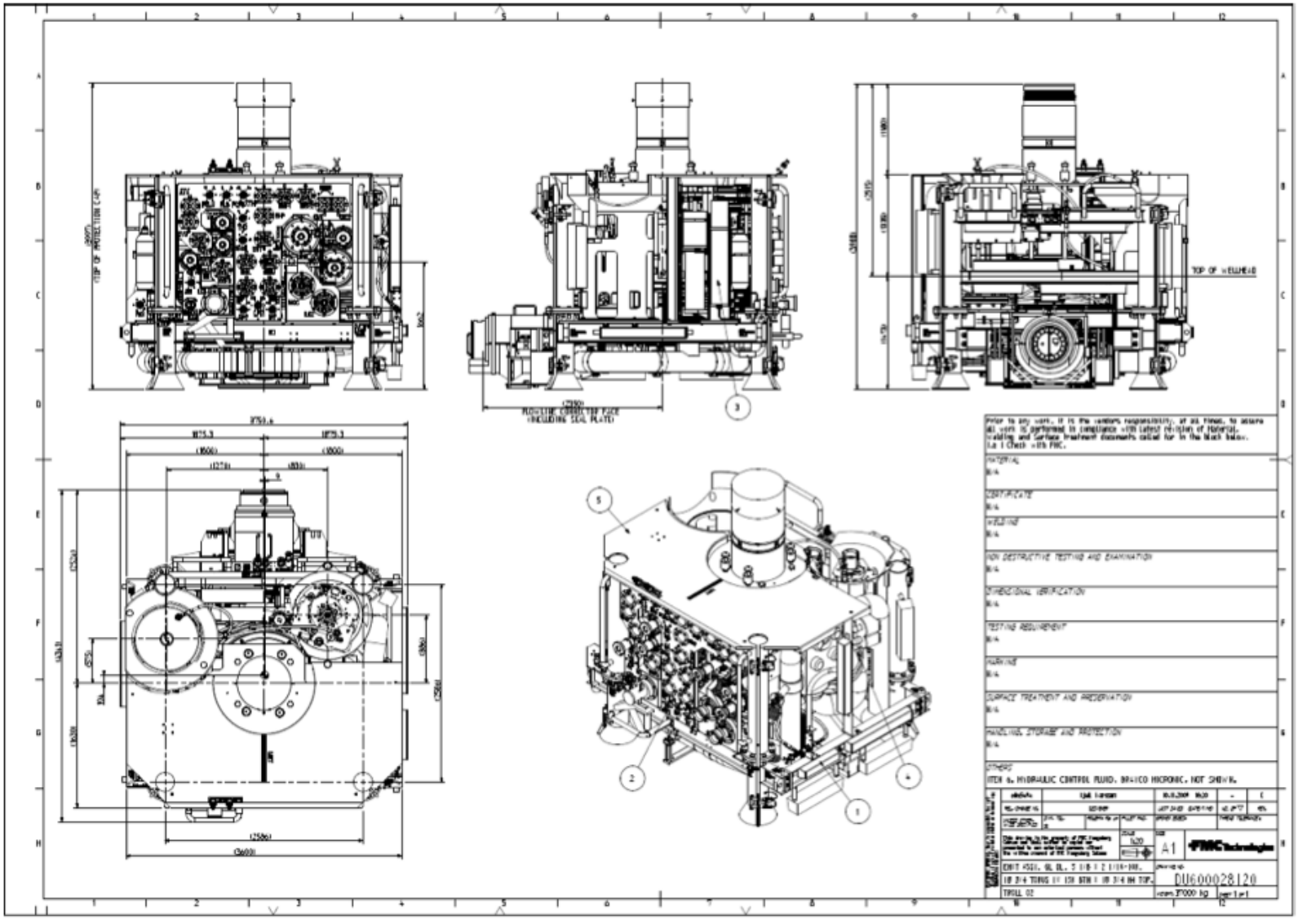

Figure A.4: Original drawings of Xmas tree

Appendix B

Model Parameters

In this appendix all parameters that were used during the different simulations is specified.

B.1 Full Scale Parameters Xmas tree parameters

Table B.1: The main physical properties of an FMC Technologies EHXT

Property	**Value**
Length	3.600 m
Width	2.586 m
Height	2.808 m
Weight	36000 kg

$$\boldsymbol{M}_{rb} = \begin{bmatrix} 36000 & 0 & 0 & 0 & 0 & 0 \\ 0 & 36000 & 0 & 0 & 0 & 0 \\ 0 & 0 & 36000 & 0 & 0 & 0 \\ 0 & 0 & 0 & 43717 & 0 & 0 \\ 0 & 0 & 0 & 0 & 62535 & 0 \\ 0 & 0 & 0 & 0 & 0 & 58942 \end{bmatrix} \tag{B.1}$$

$$\boldsymbol{M}_{a} = \begin{bmatrix} 21865 & 0 & 0 & 0 & 0 & 0 \\ 0 & 21865 & 0 & 0 & 0 & 0 \\ 0 & 0 & 21865 & 0 & 0 & 0 \\ 0 & 0 & 0 & 37477 & 0 & 0 \\ 0 & 0 & 0 & 0 & 82211 & 0 \\ 0 & 0 & 0 & 0 & 0 & 82211 \end{bmatrix} \tag{B.2}$$

$$D_l = \begin{bmatrix} 640 & 0 & 0 & 0 & 0 & 0 \\ 0 & 1336 & 0 & 0 & 0 & 0 \\ 0 & 0 & 5635 & 0 & 0 & 0 \\ 0 & 0 & 0 & 0 & 0 & 0 \\ 0 & 0 & 0 & 0 & 0 & 0 \\ 0 & 0 & 0 & 0 & 0 & 0 \end{bmatrix} \tag{B.3}$$

$$D_{nl} = \begin{bmatrix} 2807 & 0 & 0 & 0 & 0 & 0 \\ 0 & 5861 & 0 & 0 & 0 & 0 \\ 0 & 0 & 5398 & 0 & 0 & 0 \\ 0 & 0 & 0 & 2575 & 0 & 0 \\ 0 & 0 & 0 & 0 & 6956 & 0 \\ 0 & 0 & 0 & 0 & 0 & 7554 \end{bmatrix} \tag{B.4}$$

B.2 Experimental Xmas Tree Parameters

Table B.2: The main physical properties of the downscaled Xmas tree model

Property	**Value**
Length	1.0 m
Width	1.5 m
Height	1.2 m
Weight	880 kg

$$\boldsymbol{M}_{rb} = \begin{bmatrix} 880.0000 & 0 & 0 & 0 & 0 & 0 \\ 0 & 880.0000 & 0 & 0 & 0 & 0 \\ 0 & 0 & 880.0000 & 0 & 0 & 0 \\ 0 & 0 & 0 & 270.6000 & 0 & 0 \\ 0 & 0 & 0 & 0 & 178.9333 & 0 \\ 0 & 0 & 0 & 0 & 0 & 221.3113 \end{bmatrix} \tag{B.5}$$

$$\boldsymbol{M}_a = \begin{bmatrix} 499.9 & 0 & 0 & 0 & 0 & 0 \\ 0 & 499.9 & 0 & 0 & 0 & 0 \\ 0 & 0 & 499.9 & 0 & 0 & 0 \\ 0 & 0 & 0 & 1014.9 & 0 & 0 \\ 0 & 0 & 0 & 0 & 489.5 & 0 \\ 0 & 0 & 0 & 0 & 0 & 489.5 \end{bmatrix} \tag{B.6}$$

$$D_L = \begin{bmatrix} 158.6 & 0 & 0 & 0 & 0 & 0 \\ 0 & 158.6 & 0 & 0 & 0 & 0 \\ 0 & 0 & 336.4 & 0 & 0 & 0 \\ 0 & 0 & 0 & 49.8 & 0 & 0 \\ 0 & 0 & 0 & 0 & 7.2 & 0 \\ 0 & 0 & 0 & 0 & 0 & 5.8 \end{bmatrix} \tag{B.7}$$

$$D_{NL}(\boldsymbol{\nu}_r) = \begin{bmatrix} 695.7|\boldsymbol{\nu}_r| & 0 & 0 & 0 & 0 & 0 \\ 0 & 369.4|\boldsymbol{\nu}_r| & 0 & 0 & 0 & 0 \\ 0 & 0 & 869.7|\boldsymbol{\nu}_r| & 0 & 0 & 0 \\ 0 & 0 & 0 & 49.8|\boldsymbol{\nu}_r| & 0 & 0 \\ 0 & 0 & 0 & 0 & 24.0|\boldsymbol{\nu}_r| & 0 \\ 0 & 0 & 0 & 0 & 0 & 19.2|\boldsymbol{\nu}_r| \end{bmatrix} \tag{B.8}$$

B.3 Working Class ROV Model Parameters

This section presents the model parameters that is used for the Working Class ROV. These are derived in Berg [2012]. The only modification done to these are that the thrust coefficient matrix is multiplied by ten in order put the power output of the ROV in the range where typical heavy duty working class ROVs are.

B.3.1 Controller Parameters

$$K_p = \begin{bmatrix} 2000 & 0 & 0 \\ 0 & 2000 & 0 \\ 0 & 0 & 2000 \end{bmatrix} \tag{B.9}$$

$$K_i = \begin{bmatrix} 175 & 0 & 0 \\ 0 & 175 & 0 \\ 0 & 0 & 75 \end{bmatrix} \tag{B.10}$$

$$K_d = \begin{bmatrix} 8000 & 0 & 0 \\ 0 & 8000 & 0 \\ 0 & 0 & 38500 \end{bmatrix} \tag{B.11}$$

B.3.2 Inertia

$$\boldsymbol{M}_{RB} = \begin{bmatrix} 1862.87 & 0 & 0 & 0 & 0 & 0 \\ 0 & 1862.87 & 0 & 0 & 0 & 0 \\ 0 & 0 & 1862.87 & 0 & 0 & 0 \\ 0 & 0 & 0 & 525.39 & 1.44 & 33.41 \\ 0 & 0 & 0 & 1.44 & 794.20 & 2.60 \\ 0 & 0 & 0 & 33.41 & 2.60 & 691.23 \end{bmatrix} \tag{B.12}$$

$$\boldsymbol{M}_{A} = \begin{bmatrix} 779.79 & -6.8773 & -103.32 & 8.5426 & -165.54 & -7.8033 \\ -68.773 & 1222 & 51.29 & 409.44 & -5.8488 & 62.726 \\ -103.32 & 51.29 & 3659.9 & 6.1112 & -386.42 & 10.774 \\ 8.5426 & 409.44 & 6.1112 & 534.9 & -10.027 & 21.019 \\ -165.54 & -5.8488 & -386.42 & -10.027 & 842.69 & -1.1162 \\ -7.8033 & 62.726 & 10.775 & 21.019 & -1.1162 & 224.32 \end{bmatrix} \tag{B.13}$$

B.3.3 Thrust

$$\boldsymbol{K}_{T} = \begin{bmatrix} 0.0002911 & 0 & 0 & 0 \\ 0 & 0.0008734 & 0 & 0 \\ 0 & 0 & 0.0002911 & 0 \\ 0 & 0 & 0 & 0.0002911 \end{bmatrix} \cdot 10 \tag{B.14}$$

$$\boldsymbol{T} = \begin{bmatrix} 0 & 0 & 0.9063 & 0.9063 \\ 1 & 0 & -0.4226 & 0.4226 \\ 0 & 1 & 0 & 0 \\ -0.2373 & 0 & -0.4113 & 0.4113 \\ 0 & -0.2862 & 0.2179 & 0.2179 \\ 0.4878 & 0 & 0.7639 & -0.7639 \end{bmatrix} \tag{B.15}$$

B.3.4 Damping

$$\boldsymbol{D}_{NL}(\nu_r) = \begin{bmatrix} 748.22|u_r| & 0 & 0 & 0 & 0 & 0 \\ 0 & 992.53|v_r| & 0 & 0 & 0 & 0 \\ 0 & 0 & 1821.01|w_r| & 0 & 0 & 0 \\ 0 & 0 & 0 & 672|p| & 0 & 0 \\ 0 & 0 & 0 & 0 & 774.44|q| & 0 \\ 0 & 0 & 0 & 0 & 0 & 523.27|r| \end{bmatrix} \tag{B.16}$$

$$\boldsymbol{D}_L = \begin{bmatrix} 74.82 & 0 & 0 & 0 & 0 & 0 \\ 0 & 69.48 & 0 & 0 & 0 & 0 \\ 0 & 0 & 728.40 & 0 & 0 & 0 \\ 0 & 0 & 0 & 268.80 & 0 & 0 \\ 0 & 0 & 0 & 0 & 309.77 & 0 \\ 0 & 0 & 0 & 0 & 0 & 105.00 \end{bmatrix} \tag{B.17}$$

$$\boldsymbol{r}_{CG} = \begin{bmatrix} 0 \\ 0 \\ 0 \end{bmatrix}, \quad \boldsymbol{r}_{CB} = \begin{bmatrix} 0 \\ 0 \\ 0.3872 \end{bmatrix} \tag{B.18}$$

B.4 Minerva Model Parameters

This section presents the model parameters that is used for the Minerva. These are derived in Kirkeby [2010].

B.4.1 Controller Parameters

$$K_p = \begin{bmatrix} 50 & 0 & 0 \\ 0 & 50 & 0 \\ 0 & 0 & 300 \end{bmatrix} \tag{B.19}$$

$$K_i = \begin{bmatrix} 4.50 & 0 & 0 \\ 0 & 4.50 & 0 \\ 0 & 0 & 7.50 \end{bmatrix} \tag{B.20}$$

$$K_d = \begin{bmatrix} 300 & 0 & 0 \\ 0 & 300 & 0 \\ 0 & 0 & 1000 \end{bmatrix} \tag{B.21}$$

B.4.2 Inertia

$$\boldsymbol{M}_{RB} = \begin{bmatrix} 460.0 & 0 & 0 & 0 & 55.2 & 0 \\ 0 & 460.0 & 0 & -55.2 & 0 & 0 \\ 0 & 0 & 460.0 & 0 & 0 & 0 \\ 0 & -55.2 & 0 & 111.9 & 0 & 0 \\ 55.2 & 0 & 0 & 0 & 110.6 & 0 \\ 0 & 0 & 0 & 0 & 0 & 50.3 \end{bmatrix} \tag{B.22}$$

$$\boldsymbol{M}_{A} = \begin{bmatrix} 293 & 0 & 0 & 0 & 0 & 0 \\ 0 & 302 & 0 & 0 & 0 & 0 \\ 0 & 0 & 326 & 0 & 0 & 0 \\ 0 & 0 & 0 & 52 & 0 & 0 \\ 0 & 0 & 0 & 0 & 52 & 0 \\ 0 & 0 & 0 & 0 & 0 & 57 \end{bmatrix} \tag{B.23}$$

B.4.3 Thrust

$$K_{fw} = 0.4149 \tag{B.24}$$
$$K_{b} = 0.1909 \tag{B.25}$$
$$L_{lat} = 0.3334 \tag{B.26}$$
$$K_{down} = 0.3342 \tag{B.27}$$
$$K_{up} = 0.2089 \tag{B.28}$$

$$\boldsymbol{T} = \begin{bmatrix} 0.9848 & 0.9848 & 0 & 0 & 0 \\ 0.1736 & -0.1736 & 1.0 & 0 & 0 \\ 0 & 0 & 0 & 1.0 & 1.0 \\ -0.3353 & 0.3353 & 0.166 & 0 & 0 \end{bmatrix} \tag{B.29}$$

B.4.4 Damping

$$\boldsymbol{D}_{NL}(\nu_r) = \begin{bmatrix} 292|u_r| & 0 & 0 & 0 & 0 & 0 \\ 0 & 584|v_r| & 0 & 0 & 0 & 0 \\ 0 & 0 & 635|w_r| & 0 & 0 & 0 \\ 0 & 0 & 0 & 84|p| & 0 & 0 \\ 0 & 0 & 0 & 0 & 148|q| & 0 \\ 0 & 0 & 0 & 0 & 0 & |r| \end{bmatrix} \tag{B.30}$$

$$\boldsymbol{D}_L = \begin{bmatrix} 29 & 0 & 0 & 0 & 0 & 0 \\ 0 & 41 & 0 & 0 & 0 & 0 \\ 0 & 0 & 254 & 0 & 0 & 0 \\ 0 & 0 & 0 & 34 & 0 & 0 \\ 0 & 0 & 0 & 0 & 59 & 0 \\ 0 & 0 & 0 & 0 & 0 & 0.2 \end{bmatrix} \tag{B.31}$$

$$\boldsymbol{r}_{CG} = \begin{bmatrix} 0 \\ 0 \\ 0.1200 \end{bmatrix}, \quad \boldsymbol{r}_{CB} = \begin{bmatrix} 0 \\ 0 \\ -0.1500 \end{bmatrix} \tag{B.32}$$

Appendix C

Operations Manual

Operations manual: Subsea module positioning test

Where: Somewhere in Trondheims fjord where depth is between 100 m and 200 m (Closer to 200m is better)

When: 12. – 13. May

Purpose: Test an ROV control system that makes it easier/possible to deploy subsea modules and land them on a specific position on the seafloor by using one single wire, without guidelines.

Prior to operation:

- Set up navipac to output position data to control system, including information from two acoustic transponders.
- Mount Subsea module interface on to the ROV.
- Mount acoustic transponders

Operation sequence:

1) Trail assembly
   Test that all parts fit together as planned. Attach acoustic transponders to ROV and to bottom assembly. Transponder connected to bottom assembly by using a floating collar and a rope. On deck of Gunnerus. (?)
   See attached drawings for assembly.
2) Deployment bottom assembly
   i) Deploy bottom assembly, lower it to seafloor
   ii) Deploy ROV
   iii) Detach bottom assembly from lifting wire by use of ROV
   iv) Retrieve lifting wire
3) Launch Subsea module
   Launch the subsea module using crane/A-frame. Lower it to working depth by trawl winch.
4) ROV Hook-up
   i) ROV hooks up to the subsea module.
   ii) The control system is started
   iii) The heave force commended by the control system is adjusted manually so the ROV has a small downward force. This will make it follow the vertical motions of the subsea module.
5) Perform motion control tests
   The goal is to test the how well the control system can change position of subsea module
   i) Rotation test (rotate the module 180 degrees and back)
   ii) Square test (move the subsea module in a square pattern)
6) Module landing
   Land the subsea module on the bottom assembly using the control system
   Do this 3 times. (If there is enough time we should try to land the module by manual control to compare time spent and difficulty)
7) Module recovery
   Pull up and retrieve subsea module.

8) Bottom assembly recovery
    i) Lower lifting wire with ROV hook attached
    ii) Hook up bottom assembly to lifting wire
    iii) Retrieve bottom assembly
9) ROV Recovery

If there is time we could perform the following additional tests:

- Repeat the whole test (step 2-9) on another location on different depth and current conditions.
- While retrieving subsea module repeat step 5, motion control tests on a smaller depth.

Equipment needed:

- ROV Minerva
- Subsea module, bottom assembly and ROV interface
- Two acoustic transponders
- Floating collar to acoustic transponder
- Mounting equipment for transponders (hose clamps/ rope)
- Mounting equipment for ROV interface (bolts, nuts, (drill ?)
- Lifting equipment for subsea module and bottom assembly
- ROV hook for retrieval of bottom assembly
- More..?

Subsea module: parts and assembly.

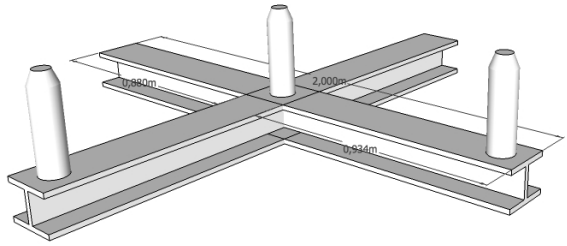

Figure 1: Bottom assembly

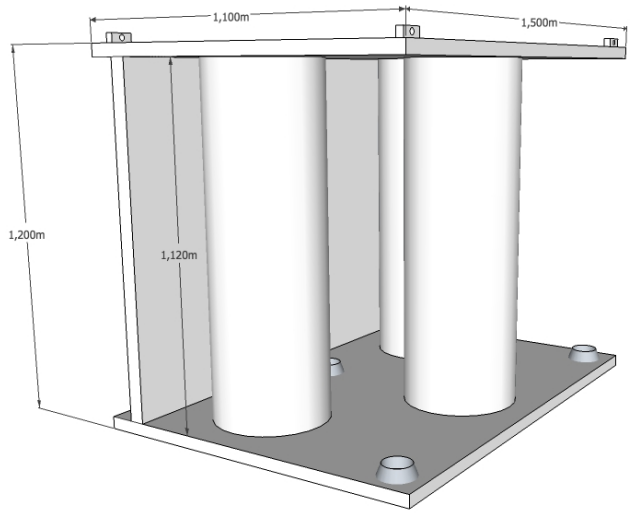

Figure 2: Subsea Module

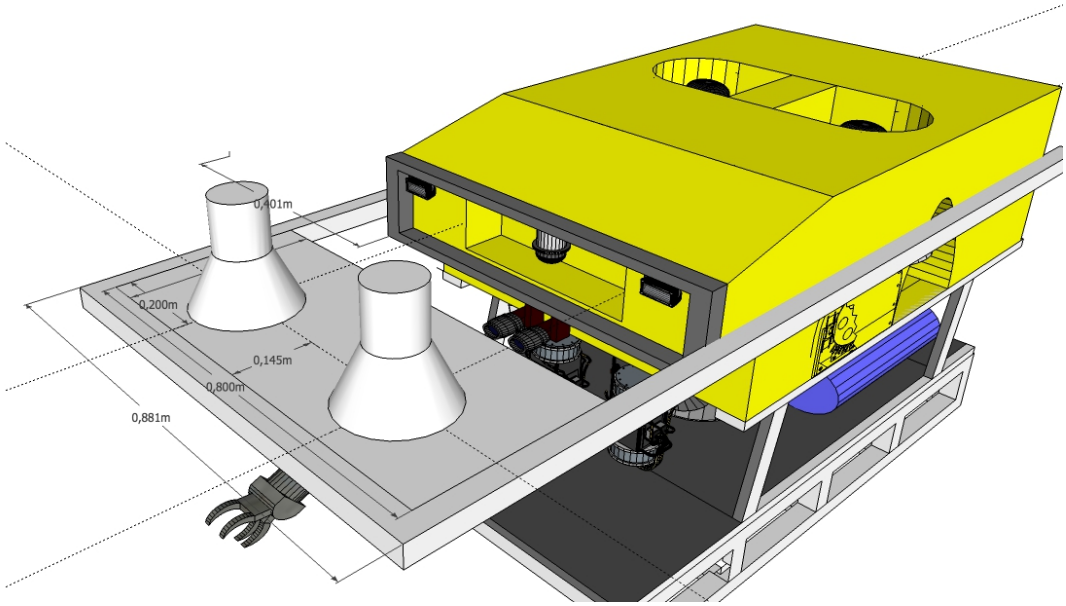

Figure 3: ROV with module interface

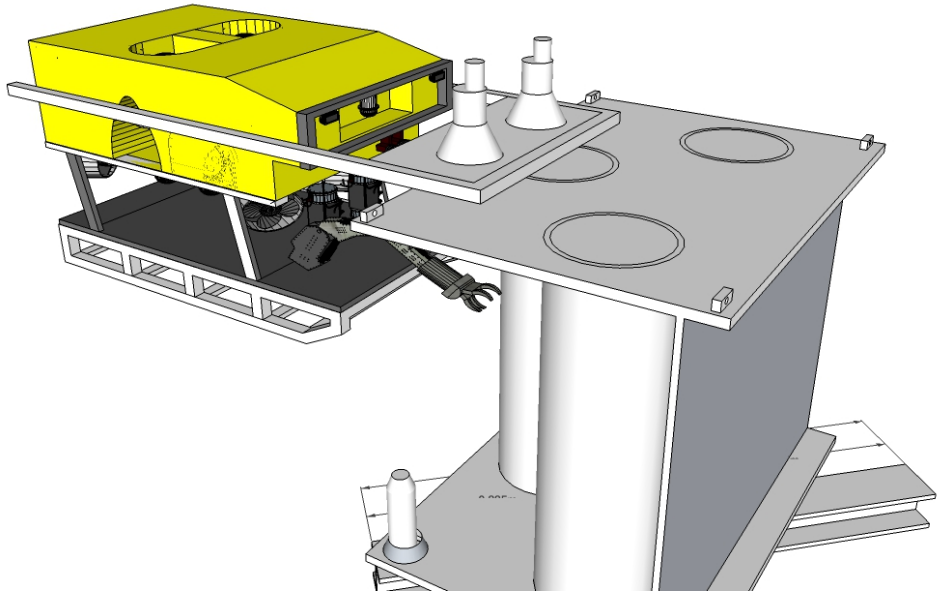

Figure 4: Complete assembly

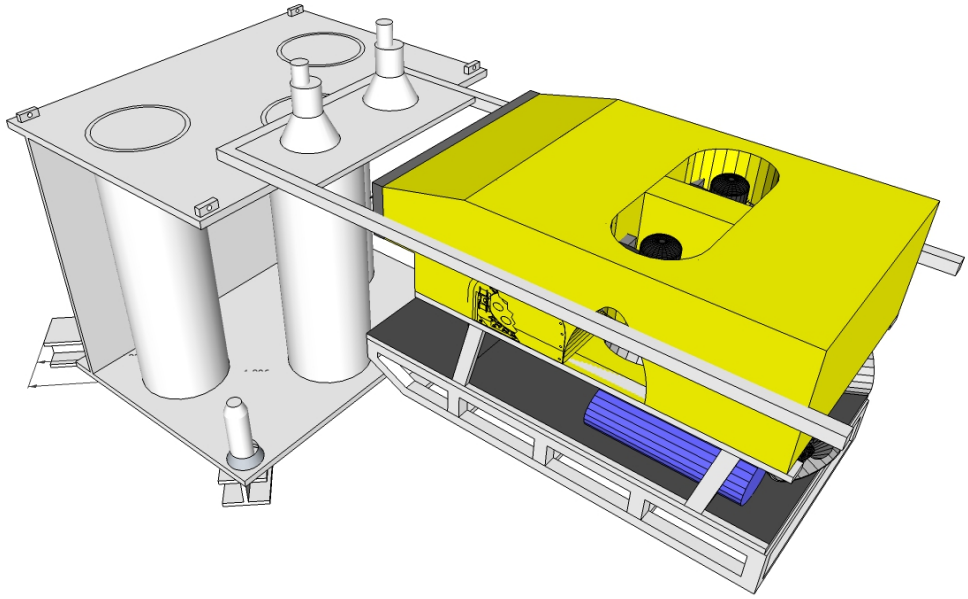

Figure 5: Complete assembly 2

Appendix D

Additional plots

In this appendix a set of additional plots that were not included in the report is presented. The plots is showing additional information about the simulations that are presented in Chapter 4.

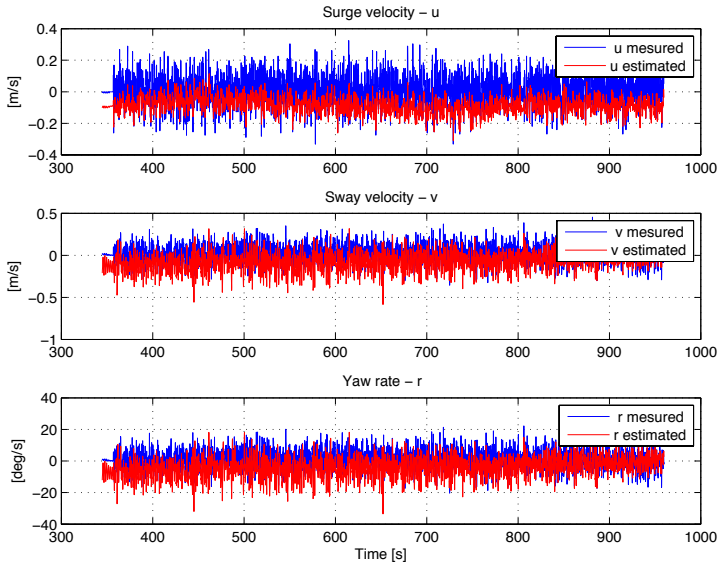

Figure D.1: Plot showing velocities during rotation move

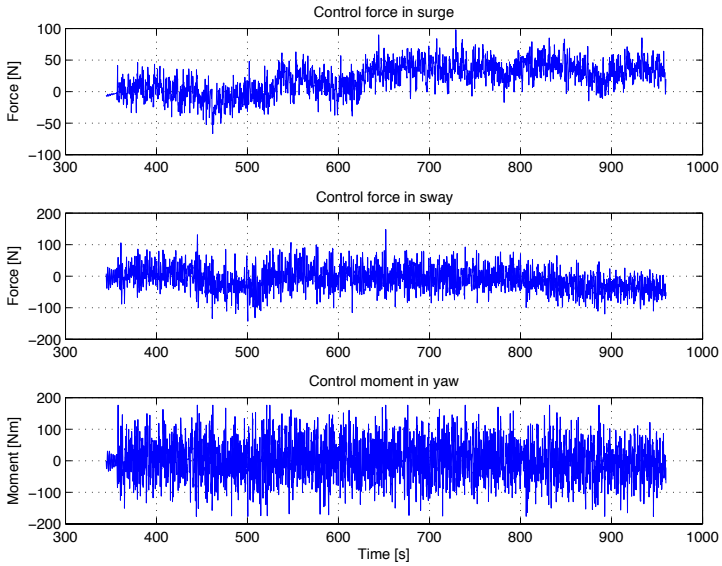

Figure D.2: Plot showing commanded control forces during rotation move

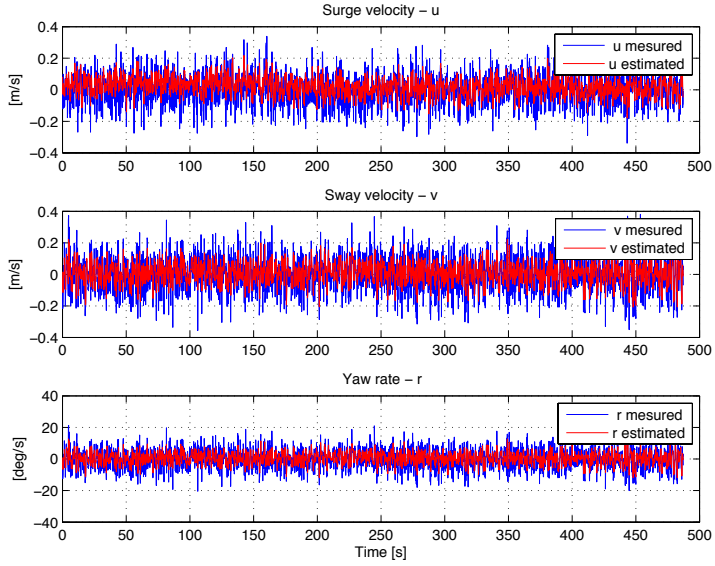

Figure D.3: Plot showing velocities during square move

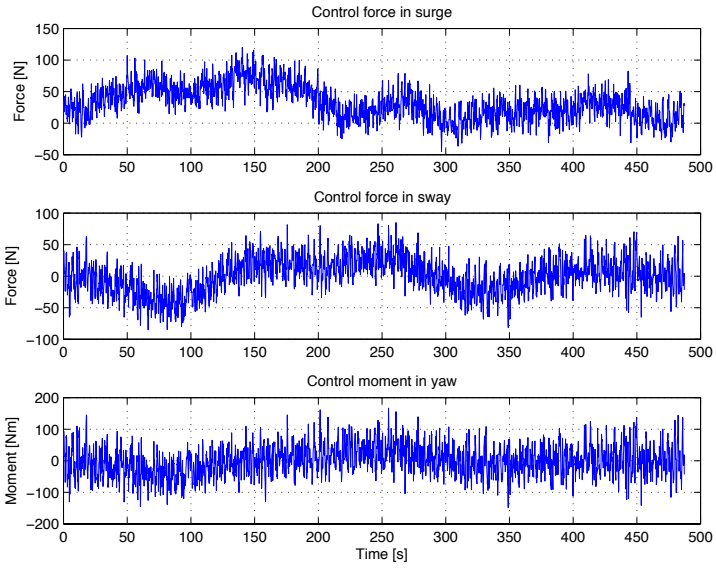

Figure D.4: Plot showing commanded control forces during square move

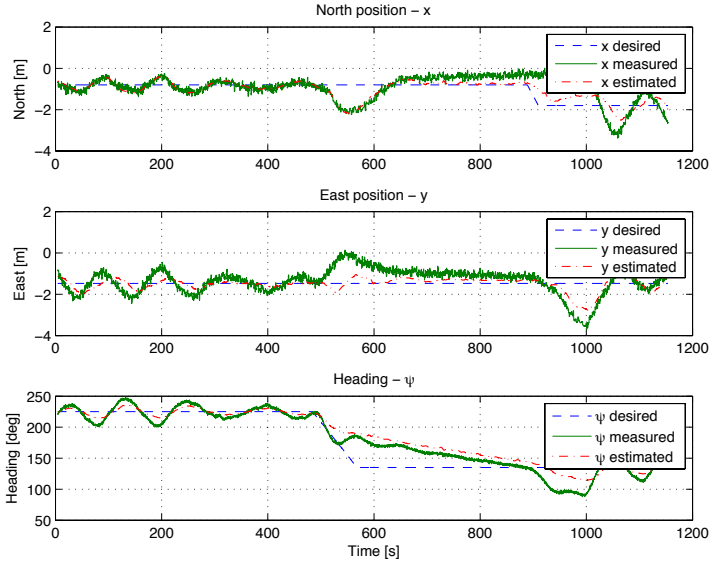

Figure D.5: Plot showing north east and heading during HIL-simulation with same parameters as in the Simulink model

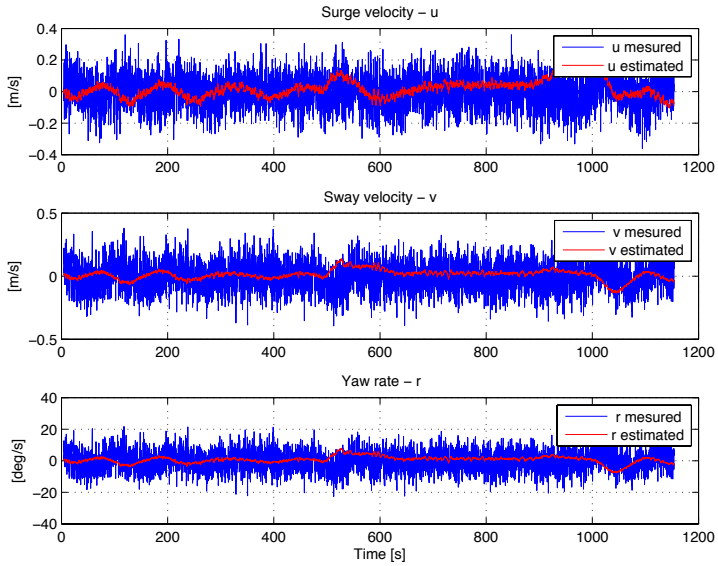

Figure D.6: Plot velocities during HIL-simulation with same parameters as in the Simulink model

Appendix E

Error Simulation

This appendix shows the result from two simulations that were conducted in order to study the effect of the error in the control system during testing.

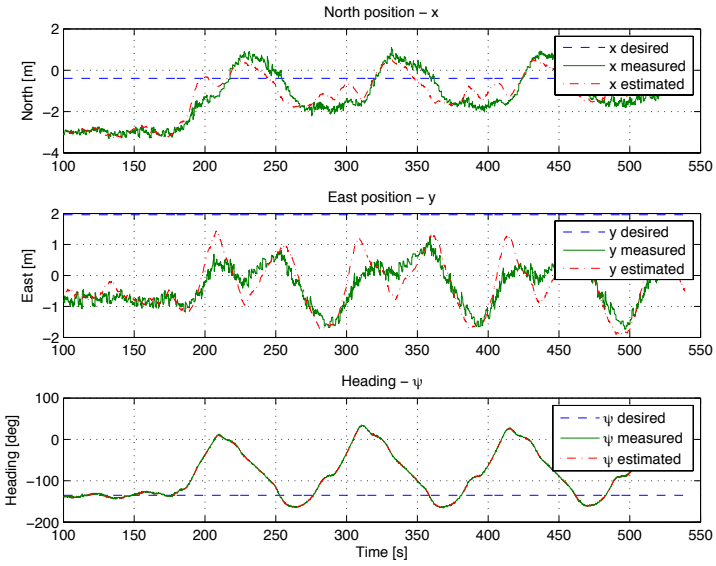

Figure E.1: plot showing the north and east position of Xmas tree

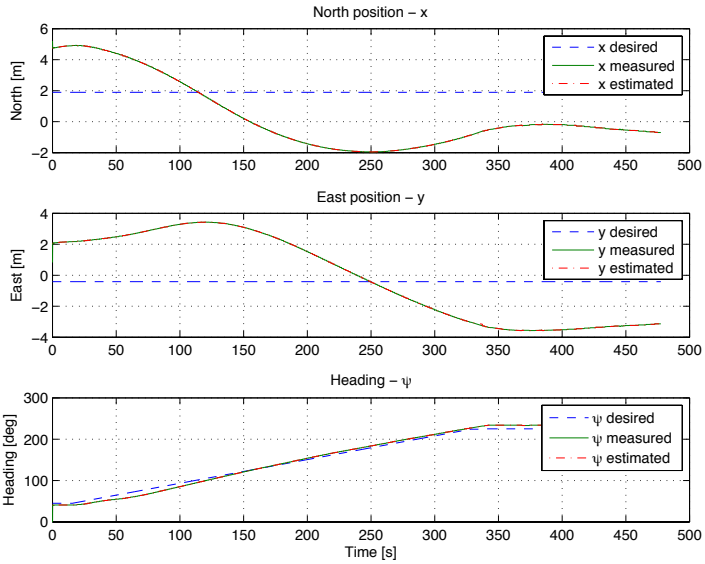

Figure E.2: Plot showing north east and heading

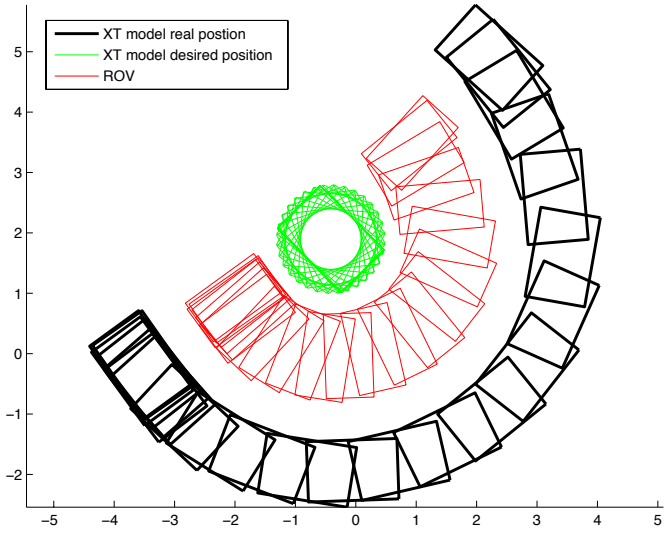

Figure E.3: plot showing the north and east position of Xmas tree

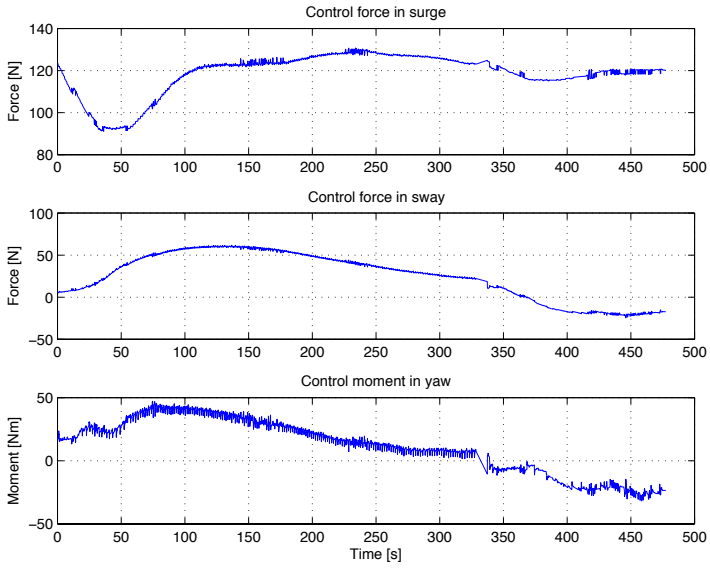

Figure E.4: plot showing the north and east position of Xmas tree

Appendix F

Digital Appendix

This appendix is including both the control system used during the experimental testing and the simulation models made in Matlab Simulink. The actual files are uploaded to the DAIM system as zipped archives.

F.1 LabView Control System

F.2 Matlab Simulink simulation models

Appendix G

Poster

This appendix includes the Scientific poster that was made to present the work done in this masters thesis during the Master Thesis Poster Exhibition at the Institute of Marine Technology.

ROV Control System for Positioning of Subsea Modules

Eirik Hexeberg Henriksen *(eirikhex@stud.ntnu.no)*
Supervisor: Asgeir J. Sørensen
Advisor: Brede Thorkildsen (FMC Technologies)

FMC Technologies
We put you first.
And keep you ahead.

NTNU

Objective and scope

Today the most common way of installing subsea Xmas trees is by lowering it down to the seabed using the drill-string of a drilling rig. Guide wires are used for positioning the module. This is a costly and time consuming operation, and there is a huge potential for saving both time and money.

A solution where the subsea Xmas tree are lowered using one single wire, and put into position by an ROV would decrease costs and time used because:

- Lowering a wire is faster than lowering a drill string
- No need for hooking up guide wires
- A smaller vessel (with a lower day rate) can be used for the installation
- No guide wires may get tangled up during the operation

The scope of my masters thesis is to design a control system for an ROV. The system should be capable of automatically placing the Xmas tree in the correct position over the well. Such a system will make the operation more effective and less prone to human errors during its last critical phase.

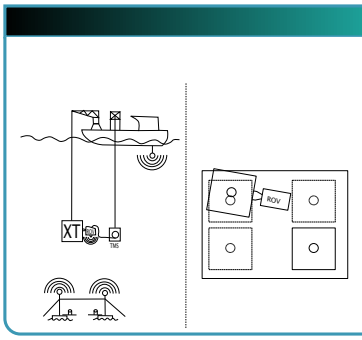

Introduction

The first objective in the project was to make a simulation model for the physical behavior of a subsea module hanging in a wire over the seabed. Then a model of an ROV was included in the model in order to study how these interacted, and if the ROV was capable of controlling the motions of the hanging module. A controller for the ROV was then designed, and simulations showed that the position of the subsea module could be controlled by the connected ROV.

The next step was to try to verify the simulation results in an experimental scale. A scaled model of a subsea Xmas tree was designed, as well as some auxiliary units that together formed an experimental setup for testing this Xmas tree installation method using R/V Gunnerus and ROV Minerva. The testing was done in the Trondheim fjord the 12. and 13. of May 2014.

Simulation results

The results from two different simulations are shown below. These simulations are done using full scale simulation model, using perfect feedback and with a small SW-going current. The two left plots are showing a motion test where the ROV is turning the Xmas tree 360° and then back while keeping its centre on the same place. In the two right plots the ROV is moving the Xmas tree in a square pattern.

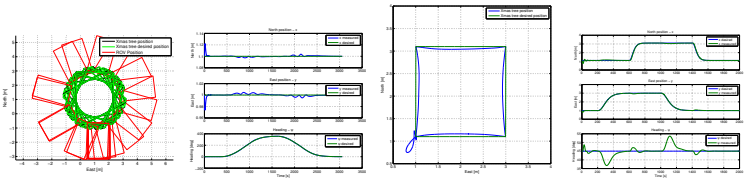

Method

Modelling

The following mathematical model for the interconnected Xmas tree and ROV system has been made. The model is expressed in the origin of the xmas tree using a compact vectorial notation.

$$\dot{\boldsymbol{\eta}} = \boldsymbol{J}_{\Theta}(\boldsymbol{\eta})\boldsymbol{\nu}$$
$$\dot{\boldsymbol{b}} = -\boldsymbol{T}_b^{-1}\boldsymbol{b} + \boldsymbol{E}_b\boldsymbol{w}$$
$$\boldsymbol{M}\dot{\boldsymbol{\nu}} + \boldsymbol{C}(\boldsymbol{\nu})\boldsymbol{\nu} + \boldsymbol{D}(\boldsymbol{\nu})\boldsymbol{\nu}_r + \boldsymbol{G}_{wire}(\boldsymbol{\eta}) = \boldsymbol{\tau}_{ctrl} + \boldsymbol{J}^{-1}(\boldsymbol{\eta})\boldsymbol{b}$$

where $\boldsymbol{\eta}$ is the position and orientation vector, $\boldsymbol{\nu}$ is the velocity vector, $\boldsymbol{b}$ is the bias vector accounting for environmental disturbances and unmodeled dynamics, $\boldsymbol{w}$ is a zero mean gaussian noise vector, $\boldsymbol{J}(\boldsymbol{\eta})$ is the euler rotation matrix rotating from the body reference frame to the North East Down (NED) frame, $\boldsymbol{M}$ is the combined rigid body mass matrix of the Xmas tree and the ROV, $\boldsymbol{C}(\boldsymbol{\nu})$ is the combined Coriolis and centripetal matrix, $\boldsymbol{D}$ is the damping matrix and $\boldsymbol{G}_{wire}(\boldsymbol{\nu})$ is the restoring forces. $\boldsymbol{\tau}_{ctrl}$ is the control force applied to the system by the thrusters of the ROV.

Controller

The controller chosen for this task is a nonlinear PID controller. It is chosen because of its simplicity and robustness. The control vector is calculated in the origin of the xmas tree by the following expression:

$$\boldsymbol{\tau}_{ctrl} = -\boldsymbol{K}_p\tilde{\boldsymbol{\eta}} - \boldsymbol{K}_s\dot{\boldsymbol{\eta}} - \int_0^t \tilde{\boldsymbol{\eta}}(\tau)d\tau \qquad (2)$$

The force vector is then transformed into the body of the ROV by the following relation:

$$\boldsymbol{\tau}_{ROV} = \boldsymbol{H}^{-T}(\boldsymbol{r})\boldsymbol{\tau}_{ctrl}$$

Where $\boldsymbol{H}$ is the system transformation matrix described in [Fossen(2011)], and $\boldsymbol{r}$ is the vector from the centre of the Xmas tree to the centre of the ROV.

Observer

An observer was implemented in order to provide a feedback to the controller with higher quality than the raw measurements. The Observer will estimate the position and speed of the system using the measurements taken on the ROV in between the slow position updates from the acoustic transponder and filter these signals.

The observer is implemented as an extended kalman filter using the model above for estimation of the states. In order to use the measurements from the ROV as input, the measured ROV states are transformed into the origin of the Xmas tree using the following kinematic relations:

$$\boldsymbol{\eta}_{xmas} = \boldsymbol{\eta}_{ROV} - \boldsymbol{J}(\boldsymbol{\eta}_{ROV})\boldsymbol{r}$$
$$\boldsymbol{\nu}_{xmas} = \boldsymbol{H}(\boldsymbol{r})\boldsymbol{\nu}_{ROV}$$

Experimental results

Experimental setup

The experimental testing was performed in the Trondheim fjord, using the NTNUs research vessel Gunnerus. The experimental setup consisted of a scaled subsea module, a docking frame, and ROV Minerva with an interface frame mounted.

The Xmas tree model was designed to have similar hydrodynamical properties as a real subsea xmas tree, but was scaled down to accommodate the thrust capacity of ROV Minerva. It was made with aligning funnels in the bottom plate, and guideposts on the top to interface with the ROV.

The docking frame was designed as a cross with guideposts that fitted the aligning funnels on the Xmas tree model. During the tests it was placed on the sea floor and served as a fixed point to land the Xmas tree model on. It was fitted with an acoustic transponder to get the position reference.

ROV Minerva was fitted with an interface frame that was going to make a connection to the xmas tree model that could transfer both linear forces and rotational moments in order to control the position of the module.

R/V Gunnerus

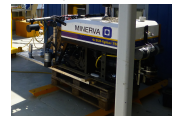

ROV Minerva with interface frame

Xmas tree model

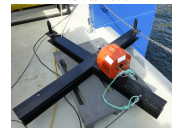

Docking frame and acoustic transponder

Experimental results

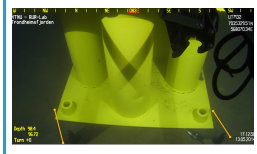

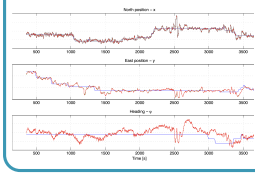

During the testing a lot of time was spent setting up and improving the equipment. When the control system was finally started, there was an error in the observer. Due to limited testing time it was decided to use raw measurements as input to the controller instead of filtered and estimated signals. It is assumed that this decreased the performance of the controller.

Even though the system did not work exactly as planned, a docking attempt was made. The module was placed about 20 cm away from the target as seen in the picture to the left. The graph is showing the desired state in blue and the measured in red.

When the testing results was analyzed, the error was found. This error applied to the controller as well, and it is assumed that it led to a somewhat decreased performance. With this in mind the testing results was promising.

Conclusions

A control system for using an ROV for controlling the position and orientation of a subsea module has been designed. Simulation results is promising, but due to an error during testing its performance was not verified. The fact that the system worked even with this error shows the robustness of the controller. Further testing without this error should be done. The main challenge for the performance of the control system is however the precision of the position measurement, it might be to low using an USBL acoustic positioning system. A way of visually confirming the alignment of the module is also needed.

References

[Fossen(2011)] Thor Inge Fossen. *Handbook of Marine Craft Hydrodynamics and Motion Control*. John Wiley Sons, Ltd, 2011.

G.2

Acknowledgements

FMC Technologies has been a sponsor for the work with this masters thesis, supplying both on the subject expertise and funding for creating the experiment setup.